

# CONTENTS

	Page	
LIST OF TABLES . . . . .	v	1/A7
LIST OF FIGURES . . . . .	vi	1/A8
LIST OF SYMBOLS . . . . .	ix	1/A11
SUMMARY . . . . .	1	1/A14
INTRODUCTION . . . . .	1	1/A14
AEROELASTIC METHODS . . . . .	5	1/B4
Aeroelastic Rigid Formats . . . . .	11	1/B10
Flutter Methods . . . . .	13	1/B12
The K-method of Flutter Solution . . . . .	14	1/B13
The KE-method of Flutter Solution . . . . .	16	1/C1
The PK-method of Flutter Solution . . . . .	17	1/C2
Frequency Response and Random Analysis . . . . .	23	1/C8
Frequency Response . . . . .	23	1/C8
Random Analysis . . . . .	29	1/C14
Transient Analysis by the Fourier Transform Method . . . . .	36	1/D7
Transient Analysis by the Fourier Method . . . . .	36	1/D7
Transformation of Loads . . . . .	39	1/D10
Calculation of Frequency Response . . . . .	41	1/D12
Inverse Transformation of the Response . . . . .	42	1/D13
Practical Considerations for Use of the Fourier Methods . . . . .	44	1/E1
AERODYNAMIC INFLUENCE COEFFICIENTS . . . . .	45	1/E2
Doublet-Lattice Method . . . . .	48	1/E5
Subsonic Wing-Body Interference Theory . . . . .	48	1/E5
Mach Box Method . . . . .	54	1/E11
Strip Theory . . . . .	56	1/E13
Piston Theory . . . . .	57	1/E14
Interconnection Between Structural and Aerodynamic Forces . . . . .	57	1/E14
Theory for Surface Splines . . . . .	59	1/F2
Theory for Linear Splines . . . . .	61	1/F4
Linear Splines . . . . .	61	1/F4
Torsion Bars . . . . .	64	1/F7
Attachment of Splines with Elastic Springs . . . . .	65	1/F8
Rigid Arms on Linear Splines . . . . .	66	1/F9
Coordinate Systems and Constraints . . . . .	66	1/F9

	Page	
DEMONSTRATION PROBLEMS . . . . .	66	1/F9
Flutter Analysis . . . . .	68	1/F11
Swept Wing . . . . .	68	1/F11
The BAH Wing . . . . .	71	1/G3
Servoelastic Stability Analysis . . . . .	79	1/G8
Aeroservoelastic Stability Analysis . . . . .	83	1/G12
Inverse Fourier Transform Characteristics . . . . .	86	2/A3
Aeroelastic Response Analysis . . . . .	96	2/A13
Discrete Gust Response . . . . .	96	2/A13
Random Gust Response . . . . .	98	2/B3
Transient Rolling Maneuver . . . . .	100	2/B5
REFERENCES . . . . .	104	2/B11

MAR 7 1979

Item 82-11-14

NAS 1.26:3094

COMPLETED

NASA Contractor Report 3094

ORIGINAL

## Aeroelastic Addition to NASTRAN

William P. Rodden, Robert L. Harder,  
and E. Dean Bellinger

CONTRACT NAS1-13034  
MARCH 1979

**NASA**

i

118

# NASA Contractor Report 3094

## Aeroelastic Addition to NASTRAN

William P. Rodden, Robert L. Harder,  
and E. Dean Bellinger  
*The MacNeal-Schwendler Corporation*  
*Los Angeles, California*

Prepared for  
Langley Research Center  
under Contract NAS1-13034



National Aeronautics  
and Space Administration

Scientific and Technical  
Information Office

1979



# CONTENTS

	Page
LIST OF TABLES . . . . .	v
LIST OF FIGURES . . . . .	vi
LIST OF SYMBOLS . . . . .	ix
SUMMARY . . . . .	1
INTRODUCTION . . . . .	1
AEROELASTIC METHODS . . . . .	5
Aeroelastic Rigid Formats . . . . .	11
Flutter Methods . . . . .	13
The K-method of Flutter Solution . . . . .	14
The KE-method of Flutter Solution . . . . .	16
The PK-method of Flutter Solution . . . . .	17
Frequency Response and Random Analysis . . . . .	23
Frequency Response . . . . .	23
Random Analysis . . . . .	29
Transient Analysis by the Fourier Transform Method . . . . .	36
Transient Analysis by the Fourier Method . . . . .	36
Transformation of Loads . . . . .	39
Calculation of Frequency Response . . . . .	41
Inverse Transformation of the Response . . . . .	42
Practical Considerations for Use of the Fourier Methods . . . . .	44
AERODYNAMIC INFLUENCE COEFFICIENTS . . . . .	45
Doublet-Lattice Method . . . . .	48
Subsonic Wing-Body Interference Theory . . . . .	48
Mach Box Method . . . . .	54
Strip Theory . . . . .	56
Piston Theory . . . . .	57
Interconnection Between Structural and Aerodynamic Forces . . . . .	57
Theory for Surface Splines . . . . .	59
Theory for Linear Splines . . . . .	61
Linear Splines . . . . .	61
Torsion Bars . . . . .	64
Attachment of Splines with Elastic Springs . . . . .	65
Rigid Arms on Linear Splines . . . . .	66
Coordinate Systems and Constraints . . . . .	66

	Page
DEMONSTRATION PROBLEMS . . . . .	66
Flutter Analysis . . . . .	68
Swept Wing . . . . .	68
The BAH Wing . . . . .	74
Servoelastic Stability Analysis . . . . .	79
Aeroservoelastic Stability Analysis . . . . .	83
Inverse Fourier Transform Characteristics . . . . .	86
Aeroelastic Response Analysis . . . . .	96
Discrete Gust Response . . . . .	96
Random Gust Response . . . . .	98
Transient Rolling Maneuver . . . . .	100
REFERENCES . . . . .	104

# LIST OF TABLES

	Page
Table 1: Matrices in Eq. 128 for Spline Interpolation . . . . .	67
Table 2: Closed Loop Servoelastic Eigenvalues, Frequencies and Damping Values . . . . .	82
Table 3: Aeroservoelastic Eigenvalues, Reduced Frequencies, Frequencies and Damping Values at Sea Level at $V = 152.4$ m/s (500 fps) . . . . .	84
Table 4: Aeroservoelastic Eigenvalues, Reduced Frequencies, Frequencies and Damping Values at Sea Level at $V = 304.8$ m/s (1000 fps) . . . . .	85
Table 5: Comparison of Exact Solution with IFT Response for FREQ105 . . . . .	87

# LIST OF FIGURES

	Page
Figure 1: Simplified Flow Diagram for Dynamic Analysis, Rigid Formats 3 and 7-12 . . . . .	6
Figure 2: Simplified Flow Diagram for Modal Flutter Analysis, Rigid Format 10 for APP AERO . . . . .	7
Figure 3: Simplified Flow Diagram for Modal Aeroelastic Response, Rigid Format 11 for APP AERO . . . . .	8
Figure 4: Basic Flow Diagram for PK-Flutter Method . . . . .	21
Figure 5: Complete Flow Diagram for PK-Flutter Analysis . . . . .	22
Figure 6: Flow Diagram for Frequency Response Module (FRRD) . . . . .	24
Figure 7: Flow Diagram for Random Analysis Module (RANDOM) . . . . .	33
Figure 8: Simplified Flow Diagram for Transient Analysis Module (TRD) . . . . .	37
Figure 9: Response of a Damped Oscillator to a Triangular Pulse . . . . .	45
Figure 10: Planform Geometry for Mach Box Method . . . . .	55
Figure 11: Splines and Their Coordinate Systems . . . . .	58
Figure 12: Fifteen Degree Sweptback Wing Model . . . . .	69
Figure 13: Aerodynamic Idealizations for Fifteen Degree Sweptback Wing Model . . . . .	71
Figure 14: Subsonic Flutter Analysis of Sweptback Wing Model Using Doublet-Lattice Aerodynamics and K-Method . . . . .	72
Figure 15: Supersonic Flutter Analysis of Sweptback Wing Model Using the PK-Method . . . . .	73
Figure 16: BAH Wing Planform and Aerodynamic Strip Idealization . . . . .	75
Figure 17: Comparison of BAH Wing Flutter Frequencies Between P- and PK-Methods . . . . .	76
Figure 18: Comparison of BAH Wing Damping Values Between P- and PK-Methods . . . . .	77
Figure 19: Comparison of BAH Wing Divergence Roots Between P- and PK-Methods . . . . .	78
Figure 20: Uniform Missile-Flipper Idealization . . . . .	79
Figure 21: Missile Servo Block Diagram . . . . .	80

	Page
Figure 22: Comparison of the Three Inverse Fourier Transform Methods . . . . .	89
Figure 23: Comparison of FREQ104 (31f's) with Solution (FREQ105, IFTM = 2) . . . . .	90
Figure 24: Comparison of FREQ106 (21f's) with Solution (FREQ105, IFTM = 2) . . . . .	91
Figure 25: Comparison of FREQ107 (6f's) with Solution (FREQ105, IFTM = 2) . . . . .	92
Figure 26: Comparison of FREQ109 (8f's) with Solution (FREQ105, IFTM = 2) . . . . .	93
Figure 27: Comparison of FREQ111 (10f's) with Solution (FREQ105, IFTM = 2) . . . . .	94
Figure 28: Comparison of FREQ112 (12f's) with Solution (FREQ105, IFTM = 2) . . . . .	95
Figure 29: Doublet-Lattice Idealization of BAH Wing for Aeroelastic Response Analyses . . . . .	97
Figure 30: Root Bending Moment per Unit Induced Gust Angle of Attack for BAH Wing due to a Sharp Unit Gust Loading . . . . .	99
Figure 31: Frequency Response of Root Bending Moment for BAH Wing due to a Random Gust Input . . . . .	101
Figure 32: Power Spectral Density of Root Bending Moment for BAH Wing . . . . .	102
Figure 33: BAH Jet Transport Roll Response . . . . .	103

**BLANK PAGE**

# LIST OF SYMBOLS

$A$	matrix defined by Eq. 9, 20, 30; tabulated coefficients or aerodynamic influence matrix
$\bar{A}$	ratio of standard deviations of the response to input loads
$a_o$	slender body half-width
$AR$	height/width ratio of slender body
$B$	damping matrix
$b$	semi-chord
$C$	defined by Eq. 83, forces along wing box quarter-chord for doublet lattice method or Theodorsen function
$\bar{c}$	reference chord
$D$	defined by Eq. 84, or substantial differentiation matrices
$E$	modulus of elasticity
$e$	missile control system inputs and outputs
$E_k$	defined by Eq. 79
$E_2$	defined by Eq. 72
$F$	real part of Theodorsen function
$f$	frequency
$G$	transformation matrix, tabulated complex function of frequency or imaginary part of Theodorsen function
$g$	artificial structural damping coefficient
$g_a$	actual structural damping coefficient
$H$	frequency response due to some excitation source
$h$	altitude
$I$	identity matrix or cross section area moment of inertia
$K$	stiffness matrix, servo time constant
$k$	reduced frequency ( $\omega\bar{c}/2V$ )
$L$	scale of turbulence
$\ell$	wing semi-span
$M$	mass matrix, or wing root bending moment
$m$	Mach number
$N_0$	mean frequency of zero crossings with a positive slope

$P$	load vector
$\tilde{P}$	Fourier transform of $P$
$p$	parameter defined by Eq. 4, operator used in missile control system transfer functions, or aircraft steady roll rate
$Q$	aerodynamic force matrix, or some excitation source
$q$	dynamic pressure
$R$	auto- or cross-correlation function
$r$	defined by Eq. 81
$\tilde{r}$	defined by Eq. 56
$S$	factor that gives proportion of k-set used in c-set, power spectral density, or integration matrix
$s$	defined by Eq. 81
$\tilde{t}$	defined by Eq. 74
$T1, T2, T3$	defined by Eqs. 69-79
$U$	airplane velocity
$u$	displacement
$\tilde{u}$	defined by Eq. 63
$V$	velocity
$W_g$	rms gust velocity
$w$	downwash, or gust velocity

#### Greek

$\alpha$	defined by Eq. 57, or used as exponential coefficient
$\beta$	defined by Eq. 58, or aileron deflection
$\gamma$	actual viscous damping, or amplification rate coefficient
$\delta$	flipper rotation, or wing tip deflection
$\epsilon$	convergence tolerance
$\zeta$	damping in missile control system transfer function
$\Theta$	twist angle
$\theta$	tabulated coefficients
$\Lambda$	sweep angle
$\lambda$	eigenvalue, or mass ratio used in Fig. 32
$\mu$	doublet strengths
$\xi_i$	set of modal coordinates
$\rho$	air density



$\tau$	tabulated coefficients
$\Phi$	power spectrum of atmospheric turbulence
$\phi$	eigenvectors of phase angle
$\psi$	defined on Fig. 32
$\omega$	circular frequency

#### Subscripts & Superscripts

a	analysis set
c	combined load set
d	dynamic analysis set for direct method
e	extra points
f	free or unconstrained structural coordinates
g	structural points
h	set used in modal analysis
i	mode index
j	indicates jth degree of freedom
k	component load set or aerodynamic points
m	multi-point constraint set
n	all points not in the m-set
o	omitted points
p	physical points
R	reference value
s	single point constraint set or slender body

## SUMMARY

An addition of aeroelastic capability for solving various problems in structural dynamics has recently been completed. Three methods of flutter analysis have been provided. The usual American method is provided and is called the K-method. A restricted form of the American method is also available which was designed specifically for speed and efficiency and is called the KE-method. The third is the British method which offers more realistic estimates of damping than does the American method and is referred to as the PK-method. Four aerodynamic theories are available for the calculation of steady and oscillatory air loads. These include the subsonic Doublet-Lattice Method with slender body interference, subsonic Strip Theory with aerodynamically balanced control surfaces, the supersonic Mach Box method, and Piston theory for use at high supersonic Mach numbers. The transient response to control surface deflections or to discrete atmospheric gusts can be analyzed using the vehicle frequency response characteristics and inverse Fourier transform procedures. Finally, the statistical properties of random response to atmospheric turbulence can be determined in terms of the vehicle frequency response characteristics and the power spectral characteristics of the turbulence. Each of the new capabilities of NASTRAN is illustrated by an appropriate example.

## INTRODUCTION

The NASA Structural Analysis Program, NASTRAN<sup>®</sup> (Refs. 1, 2, and 3), has been extended to include dynamic aeroelastic analyses. NASTRAN is a general-purpose digital computer program with a broad range of capability for static

---

<sup>®</sup>The name NASTRAN is a registered trademark of NASA and cannot be used without NASA consent.

and dynamic structural problems. This report describes the capability added for the solution of a variety of dynamic aeroelastic problems at subsonic and supersonic speeds. The implementation has followed the recommendations of the design study of Ref. 4.

The addition of extensive and diverse new capability to an already large computer program was anticipated in the original design of NASTRAN. Not only were the functional requirements for the solution of a wide range of large and complicated problems in structural analysis with high accuracy and computational efficiency recognized, but also the operational and organizational aspects of the program were considered at great length. The objectives of operational and organizational efficiency were achieved through modular separation of functional capabilities organized under a problem-independent executive system. This approach is absolutely essential in any complex multioperation, multifile application program which provides a selection of computational sequences that are controlled by the user through externally provided options and parameter values, as well as internal decision switches whose settings depend upon tests performed during the calculations which will control the computational sequences. There is, therefore, a natural separation of computational blocks into functional modules, but despite this separation it is clear that modules cannot be completely independent since they are all directed toward solution of the same general problem; in particular, they must intercommunicate data among themselves. The principal problem in organizing any application program, large or small, is designing the data interfaces among modules. This problem has been solved in NASTRAN by a separation of system functions, performed by an executive routine, from problem solution functions accomplished by modules separated strictly along functional lines. Each module is independent from all other modules in the sense that modification of a module, or addition of a new module will not, in general, require modification of other modules. The executive system is open-ended in the sense that it can accommodate an essentially unlimited number of functional modules, files and parameters, and modification of the executive system to permit modification or extension of functional modules is restricted to changes in entries in control tables stored within the executive routine.

It is the modular and executive control features of NASTRAN that allowed the addition of dynamic aeroelastic capability without compromise to the pre-existing structural program and thus permit structural analyses during the aeroelastic execution without penalty to the aeroelastician.

The new capability for dynamic aeroelastic analysis utilizes the following features.

1. Structural Model

Any of the existing NASTRAN structural finite elements can be used to build the structural model for the aeroelastic analysis. No additions or modifications are required. The structural stiffness, mass, and damping matrices are generated.

2. Aerodynamic Model

Matrices of aerodynamic influence coefficients are generated. These matrices are computed from a description of the geometry of the aerodynamic finite elements. The choice of grid points for the aerodynamic model is independent of the location of the structural grid points. Two subsonic and two supersonic aerodynamic theories are available. The subsonic theories are Strip Theory and the Doublet-Lattice Method. The Doublet-Lattice Method can account for interference among multiple lifting surfaces and bodies. The supersonic theories are the Mach Box Method and Piston Theory.

3. Interconnection

An automated procedure is provided to relate the aerodynamic and structural degrees of freedom. Linear and surface splining techniques are used to generate the transformation matrix between the aerodynamic and structural grid point deflections.

4. Modal Formulation

The number of degrees of freedom required for accurate solutions to aeroelastic problems is generally less than the number of physical degrees of freedom used in the finite element structural model. The number of independent degrees of freedom can be greatly reduced by using Galerkin's method with a series of vibration modes in which the amplitudes of the modes become the generalized coordinates. NASTRAN has the capability to compute the vibration modes and frequencies and to make the transformation to modal coordinates. The matrices of aerodynamic influence coefficients are also transformed to generalized aerodynamic forces by use of the vibration modes.

## 5. Flutter Analysis

The dynamic aeroelastic stability problem is solved by three methods. The traditional American flutter method developed by the Air Materiel Command in 1942 is available in two forms. The first is called the K-method and is the usual form; the second is a more efficient form from the point of view of tracking roots and is called the KE-method. The other available method is the British flutter method which was developed by the Royal Aircraft Establishment and is called the PK-method.

## 6. Active Control Systems

The capability to couple servo-systems with the structure was included in the original NASTRAN development. The coupling with aerodynamic forces has been added so that aero-servo-elastic analysis of flutter suppression or load alleviation systems is now possible.

## 7. Frequency Response

The coupling with aerodynamic loads has also been added to the previous NASTRAN structural frequency response capability. Frequency response to arbitrarily specified forcing functions can be determined with the oscillatory aerodynamic loads determined by any of the aerodynamic theories. Frequency response in a harmonic gust field can only be calculated at subsonic speeds using the Doublet-Lattice Method for wing-body interference.

## 8. Transient Response

Because unsteady aerodynamic loads are obtained for steady-state harmonic motion, they are known in the frequency, rather than time domain. Inverse Fourier Transform techniques provide the appropriate methods by which transient response is obtained from the frequency response. Both direct and inverse Fourier transforms are provided so that the forcing function or the gust profile can be transformed into the frequency domain. Then, after convolution with the system frequency response, the inverse transform leads to the transient response of the system to the specified forcing function or gust profile.

## 9. Random Response

Stationary random response depends on the frequency response of the system to a specified loading and the power spectral density of that loading. The loading may be either a specified force distribution or a harmonic gust field. The statistical quantities of interest in the response are  $\bar{A}$ , the ratio of standard deviations of the response to that of the input loading, and  $N_0$ , the mean frequency of zero crossings (with a positive slope) of the response. This new capability was added to NASTRAN by modifying the existing random response module to include

options to generate various atmospheric turbulence power spectra and to perform the calculation of  $N_0$ .

#### 10. Displays

In addition to all the usual numerical printout, certain output can also be requested in graphical form. Some of these graphical presentations have been standard features of NASTRAN and some have been added because they are specifically of interest in aeroelastic analyses. For checking the aeroelastic model, plots can be made of the layouts of structural and aerodynamic elements. Plots can be made of flutter analysis results in the form of velocity-damping and velocity-frequency curves; flutter mode shapes can also be plotted. Frequency response data can be plotted as functions of frequency, and transient response data can be plotted as functions of time. In random response analysis, the power spectral densities can be plotted against frequency. Several plotters are available to the user, the simplest being the printer that provides the results in a numerical format.

### AEROELASTIC METHODS

The general problem flow for Dynamic Analysis in NASTRAN is shown in Fig. 1, which is a flow diagram showing the major functional modules employed in the solution of all dynamic problems except for aeroelastic problems; the flow diagrams for aeroelastic problems are shown in Figs. 2 and 3. Three basic types of analysis are performed (Eigenvalue Extraction, Frequency Response Analysis, and Transient Response Analysis) according to either of two methods of problem formulation (Direct or Modal). In all, there are seven different paths through the flow diagram of Fig. 1 corresponding to the following seven rigid formats for dynamic analysis, which supplement five rigid formats for static analysis. (The numbers are the Rigid Format numbers assigned in the Program.)

3. Normal Modes Analysis
7. Direct Complex Eigenvalue Analysis
8. Direct Frequency and Random Response Analysis
9. Direct Transient Response Analysis
10. Modal Complex Eigenvalue Analysis

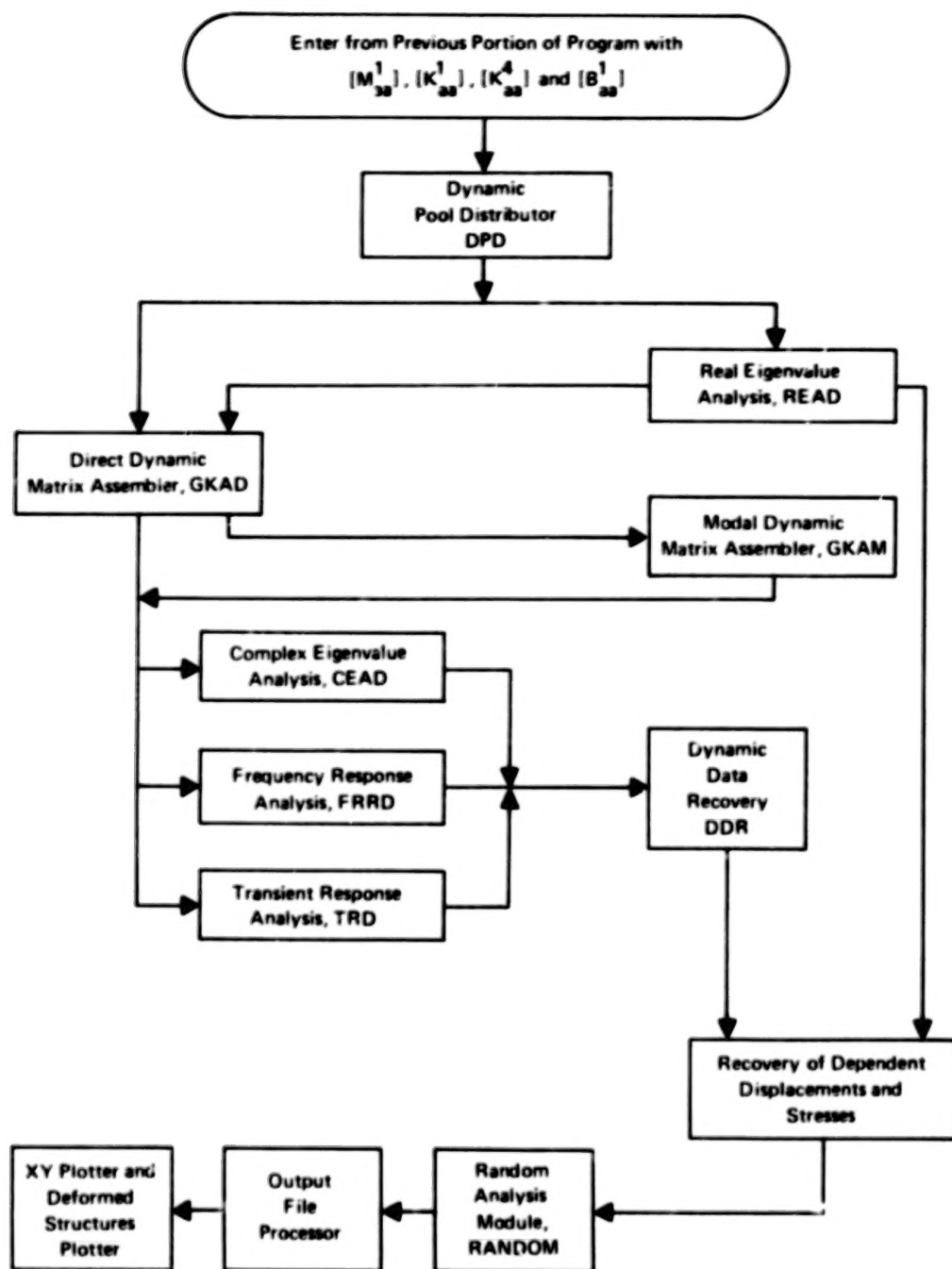


Figure 1. Simplified Flow Diagram for Dynamic Analysis, Rigid Formats 3 and 7-12.

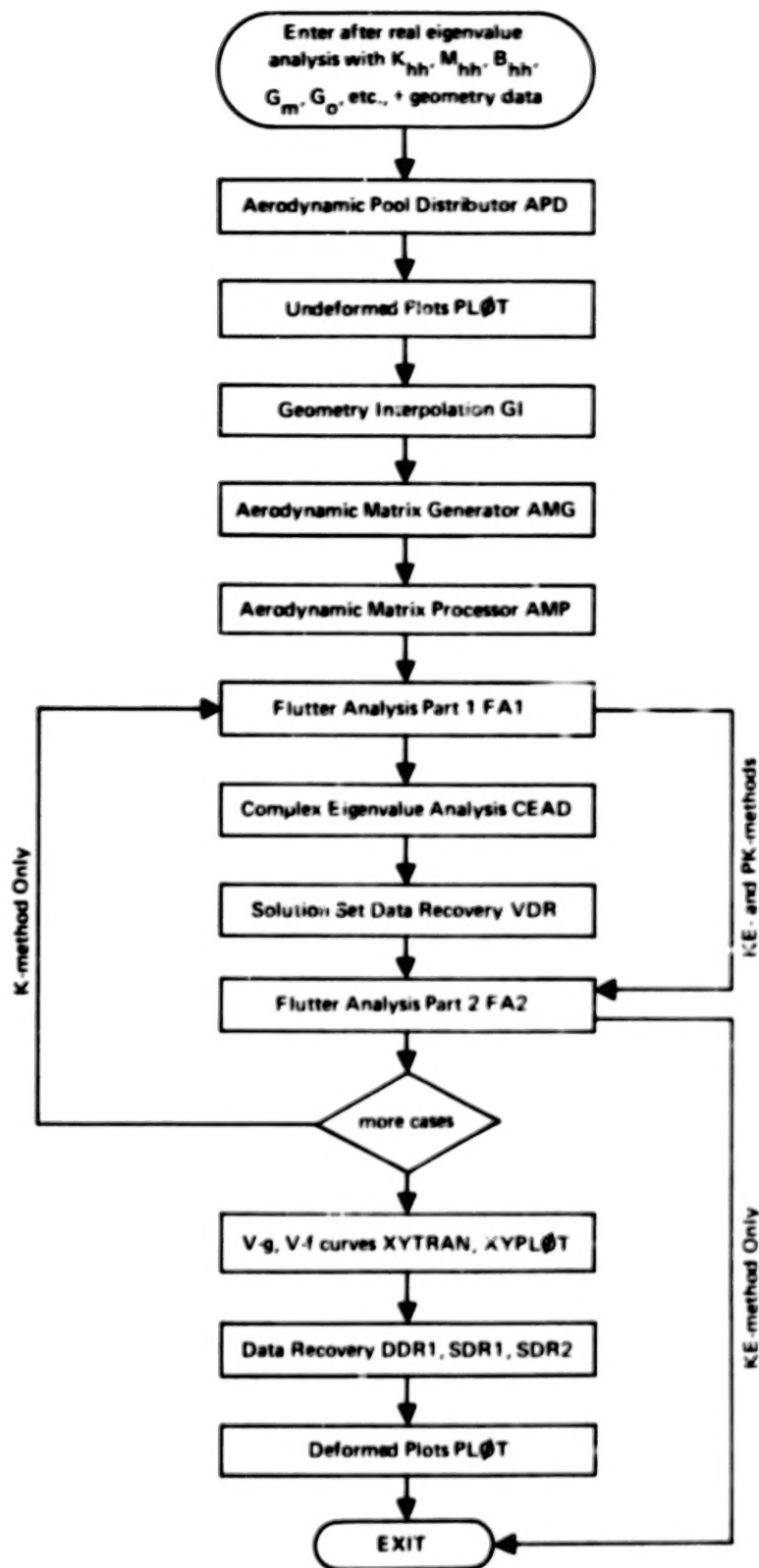


Figure 2. Simplified Flow Diagram for Modal Flutter Analysis, Rigid Format 10 for APP AERØ.





## 11. Modal Frequency and Random Response Analysis

## 12. Modal Transient Response Analysis

In the modal method of dynamic problem formulation, the vibration modes of the structure in a selected frequency range are used as degrees of freedom, thereby reducing the number of degrees of freedom while maintaining accuracy in the selected frequency range. In the direct method, the degrees of freedom are simply the displacements at grid points.

It is important to have both direct and modal methods of dynamic problem formulation in order to maximize efficiency in different situations. The modal method will usually be more efficient in problems where a small fraction of all of the modes are sufficient to produce the desired accuracy and where the bandwidth of the direct stiffness matrix is large. The direct method will usually be more efficient for problems in which the bandwidth of the direct stiffness matrix is small, and for problems with dynamic coupling in which a large fraction of the vibration modes is required to produce the desired accuracy. For problems without dynamic coupling, i.e., for problems in which the matrices of the modal formulation are diagonal, the modal method will frequently be more efficient, even though a large fraction of the modes is needed. The modal method has been chosen for the implementation of the aeroelastic addition to NASTRAN.

The flow diagram in Fig. 1 is simplified and shows only the major operations that are performed. Complete descriptions of the sequences of module calls for all rigid formats are contained in Ref. 2. The functions indicated in Fig. 1 are described in various subsections of Ref. 1.

Aeroelastic analysis brings a whole new range of capability to NASTRAN, which can be used with the structural analysis. Modules have been introduced to:

- (a) generate aerodynamic grid points,
- (b) provide connection (interpolation) between the structure and aerodynamics,
- (c) compute aerodynamic matrices, and
- (d) solve the equations for flutter or response.

Existing modules have been modified to provide, for example, a new method of eigenvalue extraction, the ability to plot aerodynamic elements and to plot the curves produced. A rigid format for modal flutter analysis by the K-, KE- or PK-methods is available.

Aerodynamic analysis, like structural analysis, is based upon a finite element approach. The finite elements are strips or boxes for which there are aerodynamic forces. There are two major points to be considered. The aerodynamic elements, even for rather complicated vehicles, tend to be in regular arrays. Thus, it is very desirable to generate the arrays of aerodynamic elements. In particular, the aerodynamic elements for lattice methods are arrays of trapezoidal boxes whose sides are parallel to the airflow. These are described simply by defining properties of the array (panel). The grid points defining the structure usually will not coincide with the aerodynamic elements. Provision has been made to generate equations of constraint between the two sets of grid points. The geometry interpolation is a key feature because it allows the choice of structural and aerodynamic elements to be based upon structural and aerodynamic considerations separately.

Aerodynamic forces are generated via the flow surrounding the structure. Each theory produces a matrix defining the forces upon the structure in terms of the deflections of the structure. State-of-the-art methods which involve interactions between aerodynamic elements are available only for sinusoidal motion. Because phase lags occur between the motions and the forces, the matrices are complex. Furthermore, these complex matrices **depend** upon parameters of the flow, namely, reduced frequency (ratio of frequency to velocity) and Mach number (ratio of velocity to speed of sound). Such matrices, if computed by an interaction theory such as the Doublet-Lattice Method or the Mach Box Method, are expensive to produce. The most effective method to evaluate the matrices for a large number of parameter values is to compute the matrices for a few selected ones, and then to interpolate for the others. This parametric interpolation is an automatic feature of the solution modules for modal aeroelastic analysis.

## Aeroelastic Rigid Formats

In NASTRAN the various phases of calculation are performed by subprograms called modules. New modules are combined with existing NASTRAN modules to solve problems. The new modules for aeroelastic analysis described in detail below are:

1. Aerodynamic Pool Distributor (APD)
2. Aerodynamic Matrix Generator (AMG)
3. Geometry Interpolator (GI)
4. Aerodynamic Matrix Processor (AMP)
5. Flutter Analysis (Part 1) (FA1)
6. Flutter Analysis (Part 2) (FA2)
7. Inverse Fourier Transform (IFT)

Several existing modules have been modified.

The term "rigid format" in NASTRAN refers to a prescribed series of module calls complete with restart tables. The new rigid formats have the following modules and characteristics:

1. The front end is similar to the existing modal-dynamics rigid formats (Nos. 10-12). Any of NASTRAN's structural elements, coordinate systems, extra points with direct matrix input for control systems, single-point constraints for boundary conditions, multipoint constraints for rigid elements, "OMIT" and "SUPPORT" for partitioning special degrees of freedom, "GENEL" elements for influence coefficient data, etc., are available.
2. The Aerodynamic Pool Distributor defines the geometry of the aerodynamic elements and adds the degrees of freedom associated with them.
3. The Geometry Interpolator produces a transformation matrix relating the aerodynamic degrees of freedom to structural degrees of freedom. Both linear and surface spline options (or combinations) are available.
4. The Aerodynamic Matrix Generator module produces a matrix which expresses the downwash at points on the aerodynamic boxes or strips in terms of the lifting pressure of the boxes or loads on the strips. The Mach number and reduced frequency are user-specified.

5. The Aerodynamic Matrix Processor combines modal, interpolation, and aerodynamic matrices to produce a matrix of generalized modal forces. The module also can output a matrix of pressure distributions for the mode shapes at the user-specified Mach numbers and frequencies.
6. The Flutter Analysis (Part 1) module produces values of  $V$  (velocity),  $g$  (artificial structural damping), and  $f$  (frequency) from user-supplied lists of  $k$  (reduced frequency), Mach number, and density, or values of  $\gamma$  (actual viscous damping) and  $f$  (frequency) from user-supplied lists of  $V$  (velocity), Mach number, and density. The calculation involves eigenvalue extraction based on the complex QR-Transformation method or the variation of the QR-Transformation for real matrices.
7. The Flutter Analysis (Part 2) module prepares the summaries of the output from the flutter analysis.
8. Both undeformed and deformed plots of the structure and aerodynamic elements can be made. Also, the  $V$ - $g$  (or  $V$ - $2\gamma$ ) and  $V$ - $f$  curves can be plotted.
9. The Inverse Fourier Transformation module converts the complex frequency response of the modal displacements to the real transient response. The numerical evaluation of the inversion integrals has been coded for both equal and unequal frequency intervals, with three curve-fitting methods available to interpolate the transformed displacements between frequencies.
10. The "RESTART" feature allows restart for several purposes. Simple restarts can continue after scheduled exits (to examine intermediate results before continuing) or to request additional output. Modified restart can be used to modify input data cards, with only the required modules being reexecuted. Rigid Formats can be switched upon restart, e.g., to start with a vibration mode analysis (Rigid Format No. 3), and then to use these results to continue with a flutter analysis.

The aeroelastic modules are arranged into two rigid formats. The flutter analysis rigid format (No. 10, APP AERØ) is shown in Fig. 2. The following capabilities are provided.

1. Complete modal flutter analysis is available. The user supplies a finite element model for structure and aerodynamics.  $V$ - $g$  and  $V$ - $f$  curves are drawn. If desired, flutter mode shapes may be plotted.
2. A change of mass or stiffness can be made without recalculating modes by means of direct matrix input (DMIG) data because there is no restriction to orthogonality in the modal solution.
3. Selection of the number of modes is made by the user. A change of modes does not require aerodynamics to be recalculated.

4. The full extra point, IMIG, transfer function capability of NASTRAN is available for control systems, etc. Special provision is made for a user-supplied matrix of downwash due to motion of extra points.
5. Data recovery is available for structural displacements, constraint forces, and element stresses and forces for any eigensolutions selected.
6. Output of the modal amplitudes can be requested using the SDISP request in Case Control.

The aeroelastic response dynamic rigid format (No. 11, APP AERD) is shown in

Fig. 3. The following capabilities are provided.

1. Choice of Frequency Response, Random Analysis, or Transient (by Fourier Transform) Analysis is provided. A transient analysis is obtained by supplying transient load and time step data. Frequency lists are required for all methods.
2. Loading by either specified loads or a gust (Doublet-Lattice Theory only) can be chosen.
3. Either times or frequencies for recovery of physical data can be selected.
4. The modal participation type of data recovery is used. The internal loads or stresses are found in each mode and the response loads are found from the linear combination of the products of the loads in each mode and its amplitude. This method of internal load response calculation is called the "mode displacement method" in Ref. 16, pp. 641-650.
5. Output can be displacements, stresses, or constraint forces. Both undeformed structure and XY-plots are available. Aerodynamic data (pressures) are also available with the frequency response analysis.
6. Random analysis obtains power spectral density, root mean square response, and mean frequency of zero crossings.

#### Flutter Methods

Flutter analysis determines the dynamic stability of the aeroelastic system. It may be solved for subsonic or supersonic flows by merely substituting the appropriate aerodynamic formulation. For the linear case assumed, the solution involves a series of complex eigenvalue solutions.

The K-method of Flutter Solution. - The first flutter analysis method used in NASTRAN includes minor variations of the usual K-method. The variations are shown in the following equations. The basic modal equation is

$$[-M_{hh}\omega^2 + i\omega B_{hh} + (1+ig)K_{hh} - (\rho V^2/2)Q_{hh}(k,m)]\{u_h\} = 0 \quad (1)$$

In Eq. 1,  $M_{hh}$ ,  $B_{hh}$ , and  $K_{hh}$  are the generalized modal mass, damping, and stiffness matrices, respectively. They are usually diagonal. However, provision is made for the user to add structural changes without recomputing the modes through the DMIG feature of NASTRAN; thus,  $M_{hh}$  and  $K_{hh}$  need not be diagonal. We also note that  $K_{hh}$  is singular when rigid body modes are included. The matrix  $Q_{hh}(k,m)$  is a complex matrix of generalized aerodynamic modal forces and depends on the reduced frequency  $k (= \omega \bar{c}/2V)$  and the Mach number  $m$ . The remaining parameters in Eq. 1 are the circular frequency  $\omega$ , the required artificial structural damping  $g$ , the density  $\rho$ , the velocity  $V$ , the reference chord  $\bar{c}$ , and the vector of modal amplitudes  $\{u_h\}$ . If the approximation,  $1+ig \approx \sqrt{1+ig}$ , is utilized\* in the damping term, Eq. 1 can be rewritten to read

$$\left[ -[M_{hh} + \frac{\rho}{2}(\frac{\bar{c}}{2k})^2 Q_{hh}] \frac{\omega^2}{1+ig} + B_{hh} \frac{i\omega}{\sqrt{1+ig}} + K_{hh} \right] \{u_h\} = 0 \quad (2)$$

or

$$\left[ [ (2k/\bar{c})^2 M_{hh} + (\rho/2) Q_{hh} ] p^2 + (2k/\bar{c}) B_{hh} p + K_{hh} \right] \{u_h\} = 0 \quad (3)$$

where

$$p^2 = -V^2/(1+ig) \quad (4)$$

\*The approximation is exact at the flutter point,  $g = 0$ , and is similar to the approximation,  $1+i(g_a+g) \approx (1+ig_a)(1+ig)$ , used in variations of the K-method that account for different actual structural dampings  $g_a$  in each mode.

An approximation to the root of Eq. 4 for small  $g$  is

$$p \approx V\left(\frac{g}{2} + i\right) \quad (5)$$

and is exact at the flutter point, i.e., where  $g = 0$ . From Eq. 5 we have

$$V = \text{Im}(p) \quad (6)$$

$$g = 2\text{Re}(p)/\text{Im}(p) \quad (7)$$

The flutter analysis is based on a series of values of  $m$ ,  $k$ , and  $\rho$  that are supplied by the user. The complex eigenvalue problem of Eq. 3 is solved by the QR-transform method of Ref. 5, as automated in the subroutine ALLMAT (Ref. 6) and modified for NASTRAN. As a preliminary step, Eq. 3 is put into the canonical form

$$[A - \lambda I]\{u\} = 0 \quad (8)$$

where

$$[A] = \begin{bmatrix} 0 & I \\ -[(2k/\bar{c})^2 M_{hh} + (\rho/2)Q_{hh}]^{-1}K_{hh} & -[(2k/\bar{c})^2 M_{hh} + (\rho/2)Q_{hh}]^{-1}(2k/\bar{c})B_{hh} \end{bmatrix} \quad (9)$$

Then

$$p = \lambda^{1/2} \quad (10)$$

where the square root with the positive imaginary part is chosen. The velocity and damping for each root are computed from Eqs. 6 and 7. The frequency of each root is given by

$$f = \omega/2\pi = kV/\pi\bar{c} \quad (11)$$



Flutter occurs when the required artificial damping is positive, i.e., when  $g > 0$  the system is unstable; the flutter speed is the lowest value of  $V$  for which  $g = 0$ .

The primary difference between the above NASTRAN algorithm for the K-method of flutter analysis and the usual K-method is that the mass matrix rather than the stiffness matrix is inverted; secondary differences appear in the approximation of Eq. 5. An advantage of the present formulation is that the user can specify  $k = 0$  and solve divergence problems for constrained systems.

As the flow chart for modal flutter analysis (Fig. 2) shows, the K-method of flutter analysis is a looping procedure. The values of  $V$ ,  $g$ , and  $f$  are solved for various values of  $k$ ,  $m$ , and  $\rho$ . Plots of  $V$  versus  $g$  can be used to determine flutter (when  $g$  goes through zero to positive values).

The KE-method of Flutter Solution. — A more efficient K-method of flutter analysis is possible if the analyst is willing to neglect viscous damping from all sources, e.g., from the structure or a control system, and to restrict his solution to eigenvalues and not require eigenvectors. Then, many of the operations can be done in-core with a consequent increase in efficiency. This efficient K-method algorithm is called the KE-method. With this increase in efficiency, a greater number of points on a flutter stability curve can be obtained for a given cost, and cases with poorly behaved stability curves can be studied more thoroughly. This method gives results similar to those of Ref. 7.

In order to sort the roots so that curves can be drawn, the roots must be ordered. For the first value of  $k$ , the roots are accepted in the order output by the eigenvalue subroutine ALIMAT. If we denote the  $i$ th eigenvalue for the  $n^{\text{th}}$  reduced frequency  $k_n$  by  $p_{i,n}$ , we may define an extrapolated eigenvalue as

$$p_{i,n}^{(c)} = p_{i,n-1} + (k_n - k_{n-1})(p_{i,n-1} - p_{i,n-2})/(k_{n-1} - k_{n-2}) \quad (12)$$

$$n = 2, 3, 4, \dots$$

in which  $p_{i,0}$  is chosen equal to  $p_{i,1}$ . Then the  $p_{i,n}$  are ordered according to closeness to  $p_{i,n}^{(e)}$  where the "closeness" is measured by a minimum value of

$$[\operatorname{Re}(p_{i,n}^{(e)} - p_{i,n})]^2 + [\operatorname{Im}(p_{i,n}^{(e)} - p_{i,n})]^2 \quad (13)$$

The PK-method of Flutter Solution. — The PK-method of flutter analysis follows the "lined-up" British method as described in Refs. 8 and 9, rather than the procedure suggested in Ref. 10. The equation to be solved for the modal amplitudes  $\{u_h\}$  is real and appears as

$$[Mp^2 + Bp + K]\{u_h\} = 0 \quad (14)$$

where the real mass matrix  $[M]$  is

$$[M] = [M_{hh}] \quad (15)$$

The real damping matrix  $[B]$  includes both the (equivalent viscous) structural damping and the aerodynamic damping

$$[B] = [B_{hh}] - (\frac{1}{4})\rho\tilde{c}V[Q_{hh}^I(k)/k] \quad (16)$$

and the real stiffness matrix  $[K]$  includes both structural and aerodynamic stiffness

$$[K] = [K_{hh}] - (\frac{1}{2})\rho V^2[Q_{hh}^R(k)] \quad (17)$$

in which  $[Q_{hh}^R(k)]$  and  $[Q_{hh}^I(k)]$  are the real and imaginary parts of the aerodynamic generalized force coefficient matrices, respectively, and the reduced frequency  $k$  is found from the eigenvalue  $p$  as

$$k = (\tilde{c}/2V)\operatorname{Im}(p) \quad (18)$$

The subroutines for real unsymmetric matrices discussed below will solve the flutter problem formulated as

$$[A - pI]\{\bar{u}_h\} = 0 \quad (19)$$

where

$$[A] = \begin{bmatrix} 0 & I \\ -M^{-1}K & -M^{-1}B \end{bmatrix} \quad (20)$$

and  $\{\bar{u}_h\}$  includes both the modal amplitudes and velocities. The eigenvalues of the real matrix  $[A]$  are either real and separate or equal, or complex conjugate pairs. Real roots indicate a convergence or divergence as in the cases of the spiral lateral-directional (rigid body) mode or a structural (torsional) divergence mode. For the real roots, the damping coefficient is related to the time or distance to half (or double) amplitude and is defined by

$$\gamma = (\bar{c}/V \ln 2) \operatorname{Re}(p) \quad (21)$$

The majority of the eigenvalues will be complex conjugate pairs. We denote a pair of complex conjugate roots as

$$p = \omega(\gamma \pm i) \quad (22)$$

where  $\omega$  is a damped system frequency and  $\gamma$  is the amplification rate coefficient. The oscillatory solutions of Eq. 14 require an iterative solution so that Eq. 18 is satisfied along with Eq. 14. The rigid body spiral root or the static structural divergence roots require no iteration but are found by setting  $k = 0$ . The oscillatory rigid body (i.e., short-period or Dutch-roll) roots and oscillatory structural roots will be found from the following algorithm. This algorithm is based on a desire for capability to determine stability

at a given speed independently of the stability at higher or lower speeds, and the observation of British experience that the reduced frequency is a secondary parameter in flutter analysis.

The algorithm begins with the given velocity  $V$  and choosing  $k = 0$ . (Note that  $k = 0$  does not lead only to static aerodynamic forces but also to a very low frequency estimate of the aerodynamic damping forces.) The eigenvalue calculation leads to all of the real and complex roots. The real roots (if any) are correct, but the complex roots do not satisfy Eq. 18. Let the complex pairs of eigenvalues be denoted by

$$p_{rs}^{(j)} = \omega_{rs}^{(j)} (\gamma_{rs}^{(j)} \pm i) \quad (23)$$

so that the next estimate of the (nonzero) reduced frequency is

$$k_s^{(j)} = \omega_{ss}^{(j)} \bar{c} / 2V \quad (24)$$

where  $r$  denotes the oscillatory mode number ordered by frequency ( $\omega_{1s} < \omega_{2s} < \dots$ ),  $s$  denotes the number of the oscillatory modes under investigation, and  $j$  denotes the iteration (eigenvalue solution) number. Iteration converges when

$$|k_s^{(j)} - k_s^{(j-1)}| < \epsilon \quad (25)$$

for which the default value is chosen as  $\epsilon = 0.001$ . Let the converged complex eigenvalues be

$$p_{rs}^{(c)} = \omega_{rs}^{(c)} (\gamma_{rs}^{(c)} \pm i) \quad (26)$$

where only  $p_{ss}^{(c)}$  satisfies both Eqs. 14 and 18. We continue to investigate the next oscillatory mode by increasing  $s$  by one. The initial estimate of the reduced frequency is

$$k_s^{(0)} = \omega_{s,s-1}^{(c)} \bar{c}/2V \quad (27)$$

and the iteration proceeds in the sequence of Eqs. 23 and 24 until convergence, Eq. 25, is again satisfied. Equations 26 and 27 begin the determination of the next oscillatory mode if the next higher mode is of interest. When all modes of interest have been determined, the solution for the given velocity is finished. The logical flow diagram for the above algorithm is shown in Fig. 4.

The complete flutter analysis by the British method requires a consideration of variations in altitude,  $h$  (i.e., density  $\rho$ ), Mach number,  $m$ , and velocity,  $V$ . Altitude, Mach number, and velocity are not independent parameters in a standard atmosphere but may be regarded as independent if compressibility effects are secondary, e.g.,  $m = 0$  is representative of compressibility effects for  $0 < m < 0.4$  or  $0.5$ . Velocity and Mach number should be considered as a user input pair, i.e., each value of  $V$  has its associated value of  $m$ . The complete flutter analysis flow diagram is shown in Fig. 5.

The principal advantage of the PK-method over the K-method (or KE-method) is that it produces results directly for given values of Mach number (or speed), whereas the other methods require iteration. In addition, the damping given by  $\gamma_{ss}^{(c)}$  in Eq. 26 is a better physical approximation of the decay rate than the artificial parameter  $g$  in Eq. 7.

The eigenvalues of Eq. 19 are also obtained by the QR-transform method of Ref. 5 but now use the algorithms of Ref. 11 for the real cases which have been automated in the subroutines HSBG (Ref. 12) and ATEIG (Ref. 13) and modified for NASTRAN. The subroutine HSBG reduces the matrix to the upper Hessenberg form, and subroutine ATEIG obtains the real or complex conjugate eigenvalues by the Double QR-Transformation method which retains entirely real arithmetic operations and obtains complex conjugate eigenvalues two at a time.

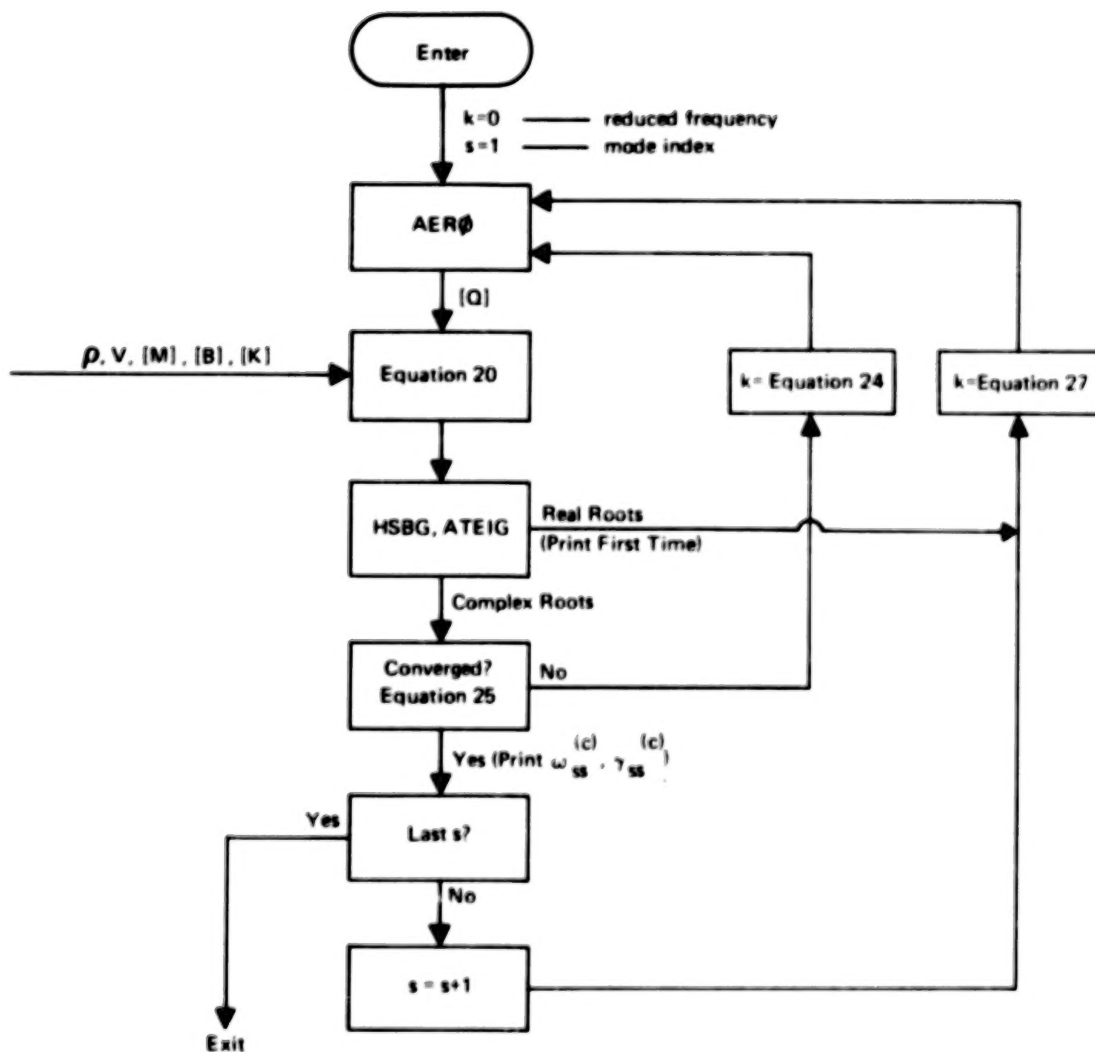


Figure 4. Basic Flow Diagram for PK-Flutter Method.

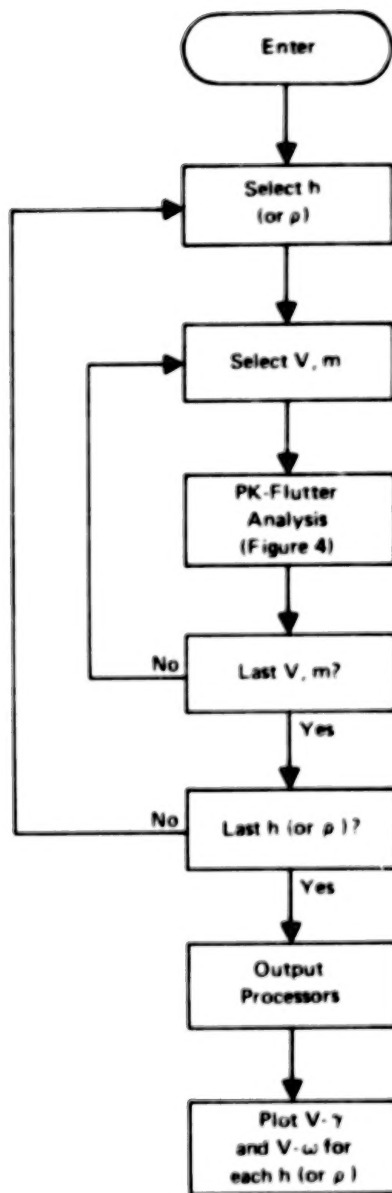


Figure 5. Complete Flow Diagram for PK-Flutter Analysis.

When requested, the eigenvectors are found in two iterations by the inverse power method with shifts (Ref. 14, p. 323 and pp. 626-628) using the subroutine EGNVCT. The subroutine EGNVCT finds the eigenvector  $\{u\}$  from the complex matrix  $[A]$  and the complex eigenvalue  $\lambda$  by solving the equation

$$[A - \lambda I]\{u\} = 0 \quad (28)$$

NASTRAN utilizes the subroutine by setting

$$\lambda = 0 \quad (29)$$

and

$$[A] = [Mp^2 + Bp + K] \quad (30)$$

in Eq. 28 in order to obtain the canonical form.

#### Frequency Response and Random Analysis

The ability to calculate the response of a system to steady sinusoidal excitation is important both because such excitation frequently exists in nature and because mathematical methods for solving other problems often require knowledge of the frequency response. The latter category of problems includes stability analysis (via Nyquist diagrams or Bode plots), random response analysis, and transient response analysis (via Fourier or Laplace transforms).

Frequency Response. — Figure 6 shows a simplified flow diagram for the frequency response module. The calculations are of two kinds: the generation of loads, and the solution of the dynamic equations to obtain a displacement response vector. Subsequent data reduction procedures are discussed in Sections 9.1 and 9.4 of Ref. 1.

In static analysis, a number of automatic load generating subroutines (gravity load, pressure load, temperature-induced load, etc.) are employed in order to simplify the user's task of input data preparation. Similar



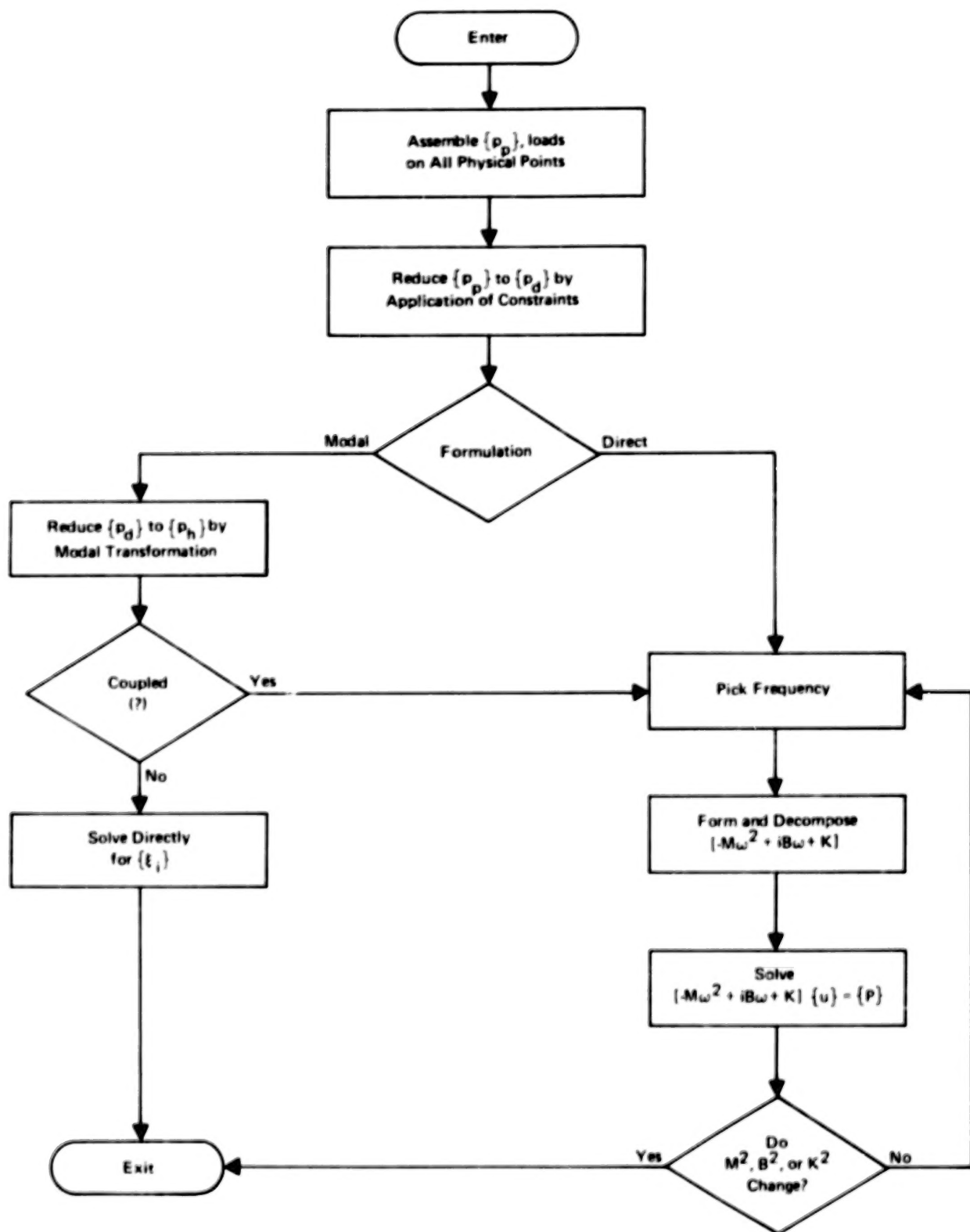


Figure 6. Flow Diagram for Frequency Response Module (FRRD).

schemes have not been made available for dynamic analysis, mainly because of the great variety in the possible sources of dynamic loads. All that is done in frequency response analysis, and perhaps all that should be done, is to provide the user with a flexible input data format which allows for a varying degree of generality vs. simplicity.

The generation of dynamic loads can, at least in principle, be a formidable task. The most general form of loading in frequency response analysis is one that varies arbitrarily in magnitude and phase with respect to the point of load application and with respect to frequency. Even for a problem of moderate size (e.g., 200 degrees of freedom and 50 frequencies), the data set required to specify a general loading is large (e.g.,  $200 \times 50 = 10,000$  entries). Thus it is desirable to have input data forms that accommodate special cases.

In NASTRAN, the dynamic load vector that is used in a specific subcase,  $\{p_j^c\}$ , is constructed as a combination of component load sets,  $\{p_j^k\}$ .

$$\{p_j^c(\omega)\} = \sum_k S_{ck} \{p_j^k(\omega)\} \quad (31)$$

where  $S_{ck}$  is a factor that gives the proportion of component load set  $k$  used in combined load set  $c$ . The advantage of this system is that it facilitates the examination of different combinations of loads from different sources. The form provided for specifying a component load set is

$$\{p_j^k(\omega)\} = \{A_{jk} e^{i(\theta_{jk} - \omega \tau_{jk})}\} \cdot G_k(\omega) \quad (32)$$

where  $A_{jk}$ ,  $\theta_{jk}$ , and  $\tau_{jk}$  are tabulated coefficients that may be different for each degree of freedom ( $j$ ).  $G_k(\omega)$  is a tabulated complex function of frequency (with two alternate forms) that is linearly interpolated to the frequencies,  $\omega_i$ , at which solutions are requested. The form provided by Eq. 32 is most useful for loads due to traveling waves (in air, in water, or underground). A meaningful interpretation of the symbols of Eq. 32 for such problems is

that  $G_k(\omega)$  is the pressure produced by the wave, that  $A_{jk}$  is the exposed area associated with the  $j$ th degree of freedom, and that  $\tau_{jk}$  is the transit time required for the wave to reach the  $j$ th degree of freedom.

The coefficients  $A_{jk}$ ,  $\theta_{jk}$ , and  $\tau_{jk}$  are tabulated separately and one list of coefficients may be referenced by several load sets. Complete generality can be obtained with Eqs. 31 and 32 by identifying each load set with a specified frequency, i.e., by specifying

$$\left. \begin{aligned} G_k(\omega) &= 1, \quad \omega = \omega_k \\ G_k(\omega) &= 0, \quad \omega \neq \omega_k \end{aligned} \right\} \quad (33)$$

The loads are referred by the user to the displacement set,  $u_p$ , that includes all physical points (structural points,  $u_g$ , and extra points,  $u_e$ ). The reduction to final form consists of applying single and multipoint constraints, the Guyan reduction (Ref. 15), and in the case of a modal formulation, the transformation to modal coordinates. Except for the modal transformation, the steps are identical to those for the reduction of static loads to final form described in Section 3.6.2 of Ref. 1. The loads on extra points are simply included in their proper sequence in each intermediate vector. The specific operations are

1. Partition  $P_p$  into  $P_m$ , the loads on points eliminated by multipoint constraints, and  $\bar{P}_n$ .

$$P_p = \begin{Bmatrix} \bar{P}_n \\ -\bar{P}_m \end{Bmatrix} \quad (34)$$

2. Apply multipoint constraints.

$$\{P_m\} = \{\bar{P}_n\} + [G_m]^T \{P_m\} \quad (35)$$

3. Partition  $P_n$  into  $P_s$ , the loads on points eliminated by single point constraints, and  $P_f$ .

$$\{P_n\} = \begin{Bmatrix} P_f \\ \bar{P}_s \end{Bmatrix} \quad (36)$$

4. Partition  $P_f$  into  $P_o$ , the loads on points eliminated by the Guyan reduction, and  $\bar{P}_d$ .

$$\{P_f\} = \begin{Bmatrix} \bar{P}_d \\ P_o \end{Bmatrix} \quad (37)$$

5. Apply the Guyan reduction.

$$\{P_d\} = \{\bar{P}_d\} + [G_o]^T \{P_o\} \quad (38)$$

6. For a modal problem formulation only, transform  $P_d$  to the modal coordinates  $u_h$  (see Section 9.3 of Ref. 1).

$$\{P_h\} = [\phi_{dh}]^T \{P_d\} \quad (39)$$

The above operations can be time consuming if there is a large number of load vectors to be transformed. If the vector of time constants,  $\tau_{jk}$ , in Eq. 32 is null, the relative magnitudes and phases of the loads at different grid points are independent of frequency. In that event, the load transformation is applied once for each load set to the complex coefficients,  $B_{jk} = A_{jk} e^{i\theta_{jk}}$ , before the transformed load sets are combined. If  $\tau_{jk}$  is not null for every load set in a particular combined load,  $\{P_p^c\}$ , the reduction procedure is applied to the combined load for each frequency.

For a direct formulation, the equation to be solved is

$$[-\omega^2 M_{dd} + i\omega B_{dd} + K_{dd}]\{u_d\} = \{P_d\} \quad (40)$$

while for a general modal formulation, including direct (nonstructural) input, the equation is

$$[-\omega^2 M_{hh} + i\omega B_{hh} + K_{hh}]\{u_h\} = \{P_h\} \quad (41)$$

The direct input matrices  $[M_{dd}^2]$ ,  $[B_{dd}^2]$ , and  $[K_{dd}^2]$  (see Section 9.3.3 of Ref. 1) are permitted to be dependent on frequency. If they are, an exit is made to the dynamic matrix assembler, GKAD, after each frequency (see Fig. 1). The user can request solutions for a specified list of frequencies, or he can request a uniform or a logarithmic distribution of frequencies in a specified range. The selection of zero as a frequency permits the user to solve static problems with nonstructural,  $[K_{dd}^2]$ , terms.

The standard matrix decomposition and solution routines provided with the program are used in the solution of Eqs. 40 and 41. The options available include single and double precision (selection is based upon the machine) and with row interchanges (partial pivoting) or without pivoting.

If, in a modal formulation, there is no direct input, i.e., if  $[M_{dd}^2] = [B_{dd}^2] = [K_{dd}^2] = 0$ , and no aerodynamic matrices, the equations are uncoupled and a separate procedure is used as indicated in Fig. 6. The solution for the modal coordinates is simply

$$\{\xi_i\} = \left\{ \frac{P_i}{-m_i \omega^2 + i b_i \omega + k_i} \right\} \quad (42)$$

where  $m_i$ ,  $b_i$ , and  $k_i$  are the generalized mass, damping, and stiffness of the  $i$ th mode (see Section 9.3.4 of Ref. 1), and  $P_i$  is the  $i$ th component of  $\{P_h\}$ .

The evaluation of Eq. 42 is trivial compared to the solution of Eq. 40. It is not true, however, that a modal formulation of an uncoupled problem is always more efficient than a direct formulation, since it is first necessary to calculate the modes and to transform the loads and then, afterwards, to obtain physical coordinates from  $\xi_i$  by the modal transformation. The question of whether the modal approach is more efficient for any given problem depends on several factors, including the number of modes, the number of response frequencies, the bandwidth of the problem when formulated directly, and the presence or absence of nonstructural coupling.

The results obtained by the Frequency Response module are passed to the Dynamic Data Recovery module for further processing and thence to other modules in the data recovery chain, see Fig. 1, Section 9.1, Ref. 1. The results that may be requested in either printed or plotted form include the components of displacement, acceleration and velocity, components of applied loads, and selected internal forces and stresses. The printed information may be sorted by frequency or by component. The plotted information consists of the magnitude and phase angle of any component plotted versus frequency. The magnitude scale is either linear or logarithmic and the frequency scale is either linear or logarithmic.

Random Analysis. — The application of frequency response techniques to the analysis of random processes requires that the system be linear and that the excitation be stationary with respect to time. The theory includes a few important theorems which will be reviewed.

An important quantity in random analysis theory is the autocorrelation function,  $R_j(\tau)$ , of a physical variable,  $u_j$ , which is defined by

$$R_j(\tau) = \lim_{T \rightarrow \infty} \frac{1}{T} \int_0^T u_j(t) u_j(t-\tau) dt \quad (43)$$

Note that  $R_j(0)$  is the time average value of  $u_j^2$ , which is an important quantity in the analysis of structural failure. The power spectral density  $S_j(\omega)$  of  $u_j$  is defined by

$$S_j(\omega) = \lim_{T \rightarrow \infty} \frac{2}{T} \left| \int_0^T e^{-i\omega t} u_j(t) dt \right|^2 \quad (44)$$

It may be shown (using the theory of Fourier integrals) that the autocorrelation function and the power spectral density are Fourier transforms of each other. Thus\*

$$R_j(\tau) = \frac{1}{2\pi} \int_0^\infty S_j(\omega) \cos(\omega\tau) d\omega \quad (45)$$

from which follows the mean-square theorem

$$\bar{u}_j^2 = R_j(0) = \frac{1}{2\pi} \int_0^\infty S_j(\omega) d\omega \quad (46)$$

The expected value of the number of zero crossings with positive slope per unit time, or mean frequency, is a quantity of interest for fatigue analysis, airplane design for gusts, etc. This mean frequency,  $N_0$ , can be found from the power spectral density:

$$N_0^2 = \frac{\left( \int_0^\infty (\omega/2\pi)^2 S_j(\omega) d\omega \right)}{\left( \int_0^\infty S_j(\omega) d\omega \right)} \quad (47)$$

The mean frequency,  $N_0$ , is thus the root mean square frequency, where the power spectral density is used as a weighting function.

---

\*The factor  $\frac{1}{2\pi}$  in Eq. 45 is omitted by some authors, or is sometimes replaced by other factors. The value of the factor depends on the definition of  $S_j(\omega)$ , Eq. 44.

The transfer function theorem (see, e.g., Ref. 16) states that if  $H_{ja}(\omega)$  is the frequency response of any physical variable,  $u_j$ , due to an excitation source,  $Q_a$ , which may be a point force, a loading condition, or some other form of excitation, i.e., if

$$u_j(\omega) = H_{ja}(\omega) \cdot Q_a(\omega) \quad (48)$$

where  $u_j(\omega)$  and  $Q_a(\omega)$  are the Fourier transforms of  $u_j$  and  $Q_a$ , then the power spectral density of the response,  $S_j(\omega)$ , is related to the power spectral density of the source,  $S_a(\omega)$ , by

$$S_j(\omega) = |H_{ja}(\omega)|^2 \cdot S_a(\omega) \quad (49)$$

Equation 49 is an important result because it allows the statistical properties (e.g., the autocorrelation function) of the response of a system to random excitation to be evaluated via the techniques of frequency response. Another useful result is that, if sources  $Q_1, Q_2, Q_3$ , etc., are statistically independent, i.e., if the cross-correlation function between any pair of sources

$$R_{ab}(\tau) = \lim_{T \rightarrow \infty} \frac{1}{T} \int_0^T Q_a(t) Q_b(t-\tau) dt \quad (50)$$

is null, then the power spectral density of the total response is equal to the sum of the power spectral densities of the responses due to individual sources. Thus,

$$S_j(\omega) = \sum_a S_{ja}(\omega) = \sum_a |H_{ja}(\omega)|^2 S_a(\omega) \quad (51)$$



If the sources are statistically correlated, the degree of correlation can be expressed by a cross-spectral density,  $S_{ab}$ , and the spectral density of the response may be evaluated from

$$S_j = \sum_a \sum_b H_{ja} H_{jb}^* S_{ab} \quad (52)$$

where  $H_{jb}^*$  is the complex conjugate of  $H_{jb}$ .

In applying the theory, it is not necessary to consider the sources to be forces at individual points. An ensemble of applied forces that is completely correlated (i.e., a loading condition) may also be treated as a source. For example, a plane pressure wave from a specified direction may be treated as a source. Furthermore, the response may be any physical variable including internal forces and stresses as well as displacements, velocities and accelerations.

In NASTRAN, Random Analysis is treated as a data reduction procedure that is applied to the results of a Frequency Response analysis. The Frequency Response analysis is performed for loading conditions,  $\{P_a\}$ , at a sequence of frequencies,  $\omega_i$ . Normal reduction procedures are applied to the output of the frequency response analysis module (see Fig. 1, Section 9.1 of Ref. 1), resulting in a set of output quantities,  $u_j$ . The calculation of power spectral densities and autocorrelation functions for the output quantities is performed in the Random Analysis module.

Figure 7 is a simplified flow diagram for the Random Analysis module. The inputs to the module are the frequency responses,  $H_{ja}(\omega_i)$ , of quantities  $u_j$  to loading conditions  $\{P_a\}$  at frequencies  $\omega_i$ , and the auto- and cross-spectral densities of the loading conditions,  $S_a$  and  $S_{ab}$ . The response quantities,  $u_j$ , may be displacements, velocities, accelerations, internal forces, or stresses. The power spectral densities of the response quantities are calculated by Eq. 52 or by Eq. 49, depending on whether the loading conditions are correlated or uncorrelated. At the user's option, the spectral densities due to all sources, considered independent, may be combined by means of Eq. 51.

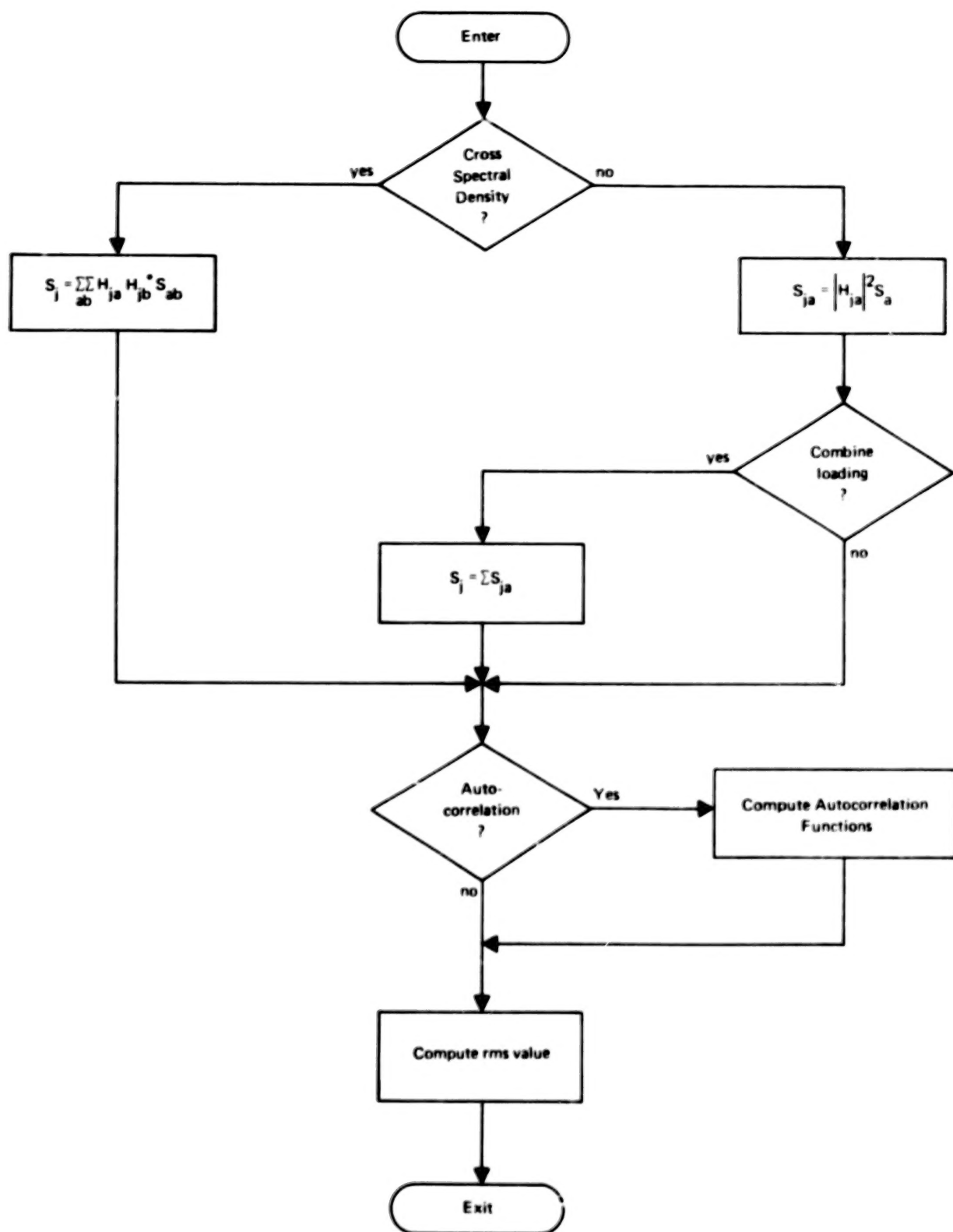


Figure 7. Flow Diagram for Random Analysis Module (RANDOM).

The autocorrelation function is computed by the following approximation to Eq. 45.

$$R_j(\tau) = \frac{1}{2\pi\tau} \sum_{i=1}^{N-1} \left\{ \frac{S_j(\omega_{i+1}) - S_j(\omega_i)}{(\omega_{i+1} - \omega_i)\tau} [\cos(\omega_{i+1}\tau) - \cos(\omega_i\tau)] + S_j(\omega_{i+1}) \sin(\omega_{i+1}\tau) - S_j(\omega_i) \sin(\omega_i\tau) \right\} \quad (53)$$

which assumes that  $S_j(\omega)$  varies linearly between  $\omega_i$  and  $\omega_{i+1}$ . The user specifies the sequence of values of  $\tau$ . The rms value of the response,  $\bar{u}_j$ , is evaluated as the square root of a trapezoidal approximation to Eq. 46, i.e.,

$$\bar{u}_j = \left[ \frac{1}{4\pi} \sum_{i=1}^{N-1} [S_j(\omega_{i+1}) + S_j(\omega_i)] (\omega_{i+1} - \omega_i) \right]^{1/2} \quad (54)$$

The mean frequency,  $N_0$ , is also evaluated from a trapezoidal curve for  $S_j(\omega)$

$$N_0 = \bar{r}_j / \bar{u}_j \quad (55)$$

where

$$\bar{r}_j = \left[ \sum_{i=1}^{N-1} (\alpha S_j(\omega_i) + \beta S_j(\omega_{i+1})) (\omega_{i+1} - \omega_i) \right]^{1/2} \quad (56)$$

$$\alpha = (3\omega_i^2 + 2\omega_i\omega_{i+1} + \omega_{i+1}^2)/96\pi^3 \quad (57)$$

$$\beta = (\omega_i^2 + 2\omega_i\omega_{i+1} + 3\omega_{i+1}^2)/96\pi^3 \quad (58)$$

The power spectral densities,  $S_j$ , are plotted versus frequency and the autocorrelation functions,  $R_j(\tau)$ , are plotted versus the time delay,  $\tau$ , at the user's request.

Cross-correlations and cross-spectral densities between different output quantities are not calculated.

The measured power spectral density function for atmospheric turbulence has been fitted with analytic functions by several authors. Two of the commonly used functions are those of Dryden and Von Kármán (see, e.g., Ref. 17). They can both be expressed by the equation,

$$S_a(\omega) = \frac{2W_g^2(L/U) [1+2(p+1)(kL\omega/U)^2]}{[1+(kL\omega/U)^2]^{p+3/2}} \quad (59)$$

where

$S_a(\omega)$  = power spectral density (per Hz),

$W_g$  = rms gust velocity,

$\omega$  = radian frequency,

$L$  = scale of turbulence (length units),

$U$  = airplane velocity (velocity units).

The values of the constant parameters  $k$  and  $p$  are given in the following table.

	Dryden	Von Kármán
$k$	1.0	1.339
$p$	1/2	1/3

A special data card (TABRNDG) is used to select this analytic form in NASTRAN. The user supplies  $W_g$ ,  $L$  and  $U$ , and selects either the Dryden or the Von Kármán parameters.

## Transient Analysis by the Fourier Transform Method

Figure 8 shows a simplified flow diagram for the basic NASTRAN transient analysis module. The equations that are solved by the module may be expressed in terms of physical coordinates,  $u_d$ , or in terms of augmented modal coordinates,  $u_h$ . If, in a modal formulation, there is no direct matrix input, and if there are no nonlinear terms, the equations of motion for the individual modal coordinates are uncoupled and the equations may be integrated by analytical rather than strictly numerical methods. When the equations are coupled, they are solved by a relatively simple numerical integration algorithm that has been developed to meet the requirements of structural analysis; see Section 11.3 of Ref. 1. The results of the transient analysis module are the displacement vectors,  $\{u_d\}$  or  $\{u_h\}$ , and their first and second time derivatives. The final results, which also include internal forces and stresses, are printed and/or plotted versus time. In addition, for a list of times provided by the user, structural displacements may be superimposed on a plot of the undeformed structure; see Section 13 of Ref. 1.

A different method to integrate the equations of motion is used for aeroelastic response problems. Aerodynamic matrices are usually known only in the frequency domain, which does not permit direct integration. A Fourier method is used in which applied loads are transformed to the frequency domain. Frequency **responses** computed by this method are then transformed back to the time domain. This section presents the new theory which is used in NASTRAN for aeroelastic transient response analysis.

Transient Analysis by the Fourier Method. — Transient analysis by a Fourier transformation is separated into three phases. First, the loads (defined as a function of time) are transformed into the frequency domain. Second, the responses are computed in the frequency domain. Third, the responses (in the frequency domain) are transformed back to the time domain.

Two forms of the transform are considered, the Fourier series and the Fourier integral, which are discussed below. Both methods must be implemented numerically which introduces approximations. The inverse transform includes an infinite sum, for which only a finite number of terms are numerically

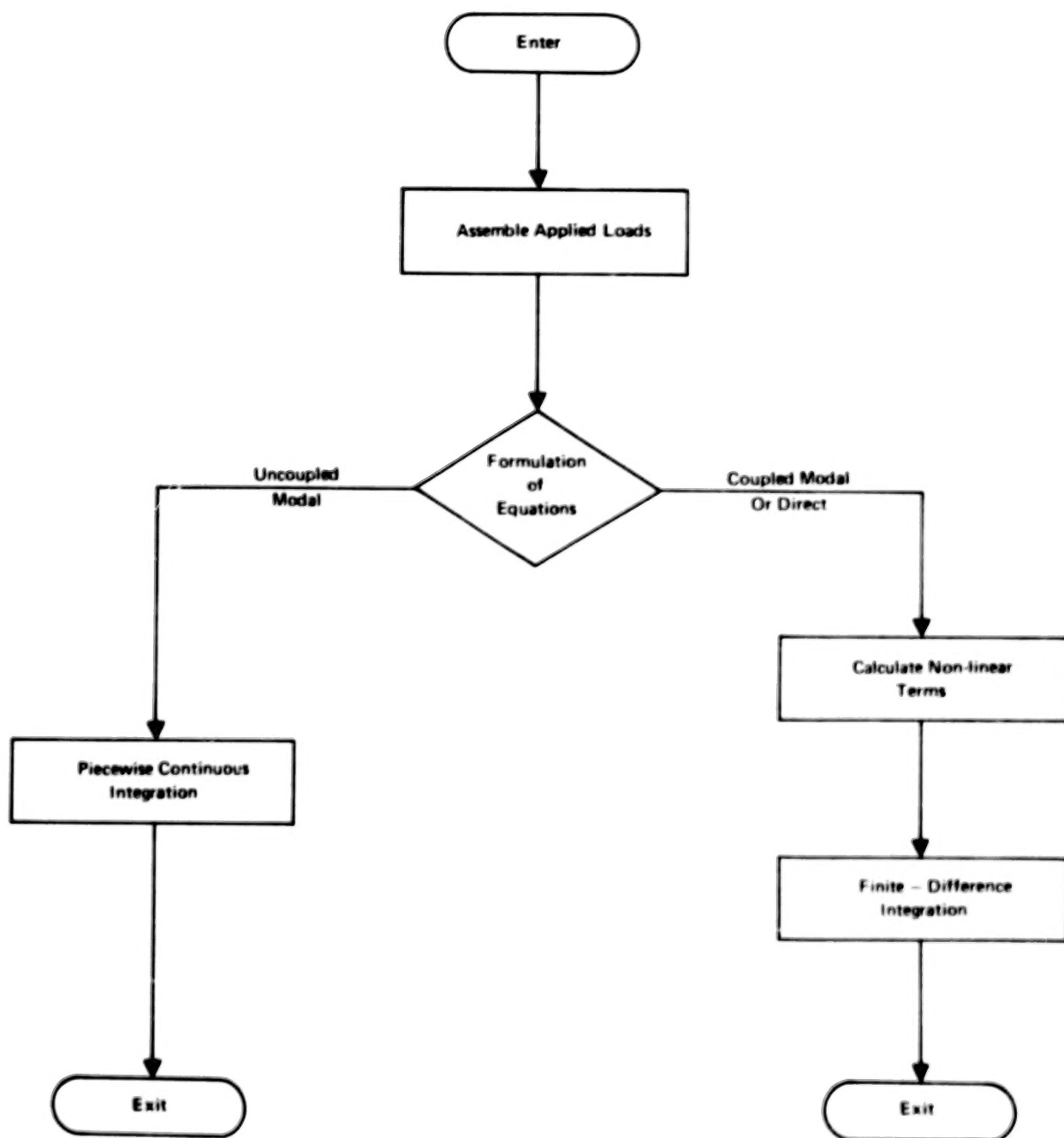


Figure 8. Simplified Flow Diagram for Transient Analysis Module, (TRD)

evaluated. This approximation leads to truncation errors. The inverse Fourier integral must be numerically integrated, which leads to integration errors. The number of frequencies at which the integrand is evaluated is limited by cost considerations. The following definitions provide the basis for the Fourier transformation.

#### A. The Fourier Series

The basic time interval is  $0 < t < T$  with the function periodic. The circular frequencies are given by

$$\omega_n = 2\pi n \Delta f \quad (60)$$

$$\Delta f = 1/T \quad (61)$$

The load transformation for a load at point a is

$$\tilde{P}_a(\omega_n) = \int_0^T P_a(t) e^{-i\omega_n t} dt \quad (62)$$

The response at point j is given by

$$\tilde{u}_j(\omega_n) = H_{ja}(\omega_n) \tilde{P}_a(\omega_n) \quad (63)$$

The response in the time domain is

$$u_j(t) = (\Delta\omega/\pi) \left[ (1/2)u(0) + \sum_{n=1}^{\infty} \text{Re}(\tilde{u}(\omega_n) e^{i\omega_n t}) \right] \quad (64)$$

where Re denotes the "real part of ( )."

## B. The Fourier Integral

This is the limit at  $T \rightarrow \infty$ ,  $\Delta f \rightarrow 0$ ,  $2\pi n\Delta f \rightarrow \omega$ , of the Fourier series. Here,  $\omega$  is a continuous variable.

$$\tilde{p}_a(\omega) = \int_0^{\infty} p_a(t) e^{-i\omega t} dt \quad (65)$$

$$\tilde{u}_j(\omega) = H_{ja}(\omega) \tilde{p}_a(\omega) \quad (66)$$

$$u_j(t) = (1/\pi) \int_0^{\infty} \text{Re}(\tilde{u}(\omega) e^{i\omega t}) d\omega \quad (67)$$

Transformation of Loads. -- The user specifies loads in two general forms which are the tabular form (Eq. 3, Sec. 11-1, Ref. 1) (piecewise linear), and the general purpose function (Eqs. 4 and 5, Sec. 11-1, Ref. 1). The transformation is given by the Fourier integral of Eq. 65, in which it is assumed that the user defines a function which vanishes for  $t > T$ .

For piecewise linear tabular functions, a table of pairs  $(x_i, Y_i)$  ( $i = 1, N$ ) is prescribed, which defines  $N-1$  time intervals. In addition, an  $X1$  shift and an  $X2$  scale factor are allowed. Thus, the time-dependent load at point  $j$  is given by

$$p_j(t) = A_j Y_T \left( \frac{t - \tau_j - X1}{X2} \right) \quad (68)$$

$A_j$  and  $\tau_j$  are an amplitude factor and a delay which may depend upon the point which is loaded, and  $Y_T(x)$  is the linearly interpolated function from the table of pairs  $(x_i, Y_i)$ . The transformed load is

$$\tilde{p}_j(\omega) = A_j e^{-i\omega\tau_j} X2 \cdot \sum_{i=1}^{N-1} (x_{i+1} - x_i) (L_i Y_i + R_i Y_{i+1}) / 2 \quad (69)$$



where

$$L_i = e^{-i\omega(X1+X2x_i)} E_2(-i\omega X2(x_{i+1} - x_i)) \quad (70)$$

$$R_i = e^{-i\omega(X1+X2x_{i+1})} E_2(+i\omega X2(x_{i+1} - x_i)) \quad (71)$$

and

$$E_2(z) = \begin{cases} \frac{2}{z^2} (e^z - 1 - z) & \text{for large } z \\ 1 + \frac{z}{3} + \frac{z^2}{3 \cdot 4} + \dots & \text{for small } z \end{cases} \quad (72)$$

The general purpose function is defined by

$$P_j(\omega) = \begin{cases} A_j \tilde{t}^n e^{a\tilde{t}} \cos(2\pi f\tilde{t} + \phi), & 0 < \tilde{t} < T_2 - T_1 \\ 0, & \text{otherwise} \end{cases} \quad (73)$$

$$\tilde{t} = t - T_1 - \tau_j \quad (74)$$

The value of  $n$  is restricted to be an integer for transient analysis by the Fourier method. The transform is given by

$$\tilde{P}_j(\omega) = A_j e^{-i\omega\tau_j} (\kappa_2 + R_1) (T_2 - T_1)^{n+1/2(n+1)} \quad (75)$$

In Eq. 75,

$$R_2 = e^y E_{n+1}(z) \quad (76)$$

$$y = i\phi + (\alpha + i2\pi f)(T_2 - T_1) - i\omega T_2 \quad (77)$$

$$z = -[\alpha + i2\pi f - i\omega](T_2 - T_1) \quad (78)$$

$R_1$  is the same as  $R_2$  except the signs of  $\phi$  and  $f$  are reversed. Also,

$$E_K(z) = \begin{cases} \frac{K!}{z^K} \left( e^z - \sum_{k=0}^{k=K} \frac{z^k}{k!} \right) \\ \text{or} \\ 1 + \frac{z}{K+1} + \frac{z^2}{(K+1)(K+2)} + \frac{z^3}{(K+1)(K+2)(K+3)} + \dots \end{cases} \quad (79)$$

The second form is used for small values of  $z$ .

These loads, which appear in the form required for frequency response, are transformed to the modal coordinates exactly as in the modal frequency response method.

One other source of loads for aeroelastic problems is a one-dimensional gust. The same time dependencies are allowed as defined above; however, the amplitude  $A_j$  and delays  $\tau_j$  for the aerodynamic elements are computed from areas, dihedrals and coordinates in the flow direction.

Calculation of Frequency Response. — The responses are computed by the method for coupled equations (see Section 12.1 of Ref. 1), because in aeroelasticity, which is the principal area of **application**, the aerodynamic matrices cause modal coupling. The aerodynamic matrices are computed at a few frequencies, and automatically interpolated to the others for computational efficiency. For small problems, a special core-held equation solver is used to increase the efficiency.

Inverse Transformation of the Response. - The response is found from the numerical approximation of Eq. 67 or from the Fourier series result (Eq. 64) which can be thought of as a special form of approximation to the integral (Eq. 67). Three approximate methods have been coded to evaluate the inverse. In all cases, the quantity  $\tilde{u}(\omega)$  is first calculated at a set of frequencies,  $\omega_i$ , by the frequency response module. The frequencies do not need to be equally spaced. For all methods  $\tilde{u}(\omega)$  is set equal to zero outside the range of frequencies. The methods and control parameter IFTM are:

Method 0 - Approximates  $\tilde{u}(\omega)e^{i\omega t}$  as a constant in each interval. This method reduces to the Fourier series approximation, Eq. 64, for equal frequency intervals. IFTM = 0.

Method 1 - Fits  $\tilde{u}(\omega)$  with a piecewise linear function, and does not approximate  $e^{i\omega t}$ . IFTM = 1.

Method 2 - Fits  $\tilde{u}(\omega)$  with a cubic spline function, and does not approximate  $e^{i\omega t}$ . IFTM = 2.

Consider Method 2. Solving the "three-moment equations," the second derivatives  $\tilde{u}''(\omega)$  can be found at each  $\omega$  for which a frequency response has been computed. Then, in any interval  $\omega_i < \omega < \omega_{i+1}$

$$\tilde{u}(\omega) = [\tilde{u}(\omega_i) \cdot s + \tilde{u}(\omega_{i+1}) \cdot r] - [(\omega_{i+1} - \omega_i)^2 / 6] \cdot [\tilde{u}''(\omega_i)(s - s^3) + \tilde{u}''(\omega_{i+1})(r - r^3)] \quad (80)$$

where

$$\left. \begin{aligned} r &= (\omega - \omega_i) / (\omega_{i+1} - \omega_i) \\ s &= 1 - r \end{aligned} \right\} \quad (81)$$

Integrate Eq. 67, using Eq. 80 for  $\tilde{u}(\omega)$ , and sum over the intervals. Then collect the terms for each  $\omega_n$ , with the result

$$u(t) = (1/\pi) \sum_{n=1}^N \operatorname{Re}\{[C_n(t)\tilde{u}(\omega_n) + D_n(t)\tilde{u}''(\omega_n)]e^{i\omega_n t}\} \quad (82)$$

$$C_n(t) = \frac{\omega_n - \omega_{n-1}}{2} E_2(-it(\omega_n - \omega_{n-1})) + \frac{(\omega_{n+1} - \omega_n)}{2} E_2(it(\omega_{n+1} - \omega_n)) \quad (83)$$

$$D_n(t) = -\frac{(\omega_n - \omega_{n-1})^3}{24} G(it(\omega_n - \omega_{n-1})) - \frac{(\omega_{n+1} - \omega_n)^3}{24} G(it(\omega_{n+1} - \omega_n)) \quad (84)$$

For the first term in Eq. 82 ( $n=1$ ), use only the second terms on the right side of Eqs. 83 and 84. Also,

$$G(z) = 2E_2(z) - E_4(z) \quad (85)$$

where  $E_Y(z)$  is given by Eq. 79.

The above form for the inverse transform has two advantages. Numerical problems for small values of  $t\Delta\omega$  are efficiently evaluated by choosing the series form of Eq. 79. Also, the other two methods are easily derived as subcases. If  $\tilde{u}''$  terms are removed from Eq. 80, a piecewise linear fit remains; thus, Method 1 results are given by deleting  $\tilde{u}''$  from Eq. 82, i.e.,

$$u(t) = (1/\pi) \sum_{n=1}^N \operatorname{Re}\left[C_n(t)\tilde{u}(\omega_n)e^{i\omega_n t}\right] \quad (86)$$

with  $C_n$  defined by Eq. 83. Method 0 results if we replace  $E_2$  by 1.0 in Eq. 83.

The above procedure for Method 0 always multiplies the first and last term in the series by  $1/2$ . In order to force agreement with the Fourier series, which is the limiting case of equal frequency intervals, the first term in the series is multiplied by  $1/2$  only if the value of the first frequency is zero.

Other special considerations are given to the equal frequency interval case. If all intervals are equal, and the first frequency is an integer multiple of  $\Delta f$ , the time step  $\Delta t$  is adjusted to make  $\Delta f \cdot \Delta t = 1/\text{integer}$ , which reduces the number of distinct values of  $\sin \omega_n t$  and  $\cos \omega_n t$  used in Eq. 86. Also,  $C_n(t)$  and  $D_n(t)$  (Eqs. 83 and 84) become independent of  $n$  and do not need to be computed at every frequency.

Practical Considerations for Use of the Fourier Methods. — Some important practical considerations must be observed to use these methods successfully. To illustrate one problem, consider the response of a simple damped oscillator to a pulse (Fig. 9). The upper three curves show the pulse and the response of the system if it is very stable and then marginally stable. Using the Fourier method, the pulse is replaced by a series of pulses with period  $1/\Delta f$ . As can be seen, this gives good results if the system is very stable, but an incorrect impression if the system is marginally stable. Thus, in order for the results of the Fourier method to be valid:

- The system should be stable;
- The forcing functions should be zero for some time interval to allow decay; and
- The frequency interval  $\Delta f \leq 1/(T_{\text{pulse}} + T_{\text{decay}})$ .

If the system has unstable modes, these will appear as a precursor before the pulse, just like a "stable mode in the reverse time." In general, Methods 1 and 2 are more accurate than Method 0. However, these methods introduce positive artificial damping into the result, which may lead to erroneous conclusions in stability studies. To see this, consider the function  $C_n(t)$  in Eq. 83. If equal frequency intervals are chosen, then

$$C_n(t) = \begin{cases} \Delta\omega \frac{1 - \cos(t\Delta\omega)}{\frac{1}{2}(t\Delta\omega)^2} = \Delta\omega(1 - (1/6)(t\Delta\omega)^2 + \dots) & \text{Method 1} \\ \Delta\omega & \text{Method 0} \end{cases} \quad (87)$$

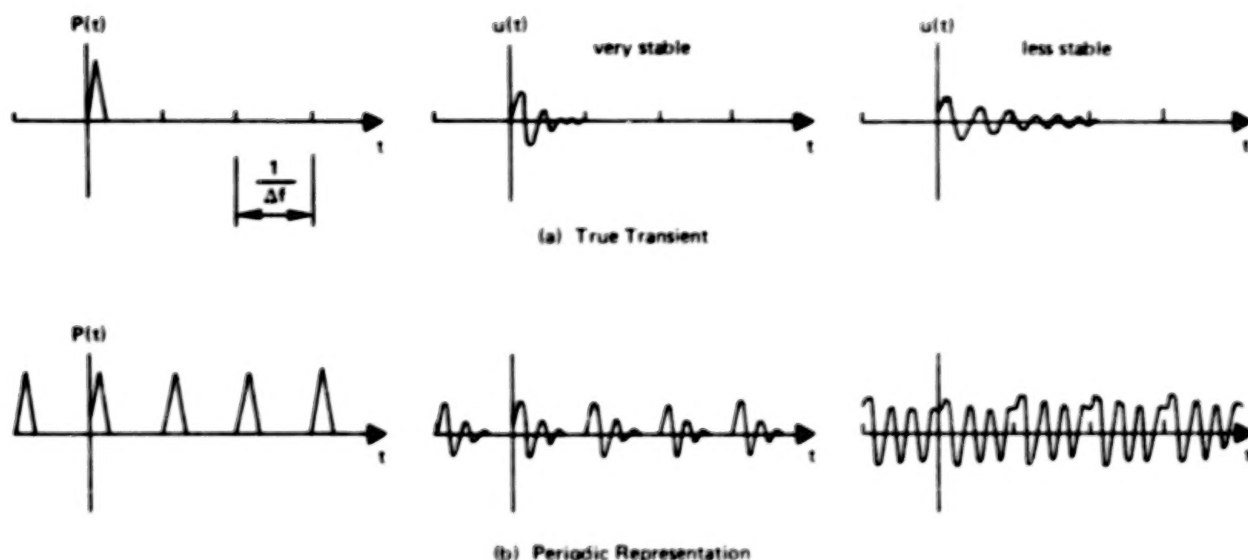


Figure 9. Response of a Damped Oscillator to a Triangular Pulse.

Thus, Method 1 (and also Method 2) produces a decaying envelope which the user may incorrectly interpret as additional damping.

The use of equal frequency intervals has been compared to unequal intervals, and the results are shown below among the demonstration problems. It has been found that the combination of a few well-chosen values near the resonant frequencies and uniformly spaced frequencies elsewhere produces excellent results for lightly damped systems.

#### AERODYNAMIC INFLUENCE COEFFICIENTS

Aerodynamic elements are strips, boxes or bodies which represent the structure for computation of aerodynamic forces. These elements, like the structural elements, are defined by their geometry, and their motions are defined by degrees of freedom at associated aerodynamic grid points. Often requirements of the aerodynamic theory dictate the geometry of the boxes. For example, the Doublet-Lattice Method requires trapezoidal boxes with their

parallel edges along the streamlines, and also, if one box lies in the wake of another, their edges must be the same two streamlines. Aerodynamic elements and grid points are generated to reduce the labor of the user (many less data cards are required) and to help insure that theoretical requirements are met.

Aerodynamic calculations are made in a Cartesian aerodynamic coordinate system. By the usual convention, the flow is in the positive x-direction. The basic coordinate system was not chosen, because it would place an undesirable restriction upon the description of the structural model. Any NASTRAN Cartesian system may be specified, and flow will be defined in the direction of its positive x-axis. All aerodynamic calculations are made initially in the aerodynamic coordinate system. All element and aerodynamic grid point data, computed initially in the basic coordinate system, are converted to the aerodynamic coordinate system. The global (displacement) coordinate system of the aerodynamic grid points has its T1 direction in the flow direction. T3 is normal to the element for boxes, and parallel to the aerodynamic T3 in the case of bodies. Coordinate system data are generated for the aerodynamic grid points.

The grid points are physically located at the centers of the boxes and body elements. Permanent constraints are generated for the unused degrees of freedom. A second set of grid points, used only for undeformed plotting, is located at the element corners. All six degrees of freedom are permanently constrained. Grid point numbers are generated based upon the element identification number. For any panel, the external grid point numbers for the boxes start with the panel identification number and increase consecutively.

Aerodynamic degrees of freedom, along with the extra points, are added after the structural matrices and modes have been determined. This introduces the following displacement sets:

- $u_k$  Aerodynamic box and body degrees of freedom;
- $u_{sA}$  Permanently constrained degrees of freedom associated with aerodynamic grid points;
- $u_{ps}$  Union of  $u_p$  (physical) and  $u_{sA}$ ;
- $u_{pA}$  Union of  $u_k$  and  $u_{ps}$  (physical and aerodynamic).

The set  $u_{pA}$  replaces  $u_p$  as the set available for output at grid, scalar and extra points.

Three matrix equations summarize the relationships required to define a set of aerodynamic influence coefficients (Ref. 18). These are the basic relationship between pressure and downwash (normalwash),

$$\{w_j\} = [A_{jj}]\{P_j\} \quad (88)$$

The substantial differentiation of the deflections to obtain downwash,

$$\{w_j\} = [D_{jk}^1 + ik D_{jk}^2]\{u_k\} \quad (89)$$

and the integration of the pressure to obtain forces,

$$\{P_k\} = [S_{kj}]\{P_j\} \quad (90)$$

where

- $u_k, P_k$  = displacement and forces at aerodynamic grid points,
- $w_j$  = downwash (normalwash),
- $P_j$  = pressure on lifting element,
- $A_{jj}(k,m)$  = aerodynamic influence matrix,
- $D_{jk}^1, D_{jk}^2$  = substantial differentiation matrices, and
- $S_{kj}$  = integration matrix.

In general, the matrices  $A$ ,  $D^1$ ,  $D^2$ , and  $S$  are computed, although for some aerodynamic theories  $A^{-1}$  is obtained directly; in the case of extra points, e.g., when an active control system is included, some partitions of the matrices  $D^1$  and  $D^2$  must be supplied by the user. The matrix  $A$  (or  $A^{-1}$ ) is computed for a user supplied list of  $(k,m)$ .



Doublet-Lattice Method. — The Doublet-Lattice Method (DLM) can be used for interfering lifting surfaces in subsonic flow. The theory is presented thoroughly in the literature (Refs. 19, 20 and 21) and will not be reproduced here. The following general remarks summarize the essential features of the method.

The theoretical basis of the DLM is linearized aerodynamic theory. The undisturbed flow, about which the perturbations occur, is uniform, i.e., there are no spatial variations, and it is either steady or gusting harmonically. Thus, all lifting surfaces must lie nearly parallel to the flow. The DLM is an extension of the steady Vortex-Lattice Method to unsteady flow.

Each of the interfering surfaces is divided into small trapezoidal lifting elements ("boxes") such that the boxes are arranged in strips parallel to the free stream so that surface edges, fold lines, and hinge lines lie on box boundaries. The unknown lifting pressures are assumed to be concentrated uniformly across the one-quarter chord line of each box. There is one control point per box and the surface normalwash boundary condition is satisfied at each of these points. The control point is centered spanwise on the three-quarter chord line of the box.

The code for computing  $A_{jj}$  was taken directly from Ref. 22. Any number of arbitrarily shaped interfering surfaces can be analyzed, provided that each is idealized as one or more trapezoidal planes. Various symmetry options are also available. These include geometry (planform), motion (symmetric or antisymmetric), and ground effect.

Subsonic Wing-Body Interference Theory. — The Method of Images, along with Slender Body Theory has been added to the Doublet-Lattice Method (DLM) (Refs. 22, 23 and 24). The DLM is used to represent the configuration of interfering lifting surfaces, while Slender Body Theory is used to represent the lifting characteristics of each body, i.e., fuselage, nacelle, or external store. The primary wing-body interference is accounted for by a system of images of the DLM vortices and doublets within a cylindrical interference body that circumscribes each slender body. The secondary wing-body interference that results from the DLM bound vortices and doublets is accounted for by a

line of doublets located on the longitudinal axis of each slender body. The boundary conditions of no flow through the lifting surfaces or through the body (on the average about the periphery) leads to the equations for the lifting pressures on the surfaces and for the longitudinal (and/or lateral) loading on the bodies in terms of the normalwashes on the wing-body combination.

The code for computing the aerodynamic matrices was adapted for NASTRAN from Ref. 22. The adaptation required matrix formulations of all of the body interference and body loading calculations. These equations are written using the symbols adopted for NASTRAN and the equivalences to **names** used in the documentation of Ref. 22 are shown below.

The program of Ref. 22 finds the forces on the lifting boxes and bodies of an idealized airplane in terms of the motions of these elements. The lifting surfaces are divided into boxes. The bodies are divided into elements. There are two types of body elements: slender elements are used to simulate the body's own motion; and interference elements are used to simulate the interaction with other bodies and boxes. The body elements may have y (lateral), z (vertical), or both degrees of freedom.

The basic method is the superposition of singularities and their images. There are two basic types, which are "forces" and modified acceleration potential "doublets." Each "force" singularity may be shown to be equivalent to a line of doublets in the wake. The wing boxes use the "force" type of singularity concentrated along the box quarter chord. The interference elements use the "doublet" type of singularity. The slender elements use both types. The first equation relates the downwashes to the singularities.

$$\begin{pmatrix} w_w \\ 0 \\ w_s \end{pmatrix} = \begin{bmatrix} A_{ww} & A_{wI} & A_{ws} \\ A_{Iw} & A_{II} & A_{Is} \\ 0 & 0 & A_{ss} \end{bmatrix} \begin{pmatrix} C_w \\ \mu_I \\ \mu_s \end{pmatrix} \quad (91)$$

where

- $w_w$  = the wing box downwashes at the 3/4-chord,
- $0$  = the downwashes for interference elements due to singularities other than slender elements in the same body,
- $w_s$  = the downwashes for slender body elements,
- $C_w$  = the forces distributed along wing box quarter-chords,
- $\mu_I$  = the interference doublet strengths,
- $\mu_s$  = the slender element doublet strengths,

$$\begin{bmatrix} A_{ww} & \vdots & A_{wI} \\ \text{---} & \text{---} & \text{---} \\ A_{Iw} & \vdots & A_{II} \end{bmatrix} = [DT], \text{ from Section 5.3.1, Ref. 22,}$$

$$\begin{bmatrix} A_{ws} \\ \text{---} \\ A_{Is} \end{bmatrix} = [DZ \quad DY], \text{ from Section 5.5.3, Ref. 22, and}$$

$$\begin{bmatrix} A_{ss} \end{bmatrix} = \begin{bmatrix} D2D^{-1} \end{bmatrix}, \text{ which is diagonal and will be discussed later.}$$

The next equation relates the forces to the singularity strengths.

$$\begin{Bmatrix} f_w \\ \text{---} \\ f_s \end{Bmatrix} = \begin{bmatrix} S_{ww} & \vdots & 0 & \vdots & 0 \\ \text{---} & \text{---} & \text{---} & \text{---} & \text{---} \\ S_{sw} & \vdots & S_{sl} & \vdots & S_{ss} \end{bmatrix} \begin{Bmatrix} C_w \\ \text{---} \\ \mu_I \\ \text{---} \\ \mu_s \end{Bmatrix} \quad (92)$$

where

$C_s$  = the slender element forces,

$[S_{ww}]$  = box areas (diagonal), and

$[S_{sw} \quad S_{sl} \quad S_{ss}]$  = [BFS] from Section 5.8.1, Ref. 22, but rearranged

in the order of the rows. These equations use Method 1 of Ref. 22 (Method 2 was not put into NASTRAN). All of the above matrices have been modified to include the images of the sources on the symmetry plane. Reference 22 uses the convention that images are not used for bodies or surfaces on a plane of symmetry.

In the slender body part of the program developed in Ref. 22, there is no matrix which relates the slender body forces,  $C_s$ , to the slender body modified doublets,  $\mu_s$ . This relationship involves only elements of the same body and of the same orientation. Hence, we must derive this matrix. The differential equation relating distributions of these is

$$C(x) = \left( \frac{\partial}{\partial x} + i \frac{\omega}{U} \right) \mu(x) \quad (93)$$

where

$C(x)$  = lift per unit length/dynamic pressure (i.e., has units of length),

$\mu(x)$  = doublet strength per unit length/free stream velocity (i.e., has units of area),

$x$  = axial coordinate, and

$\omega/U$  = dimensional reduced frequency.

The elements of the vector  $\{C_s\}$  are  $\Delta x \cdot C(x_{\text{center}})$ , which are the total forces on the elements divided by the dynamic pressure. The elements of  $\{\mu_s\}$  are  $\mu(x_{\text{center}})$ . In subroutine MUZYC (Section 5.5.4, Ref. 22), the values of  $C_s$  (called  $\Delta C_p \Delta A$  in the reference) are evaluated from an equation which is equivalent to

$$C_s = \Delta x \left[ \left( \frac{d}{dx} + i \frac{\omega}{U} \right) \mu(x) \right]_{x=x_{\text{center}}} \quad (94)$$

$$\mu(x) = (D2D)^{-1} w_s(x) \quad (95)$$

and

$$w_s(x) = \tilde{c} \left( \frac{d}{dx} + i \frac{\omega}{U} \right) \Sigma \Lambda_n (x_s / \tilde{c})^n \quad (96)$$

where

$$(D2D)^{-1} = 2\pi(1+AR)a_0^2(x) \quad (z \text{ bodies}),$$

$$w_s = \text{downwash} \quad (\text{dimensionless}),$$

$$a_0(x) = \text{half-width} \quad (\text{radius}),$$

$$AR = \text{height/width ratio of body, and}$$

$$\Sigma \Lambda_n (x_s / \tilde{c})^n = \text{polynomial mode shape, which is input data in Ref. 22.}$$

The method used was to derive a matrix,  $[G]$ , which relates the vector of  $\{C_s\}$  to  $\{\mu_s\}$

$$\{C_s\} = [G]\{\mu_s\} \quad (97)$$

The derivation of  $[G]$  assumes that  $\mu/a_0^2$ , which is proportional to  $w$ , is a smooth function. Thus,  $\mu(x) = a_0^2(x) [\mu(x)/a_0^2(x)]$ . Using Eq. 93,

$$\begin{aligned} C(x) &= \left( \frac{\mu}{a_0^2} \right) \frac{\partial}{\partial x} (a_0^2) + a_0^2 \left( \frac{\partial}{\partial x} + i \frac{\omega}{U} \right) \left( \frac{\mu}{a_0^2} \right) \\ &= \left( \frac{2}{a_0} \frac{da_0}{dx} + i \frac{\omega}{U} \right) \mu + a_0^2 \frac{\partial}{\partial x} \left( \frac{\mu}{a_0^2} \right) \end{aligned} \quad (98)$$

The numerical derivatives required for the last term in Eq. 98 are evaluated by the following rules:

One point per body: derivative = 0

Two or more points per body: derivative =  $\begin{cases} \text{2-point rule at end points} \\ \text{3-point rule at interior points} \end{cases}$

The 2-point rule comes from a linear fit, the 3-point rule from a quadratic fit. Examples are

$$\left(\frac{dy}{dx}\right)_1 = \frac{y_2 - y_1}{x_2 - x_1} \quad (2\text{-point}) \quad (99)$$

$$\left(\frac{dy}{dx}\right)_2 = \frac{y_2 - y_1}{x_2 - x_1} + \frac{y_3 - y_2}{x_3 - x_2} - \frac{y_3 - y_1}{x_3 - x_1} \quad (3\text{-point}) \quad (100)$$

Using this, the part of [G] for one body is given by

$$[G_{ij}] = (\Delta x)_i \left[ \delta_{ij} \left( \frac{2}{a_0} \frac{da_0}{dx} + i \frac{2k}{c} \right) + g_{ij} \right] \quad (101)$$

where  $g_{ij}$  is tridiagonal:

$$g_{ij} = \frac{(a_0^2)_i}{(a_0^2)_j} \begin{cases} \frac{1}{x_{i+1} - x_{i-1}} - \frac{1}{x_i - x_{i-1}}, & j = i-1 \\ \frac{1}{x_i - x_{i-1}} - \frac{1}{x_{i+1} - x_i}, & j = i \\ \frac{1}{x_{i+1} - x_i} - \frac{1}{x_{i+1} - x_{i-1}}, & j = i+1 \\ 0, & \text{otherwise} \end{cases} \quad (102)$$

For the first element ( $i=1$ ), delete terms involving ( $i-1$ ). For the last point ( $i=N$ ), delete terms involving  $x_{i+1}$ .

Equation 97 is used to eliminate the slender element forces  $C_s$  from Eq. 92 giving

$$\begin{Bmatrix} f_w \\ f_s \end{Bmatrix} = \begin{bmatrix} S_{ww} & 0 & 0 \\ S_{sw} & S_{sl} & S_{ss} G \end{bmatrix} \begin{Bmatrix} C_w \\ u_I \\ u_s \end{Bmatrix} = [S_{kj}] \{P_j\} \quad (103)$$

Equations 91 and 103 relate forces to downwashes. The relationship of deflections to downwashes is given by Eq. 89. As can be seen from Eq. 81, there is zero "downwash" for all interference body elements, hence the rows of  $D_{jk}^1$  and  $D_{jk}^2$  associated with interference body elements vanish. All other rows represent total derivatives for downwashes of boxes and slender body elements. The basic forms of Eqs. 88-90 are kept, even in the case of panels with interference and slender bodies.

Mach Box Method. — The Mach Box Method (MBM) can be used to estimate generalized aerodynamic forces on isolated planar wings with two (adjacent) control surfaces oscillating in supersonic flow. The MBM is based on the box method first proposed in Ref. 25, and refined in Refs. 26 and 27. The general features of the method are summarized in the following remarks.

The MBM is a numerical solution of the linearized, three-dimensional, oscillatory, supersonic perturbation potential flow equation. The regions disturbed by the lifting surface are divided into a grid of rectangular lifting elements, called Mach boxes, i.e., rectangles whose diagonals are parallel to the Mach lines. The regions divided into Mach boxes include the wing and control surfaces, and regions off the lifting surface affected by any subsonic edge of the surface, i.e., an edge whose normal Mach number is less than unity. Calculations are made of the influence of unit sources, distributed uniformly over the area of each box, on the aerodynamic loading at the center of every box assuming that the constant source strength on each box is equal to the value at the box center. These calculations generate the aerodynamic influence coefficients for the surface. The coefficients obtained are velocity potential influence coefficients and are independent of the mode shapes of the structure.

For a prescribed mode, its downwash distribution and the influence coefficients determine the source strengths associated with the mode, and we obtain the corresponding velocity potential distribution over the planform. The knowledge of the modal velocity potential distributions and the mode shapes permits the calculation of the generalized aerodynamic force coefficients. The accuracy of the MBM depends on the validity of supersonic linearized theory which is generally assumed to be in the Mach number range from about 1.2 up to 3.0. At high Mach numbers the results approach those from first order Piston Theory.

The supersonic Mach Box code used by NASTRAN is based on subroutines of a modified version of the program of Ref. 27 (the modifications were made by L. V. Andrew, G. V. Owens, and J. W. Sleison of the Space Division of Rockwell International). The subroutines have been adapted to calculate the aerodynamic influence coefficients  $A_{jj}^{-1}$  directly. The general planform that can be analyzed is shown in Fig. 10. The following options are available to the user:

1. Leading- and/or trailing-edge cranks;
2. None, one or two adjacent trailing-edge control surfaces with swept-back hinge lines; and
3. Symmetric or antisymmetric motion (no harmonic gust fields are considered).

The freestream velocity is parallel to the x-axis as shown in Fig. 10.

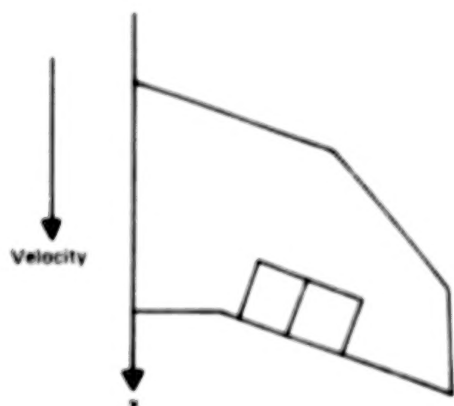


Figure 10. Planform Geometry for Mach Box Method.



Strip Theory. - The first solutions to the unsteady theoretical aerodynamic problem were obtained in two dimensions (Refs. 28 and 29). These solutions were utilized in flutter analysis by assuming that the loads at each spanwise station of a wing depended only on the motion of that station. Practical flutter analyses (e.g., Ref. 30) divided the wing into a number of strips and the aerodynamic loads on each strip were calculated on the basis of the two-dimensional coefficients evaluated at the centerline of the strip. This "Strip Theory" was surprisingly accurate although its successes were primarily in application to unswept wings with high aspect ratios.

The NASTRAN code for computing the aerodynamic influence coefficient matrix or  $A_{jj}^{-1}$  directly is based on Ref. 29 and is an extension of an existing program (written by E. Albano at the Northrop Corporation). Although Ref. 29 includes a trim tab, only the airfoil and an aerodynamically balanced control surface are considered herein; both the airfoil and the control surface are assumed to be rigid in the chordwise direction, and the control surface hinge line is assumed to remain on the wing chord line. The gap between the airfoil and the control surfaces can be assumed to be sealed or open (unsealed). The Theodorsen function for the unsteady circulatory loads is written as

$$C(k) = F(k) + iG(k) \quad (104)$$

where  $k = \omega b/V$  is the local reduced frequency, i.e.,  $b$  is the semi-chord of the strip. The user has the option of calculating  $F(k)$  and  $G(k)$  from their exact expressions in terms of Bessel functions, or from approximations of the form

$$F(k) = \sum_{n=0}^{\infty} \frac{b_n}{1 + (\beta_n/k)^2} \quad (105)$$

$$G(k) = \sum_{n=1}^{\infty} \frac{b_n (\beta_n/k)}{1 + (\beta_n/k)^2} \quad (106)$$

in which  $\beta_0 = 0$ . The choice of values for the parameters  $b_n$  and  $\beta_n$  is left to the user. In this way, Strip Theory can be adjusted to account for compressibility or aspect ratio effects. Some values of  $b_n$  and  $\beta_n$  are tabulated on pages 350 and 394 of Ref. 16. An approximate sweep correction is also incorporated; the correction is the factor  $\cos \Lambda$ , where  $\Lambda$  is the one-quarter chord line sweep angle for the aerodynamic macro-element defined on a bulk data card, and is applied as a multiplier to all loads acting on the element.

**Piston Theory.** — In the limit of high Mach number ( $M^2 \gg 1$ ) or high reduced frequency ( $m^2 k^2 \gg 1$ ), the three-dimensional pressure-downwash relationship on a lifting surface becomes a nonlinear point relationship. The nonlinear point relationship can be linearized for small oscillatory disturbances while retaining the nonlinear aspects of the steady-state condition. The result is known as third order Piston Theory (Ref. 31).

A computer program to obtain  $A_{jj}^{-1}$  has been written (Ref. 32) in the form of a strip theory (as above). This computer code has been modified for NASTRAN only to adjust the sign conventions. It has the following general features. It is an extension of Ref. 31 to account for sweep and steady angle of attack and to reduce the lower supersonic Mach number limit so that agreement with Ref. 33 is obtained through the second-order terms. A rigid chord is assumed as well as a rigid control surface hinged at its leading edge, i.e., no aerodynamic balance is considered because balance is not a desirable design feature on supersonic vehicles. Experimental correlations have indicated the validity of Piston Theory in the range of Mach number from about 2.5 to 7.0.

#### Interconnection Between Structural and Aerodynamic Forces

A very general means is provided to relate structural and aerodynamic degrees of freedom. The method allows the selection of grid points and elements for the structure and for the aerodynamics so that each may be chosen by a method which is well-suited to the particular problem. The structural model for a wing may involve a one-, two- or three-dimensional array of grid points. The aerodynamic theory may involve a strip theory or a lifting surface theory. A general interpolation method is available which can interconnect the various

combinations. Any aerodynamic panel or body can be subdivided into subzones for interpolations, using a separate function for each.

The interpolation method used is called "splining." The theory involves the mathematical analysis of beams and plates (see Fig. 11). A linear spline

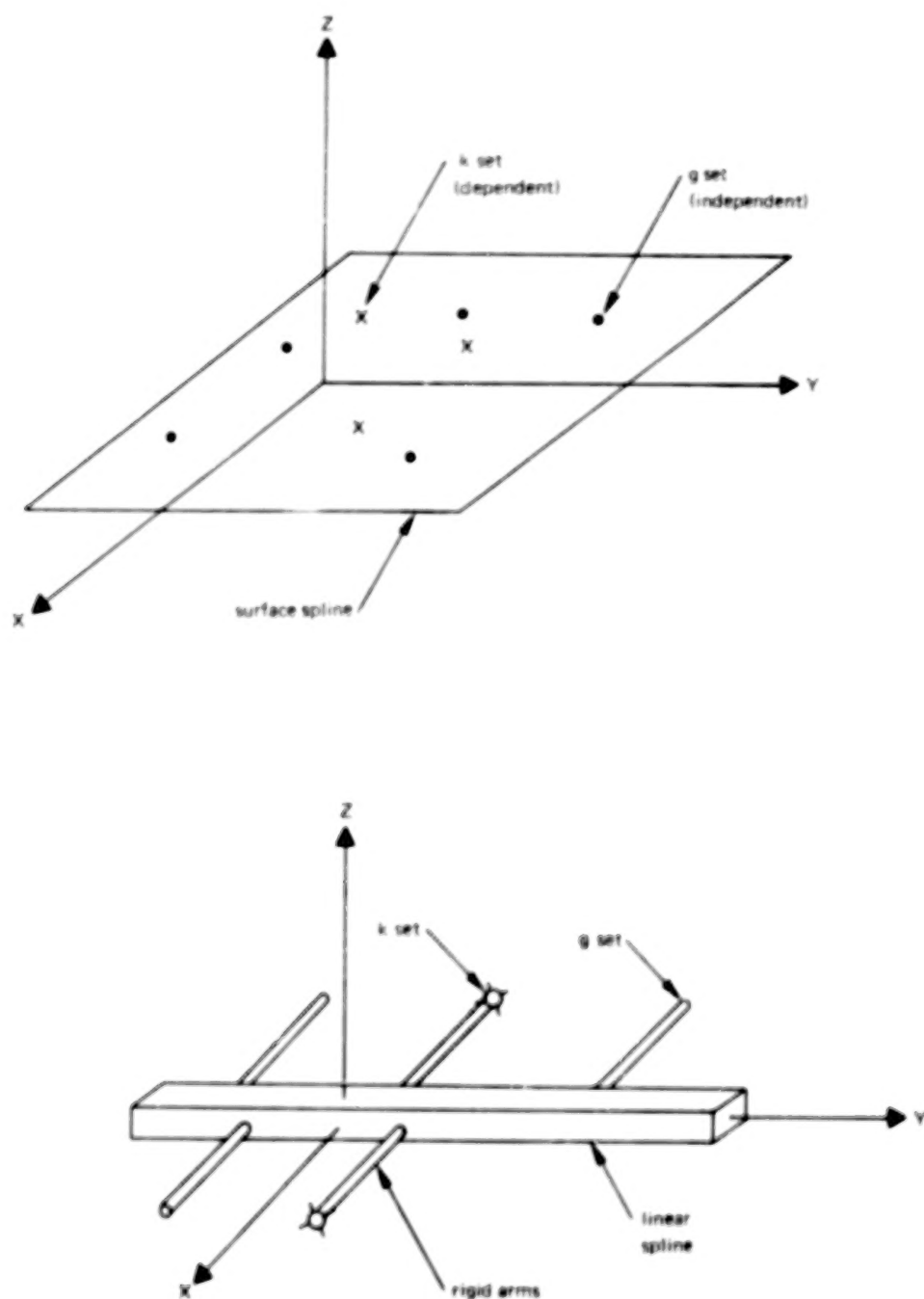


Figure 11. Splines and Their Coordinate Systems.

is a generalization of the simple beam, which allows torsional as well as bending degrees of freedom. A surface spline is a solution for an infinite uniform plate. Several splines, including combinations of the two types, can be used in one model. For example, a model may use one linear spline for the horizontal tail, and three surface splines for the wing (inboard section, outboard section, and aileron). This local splining allows discontinuous slopes (at the wing-aileron hinge), separate functions (for wing and tail), and smaller zones. Smaller zones will reduce the computing effort (cost).

The structural degrees of freedom have been chosen as the independent degrees of freedom; the aerodynamic degrees of freedom are dependent. A matrix is derived which relates the dependent degrees of freedom to the independent ones. The structural degrees of freedom may include any grid components.

Theory for Surface Splines. - The problem of an infinite plate on multiply deflected supports has been studied in Ref. 34. The solution for the deflections is summarized here. The deflection function becomes the surface spline and provides one basis for two-dimensional interpolation in NASTRAN.

The deflection of the infinite plate under a single concentrated load is the fundamental solution and it has polar symmetry. In polar coordinates ( $X = r \cos \theta$ ,  $Y = r \sin \theta$ ), the governing differential equation of the plate deflection is

$$D \nabla^4 W = D \frac{1}{r} \frac{d}{dr} \left\{ r \frac{d}{dr} \left[ \frac{1}{r} \frac{d}{dr} \left( r \frac{dw}{dr} \right) \right] \right\} = q \quad (107)$$

The load  $q$  vanishes except near  $r = 0$ . A solution to the general spline problem, formed by superimposing solutions of Eq. 107 is given by

$$W(X,Y) = a_0 + a_1 X + a_2 Y + \sum_{i=1}^N K_i(X,Y) P_i \quad (108)$$

where

$$K_i(X,Y) = (1/16\pi D) r_i^2 \ln r_i^2, \quad (109)$$

$$r_i^2 = (X-X_i)^2 + (Y-Y_i)^2 \quad (110)$$

and  $P_i$  is a concentrated load at  $(X_i, Y_i)$ . The  $N+3$  unknowns ( $a_0, a_1, a_2, P_i$  where  $i=1,N$ ) are determined from the  $N+3$  equations

$$\sum P_i = \sum X_i P_i = \sum Y_i P_i = 0 \quad (111)$$

and

$$W_j = a_0 + a_1 X_j + a_2 Y_j + \sum_{i=1}^N K_{ij} P_i \quad (j=1,N) \quad (112)$$

where

$$K_{ij} = K_i(X_j, Y_j). \text{ Note that } K_{ij} = K_{ji}, \text{ and } K_{ij} = 0 \text{ when } i = j.$$

These equations can be summarized in matrix form.

$$W(X,Y) = [1, X, Y, K_1(X,Y), K_2(X,Y), \dots, K_N(X,Y)] \begin{Bmatrix} a_0 \\ a_1 \\ a_2 \\ \text{---} \\ P_1 \\ P_2 \\ \vdots \\ P_N \end{Bmatrix} \quad (113)$$

where  $K_i(X,Y)$  is defined in Eq. 109. The vector of planar coefficients and loads is found by solving

$$\begin{Bmatrix} 0 \\ 0 \\ 0 \\ \hline w_1 \\ w_2 \\ \vdots \\ w_N \end{Bmatrix} = \begin{bmatrix} 0 & 0 & 0 & | & 1 & \dots & 1 \\ 0 & 0 & 0 & | & x_1 & \dots & x_N \\ 0 & 0 & 0 & | & y_1 & \dots & y_N \\ \hline 1 & x_1 & y_1 & | & 0 & \dots & K_{1N} \\ 1 & x_2 & y_2 & | & \cdot & \dots & K_{2N} \\ \vdots & \vdots & \vdots & | & \vdots & \ddots & \vdots \\ 1 & x_N & y_N & | & K_{N1} & \dots & 0 \end{bmatrix} \begin{Bmatrix} a_0 \\ a_1 \\ a_2 \\ \hline p_1 \\ p_2 \\ \vdots \\ p_N \end{Bmatrix} \quad (114)$$

where  $K_{ij}$  is defined in Eq. 112.

The interpolation to any point in the plane  $(X,Y)$  is then achieved by evaluating  $W(X,Y)$  from Eq. 108. Slopes can be found by analytic differentiation of Eq. 108.

Theory for Linear Splines. - Linear splines are easily solved by the three-moment method, which is appropriate for simple linear splines. Unfortunately, the method does not work as well for splines with torsion, rigid arms, and attachment springs. The derivations outlined below are based upon an analogy with the surface spline derivation.

Linear Splines. - The beam deflection equation is

$$EI \frac{d^4 w}{dx^4} = q + \frac{dm}{dx} \quad (115)$$

where  $q$  is an applied load and  $m$  is an applied moment. A symmetric fundamental solution for  $x \neq 0$  is used for loads  $q = P\delta(X)$ , and an antisymmetric fundamental solution is used for moments. The solution for the general case is found by superimposing the fundamental solutions as before.

$$W(X) = a_0 + a_1 X + \sum_{i=1}^N \left( -\frac{M_i (X-X_i) |X-X_i|}{4EI} + \frac{P_i |X-X_i|^3}{12EI} \right) \quad (116)$$

$$\theta(X) = \frac{dw}{dx} = a_1 + \sum_{i=1}^N \left( -\frac{M_i |X-X_i|}{2EI} + \frac{P_i (X-X_i) |X-X_i|}{4EI} \right) \quad (117)$$

These are written in matrix notation as

$$\begin{Bmatrix} W(X) \\ \theta(X) \end{Bmatrix} = \begin{bmatrix} 1 & X & \frac{|X-X_1|^3}{12EI} & \dots & -\frac{(X-X_i) |X-X_i|}{4EI} & \dots \\ 0 & 1 & \frac{(X-X_1) |X-X_1|}{4EI} & \dots & -\frac{|X-X_i|}{2EI} & \dots \end{bmatrix} \begin{Bmatrix} a_0 \\ a_1 \\ P_1 \\ \vdots \\ P_N \\ M_1 \\ \vdots \\ M_N \end{Bmatrix} \quad (118)$$

The unknown planar coefficients and loads are found from

$$\begin{Bmatrix} 0 \\ 0 \\ \vdots \\ 0 \\ W_1 \\ \vdots \\ W_N \\ \theta_1 \\ \vdots \\ \theta_N \end{Bmatrix} = \begin{bmatrix} 0 & R_1^T & R_2^T \\ R_1 & A_{11} & A_{21}^T \\ R_2 & A_{21} & A_{22} \end{bmatrix} \begin{Bmatrix} a_0 \\ a_1 \\ P_1 \\ \vdots \\ P_N \\ M_1 \\ \vdots \\ M_N \end{Bmatrix} \quad (119)$$

in which the various partitions in Eq. 119 are

$$R_1^T = \begin{bmatrix} 1 & 1 & \dots & 1 \\ x_1 & x_2 & \dots & x_N \end{bmatrix} \quad (120)$$

$$R_2^T = \begin{bmatrix} 0 & 0 & \dots & 0 \\ 1 & 1 & \dots & 1 \end{bmatrix} \quad (121)$$

$$A_{11} = \begin{bmatrix} 0 & \frac{|x_2 - x_1|^3}{12EI} & \dots & \frac{|x_N - x_1|^3}{12EI} \\ \frac{|x_2 - x_1|^3}{12EI} & 0 & \dots & \frac{|x_N - x_2|^3}{12EI} \\ \vdots & \vdots & \ddots & \vdots \\ \frac{|x_N - x_1|^3}{12EI} & \frac{|x_N - x_2|^3}{12EI} & \dots & 0 \end{bmatrix} \quad (122)$$

$$A_{21} = \begin{bmatrix} 0 & -\frac{(x_2 - x_1)|x_2 - x_1|}{4EI} & \dots & -\frac{(x_N - x_1)|x_N - x_1|}{4EI} \\ \frac{(x_2 - x_1)|x_2 - x_1|}{4EI} & 0 & \dots & -\frac{(x_N - x_2)|x_N - x_2|}{4EI} \\ \vdots & \vdots & \ddots & \vdots \\ \frac{(x_N - x_1)|x_N - x_1|}{4EI} & \frac{(x_N - x_2)|x_N - x_2|}{4EI} & \dots & 0 \end{bmatrix} \quad (123)$$



$$A_{22} = \begin{bmatrix} 0 & -\frac{|x_2 - x_1|}{2EI} & \dots & -\frac{|x_N - x_1|}{2EI} \\ -\frac{|x_2 - x_1|}{2EI} & 0 & \dots & -\frac{|x_N - x_2|}{2EI} \\ \vdots & \vdots & \ddots & \vdots \\ -\frac{|x_N - x_1|}{2EI} & -\frac{|x_N - x_2|}{2EI} & \dots & 0 \end{bmatrix} \quad (124)$$

Torsion Bars. — The twist equation for a torsion bar is

$$GJ \frac{d^2 \theta}{dx^2} = -t \quad (125)$$

where  $t$  is a distributed applied torque, and the solution is

$$\theta(x) = \left[ 1 \mid 0, -\frac{|x_2 - x_1|}{2GJ}, \dots, -\frac{|x_N - x_1|}{2GJ} \right] \begin{Bmatrix} a_0 \\ T_1 \\ \vdots \\ T_N \end{Bmatrix} \quad (126)$$

where the unknowns are solved from

$$\begin{Bmatrix} 0 \\ \vdots \\ \theta_1 \\ \vdots \\ \theta_2 \\ \vdots \\ \theta_N \end{Bmatrix} = \begin{bmatrix} 0 & 1 & 1 & \dots & 1 \\ \vdots & \vdots & \vdots & \ddots & \vdots \\ 1 & 0 & -\frac{|x_2 - x_1|}{2GJ} & \dots & -\frac{|x_N - x_1|}{2GJ} \\ \vdots & -\frac{|x_2 - x_1|}{2GJ} & 0 & \dots & -\frac{|x_N - x_2|}{2GJ} \\ \vdots & \vdots & \vdots & \ddots & \vdots \\ 1 & -\frac{|x_N - x_1|}{2GJ} & -\frac{|x_N - x_2|}{2GJ} & \dots & 0 \end{bmatrix} \begin{Bmatrix} a_0 \\ T_1 \\ T_2 \\ \vdots \\ T_N \end{Bmatrix} \quad (127)$$

Attachment of Splines with Elastic Springs. — Springs can be inserted between the structure and the spline to provide a smoother interpolation. The change in the formulas for splines to accommodate the springs is simple. A derivation, valid for the several types of splines, is as follows. The spline deflection is given by Eq. 113, 118 or 126 and can be written

$$\{u_k(r)\} = [R(r)]\{a\} + [A_j(r)]\{P\} \quad (128)$$

where  $u_k$  is the deflection of the spline and the  $r$  may be a one- or two-dimensional argument. Thus, writing of the equilibrium equations and introducing subscripts into Eq. 128, we have

$$0 = [R_i]^T\{P\} \quad (129)$$

and

$$\{u_k\} = [R_i]\{a\} + [A_{ij}]\{P\} \quad (130)$$

The structural deflection,  $u_g$ , will differ from the spline deflection by the deformation of the spring, resulting in forces

$$\{P\} = [K_s]\{u_g - u_k\} \quad (131)$$

where the matrix,  $K_s$ , has the spring constant,  $K$ , along the diagonal. These are nonzero (Note: if  $K$  were = 0, then there would be no attachment and we would discard that grid point) and thus the inverse of  $K_s$  is

$$[K_s]^{-1} = \begin{bmatrix} \frac{1}{K} & & 0 \\ & \ddots & \\ 0 & & \frac{1}{K} \end{bmatrix} \quad (132)$$

Eliminating  $u_k$  between Eq. 130 and 131 we get

$$\{u_g\} = [R_i]\{a\} + ([A_{ij}] + [K_s]^{-1})\{P\} \quad (133)$$

Thus, all that is required to accommodate springs is to add the spring flexibilities ( $1/K$ ) to the diagonal of the spline influence coefficient matrix, which is obvious from physical reasoning, since the spring and spline flexibilities are in series and can be added directly.

Rigid Arms on Linear Splines. — The linear splines used for geometry interpolation have rigid arms (see Fig. 11). Mathematically, these represent equations of constraint between the displacements and rotations at the spline and at the attachment points. The constraint equations are used to transform the influence functions from the spline ends to influence functions at the attachment ends. The complete transformed influence functions are shown in Table 1.

Coordinate Systems and Constraints. — The spline constraints are derived in spline coordinates, transformed to the global coordinate system, and then all splines are appended to a common constraint matrix,  $G_{kg}$ . Finally, the multi-, single- and omit-constraints are applied to reduce this to  $G_{ka}$ . The subscript  $k$  refers to points on the aerodynamic boxes and bodies. Subscripts  $g$  and  $a$  are standard NASTRAN sets. The sets are defined in Ref. 1, Section 3.3, and the method of reduction is in Ref. 1, Section 3.5. The set "g" contains all of the degrees of freedom at the grid and scalar points, while the set "a" contains the "analysis" set.

#### DEMONSTRATION PROBLEMS

A large number of problems is necessary to illustrate the principal features of the dynamic aeroelastic capability of NASTRAN. The problems can be grouped under two headings: those requiring a stability (flutter) analysis, and those requiring a frequency response analysis. Flutter analyses by the three available methods have been selected to demonstrate

TABLE 1. MATRICES IN EQ. 128 FOR SPLINE INTERPOLATION

The R Matrix for Surface and Linear Splines:

$$\begin{Bmatrix} u_z \\ \vdots \\ \partial_x \\ \vdots \\ \partial_y \end{Bmatrix}_i = \begin{bmatrix} 1 & x_i & -x_i \\ 0 & 1 & 0 \\ 0 & 0 & 1 \end{bmatrix} \begin{Bmatrix} u_z \\ \partial_x \\ \partial_y \end{Bmatrix}_r$$

The A Matrix for Surface Splines:

$$\begin{Bmatrix} u_z \\ \vdots \\ \partial_x \\ \vdots \\ \partial_y \end{Bmatrix}_i = \begin{bmatrix} \frac{r_{ij}^2 \ln r_{ij}^2}{16\pi D} + \frac{x_{ij}}{k_z} \\ \frac{(y_i - y_j)(1 + \ln r_{ij}^2)}{32\pi D} \\ \frac{(x_i - x_j)(1 + \ln r_{ij}^2)}{32\pi D} \end{bmatrix} \quad (P_{ij})_f$$

where

$$r_{ij}^2 = (x_i - x_j)^2 + (y_i - y_j)^2$$

$$x_{ij} = \begin{cases} 1 & \text{for } i = j \\ 0 & \text{for } i \neq j \end{cases}$$

The A Matrix for Linear Splines:

$$\begin{Bmatrix} u_z \\ \vdots \\ \partial_x \\ \vdots \\ \partial_y \end{Bmatrix}_i = \begin{bmatrix} \frac{y_i - y_j}{4\pi D} + \frac{x_i x_j (y_i - y_j)}{2GJ} + \frac{x_{ij}}{k_z} & -\frac{y_i - y_j}{4\pi D} + \frac{x_i (y_i - y_j)}{2GJ} \\ \frac{y_i - y_j}{4\pi D} + \frac{y_i (y_i - y_j)}{2GJ} & -\frac{y_i - y_j}{4\pi D} + \frac{x_i}{k_x} \\ \frac{x_i (y_i - y_j)}{2GJ} & 0 \end{bmatrix} \begin{Bmatrix} P_z \\ M_x \\ M_y \end{Bmatrix}_j$$

the five aerodynamic theories. Examples of transient and random responses are chosen as applications of the frequency response analysis.

A physical description of each problem, along with its mathematical model, is given here and a summary of the results of the analysis is presented. (The details of the Executive, Case Control, and Bulk Data cards are presented in Ref. 2.)

### Flutter Analysis

Swept Wing. — A simple flat-plate wing with fifteen degrees of sweepback is shown in Fig. 12a. This wing has been tested in a wind tunnel at subsonic and supersonic speeds and the results have been reported (Ref. 35). A number of models of the same shape but of different materials were tested. The models were made of 1.04 mm (0.041 in.) thick sheet with beveled leading and trailing edges; the low speed models were made of aluminum and the high speed models were made of magnesium. The example problems chosen here are correlated with the subsonic test at a Mach number  $m = 0.45$ , and with the supersonic test at  $m = 3.00$ .

The structural model was chosen as a classical "stick" model with bending and torsion of the elastic axis. Although NASTRAN has the capability to treat the model more accurately as a plate, the aspect ratio of the model is high enough and the sweepback angle is low enough so that its idealization as an elementary beam elastic axis is a reasonable approximation. The structural idealization is shown in Fig. 12b. The section properties (bending and torsional stiffnesses) for both models were adjusted slightly to improve the agreement between the calculated and the measured natural frequencies.

The subsonic flutter analysis of the aluminum model used the Doublet-Lattice oscillatory aerodynamic theory and the K-method of flutter analysis. The planform idealization into 24 aerodynamic boxes is shown in Fig. 13a. The interpolation for the downwashes at the 24 boxes and for the generalized aerodynamic forces from the 24 boxes was carried out using a linear spline along the elastic axis. The aerodynamic matrices were obtained for the

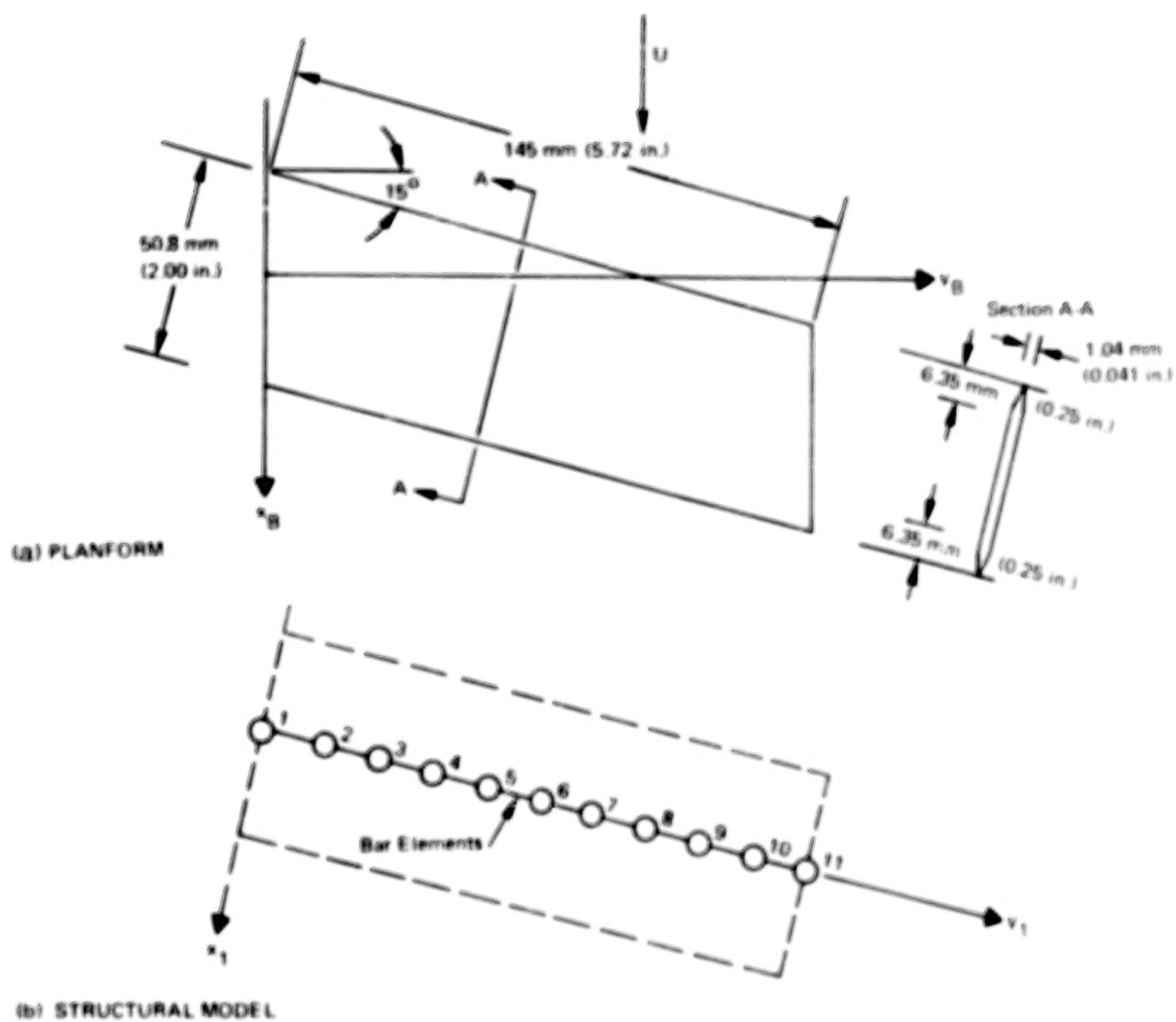


Figure 12. Fifteen Degree Sweptback Wing Model.

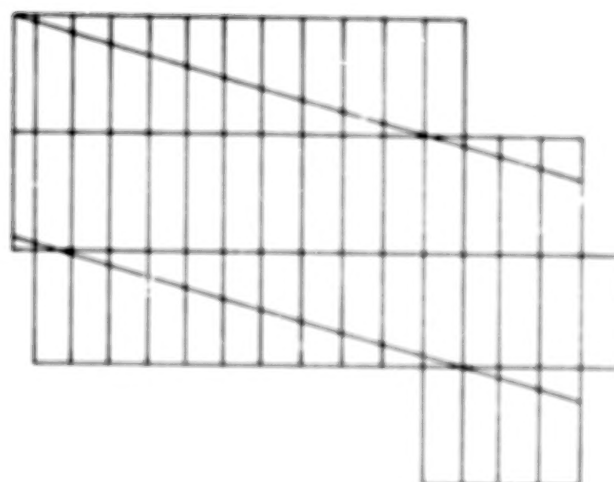
three reduced frequencies  $k = 0.001$ ,  $0.1$  and  $0.2$  at the Mach number  $M = 0.45$ , and the flutter solutions were obtained at the four interpolated reduced frequencies  $k = 0.125$ ,  $0.143$ ,  $0.167$ , and  $0.200$  ( $1/k = 8.0$ ,  $7.0$ ,  $6.0$ , and  $5.0$ ). Linear spline interpolation on  $k$  was used to obtain the generalized aerodynamic forces for intermediate values of  $k$ . The results of the flutter analysis give good agreement with the experimental flutter velocity. The V-g curve is shown in Fig. 14. The V-g curve is steep and gives a well-defined flutter point. The calculated flutter speed is less than 2 percent higher than the experimental value. The calculated flutter frequency does not agree with the experimental value as well as the velocity; it is high by about 20 percent.

The supersonic flutter analysis of the magnesium model was done by the PK-method of flutter analysis and two aerodynamic theories: the Mach Box Method and Piston Theory. Both flutter analyses used the test Mach number  $M = 3.00$  and the test air density  $\rho = 0.479 \text{ kg/m}^3$  ( $0.00093 \text{ slugs/cu. ft.}$ ). The planform idealization into 45 boxes for the Mach Box Method is shown in Fig. 13b, and the idealization into six equal strips for Piston Theory is shown in Fig. 13c. The linear spline along the elastic axis was used again to determine the box deflections and downwashes for the generalized force calculation. The aerodynamic solutions were found at  $k = 0.001$ ,  $0.1$  and  $0.2$  for the Mach Box Method and  $0.001$ ,  $0.04$ ,  $0.1$  and  $0.2$  for Piston Theory, and again linear spline interpolation on  $k$  was used to obtain the generalized aerodynamic forces for the intermediate values of  $k$  required during the iterative PK-flutter solution.

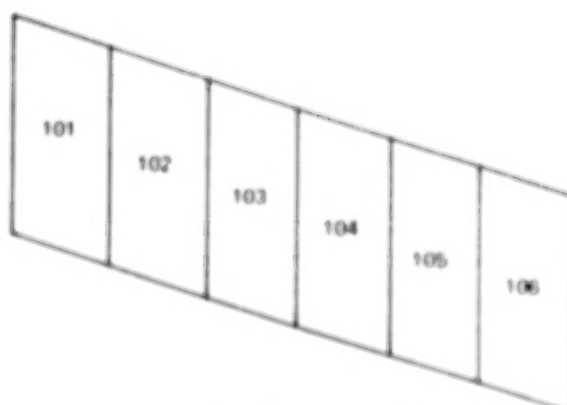
The flutter results for the magnesium  $15^\circ$  swept wing are summarized in Fig. 15. The theoretical flutter results based on both Mach Box and Piston Theory unsteady aerodynamics are compared with the experimental data from Ref. 35. The results which were calculated using Piston Theory agree reasonably well with the experimental data. The theoretical flutter speed is 7 percent higher than the test speed and the flutter frequency is 28 percent higher than the experimental value. The flutter results based on Mach Box aerodynamics did not predict the experimental data at all. No flutter speed was obtained and the flutter frequency was 79 percent high. Because there were effectively only two Mach boxes on the chord in the outboard wing

101	105	109	113	117	121
102	106	110	114	118	122
103	107	111	115	119	123
104	108	112	116	120	124

(a) Subsonic Model



(b) Supersonic Mach Box Model



(c) Piston Theory Model

Figure 13. Aerodynamic Idealizations for Fifteen Degree Sweptback Wing Model.



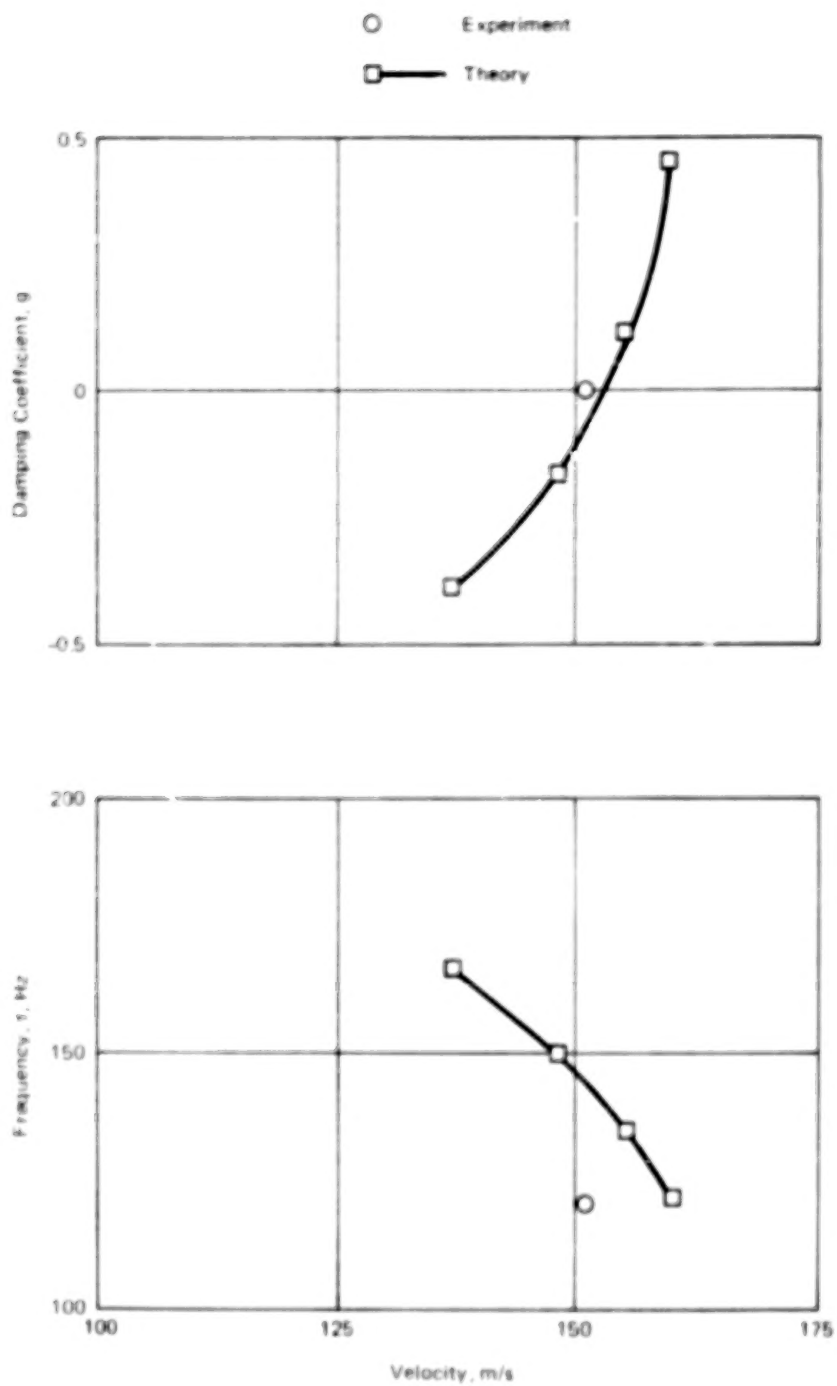


Figure 14. Subsonic Flutter Analysis of Sweptback Wing Model Using Doublet-Lattice Aerodynamics and K-Method.

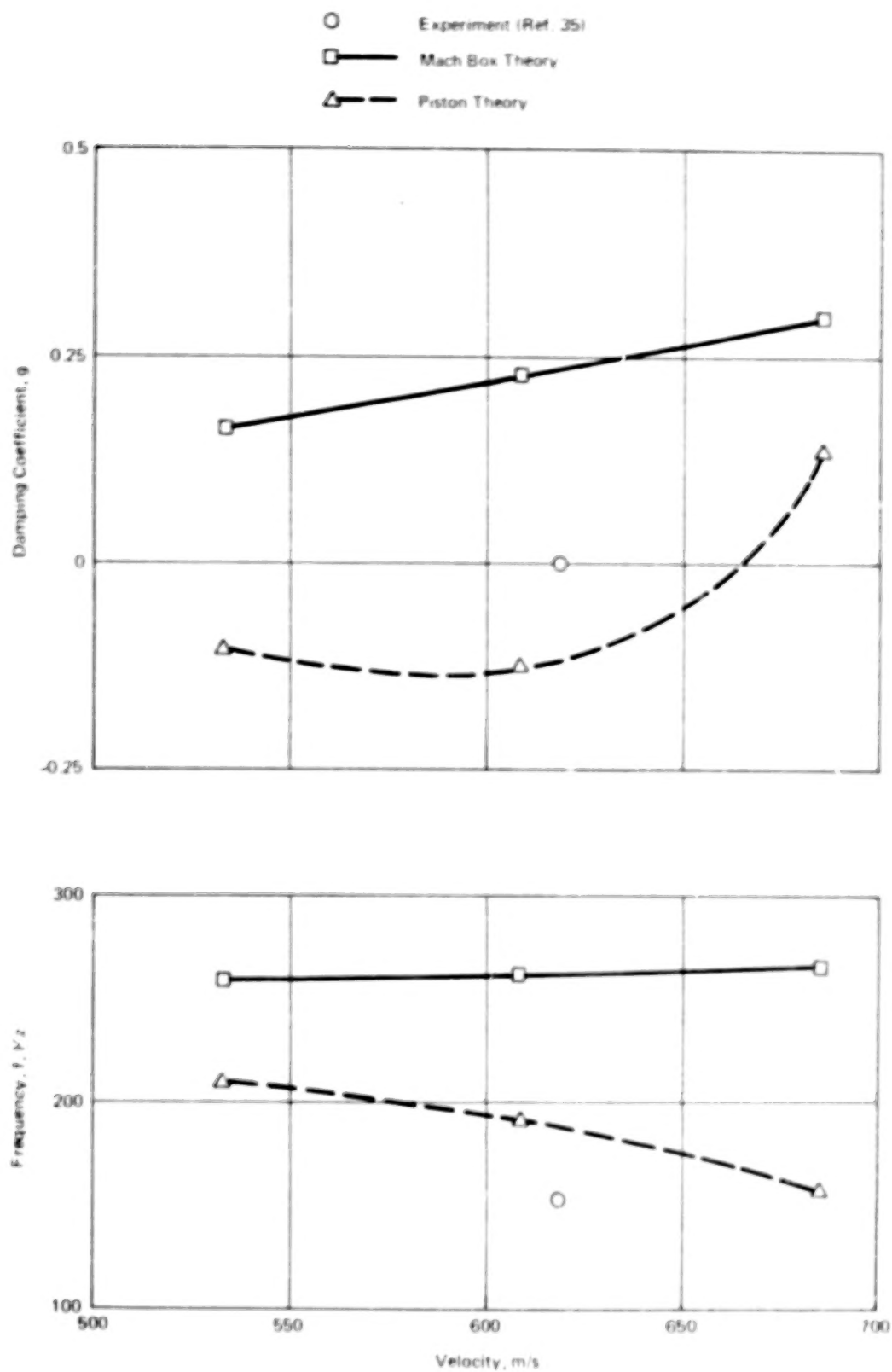


Figure 15. Supersonic Flutter Analysis of Sweptback Wing Model Using the PK-Method

region, one would not expect an accurate converged solution; no convergence study of this case has been made although three or four boxes per chord is probably a practical minimum.

The BAH\* Wing. — The BAH wing was chosen as an example to demonstrate the accuracy of the aerodynamic damping calculated by the PK-method of flutter analysis. This example was analyzed in Ref. 36 using a rigorous approach to the transient aerodynamic loading based on strip theory and an exponential approximation to the Wagner function given in Ref. 37. The approach of Ref. 36 has been extended to three-dimensional aerodynamic lifting surface theories in Ref. 38, but strip theory was adequate for the present purpose of demonstration.

The BAH wing flexibility influence coefficients and mass matrix are given in Ref. 39 for the idealization shown in Fig. 16. With the flexibility matrix, the NASTRAN general element (GENEL) was set up and the vibration analysis was based on that and the available mass matrix. Ten cantilever modes were used. The flutter analyses of Refs. 36 and 39, i.e., by the P- and K-methods, respectively, neglected structural damping so that assumption was also made here. The generalized aerodynamic forces were obtained from the geometry of Fig. 16 and the strip theory option that uses approximations to the Theodorsen function. In this case, for comparison to Ref. 36, the constants developed in Ref. 37 for incompressible flow were used.

The flutter analysis was made for sea level density. The rigid chord assumed in the calculation of the flexibility matrix was also considered in the aerodynamic analysis through a linear spline interpolation for the deflections and downwashes at the one-quarter chord point on each of the five strips. The basic aerodynamic matrices were calculated for  $k = 0.02, 0.05, 0.10, 0.20, 0.50, 1.00$  and  $2.00$ , and linear spline interpolation on  $k$  was used for intermediate values of  $k$  required in the PK-iteration. The large number of values of  $k$  were more than necessary but were used to ensure accuracy so that the comparison between dampings given by the P- and PK-methods could be made properly.

---

\*This is the example problem of a jet transport wing considered throughout Ref. 16.

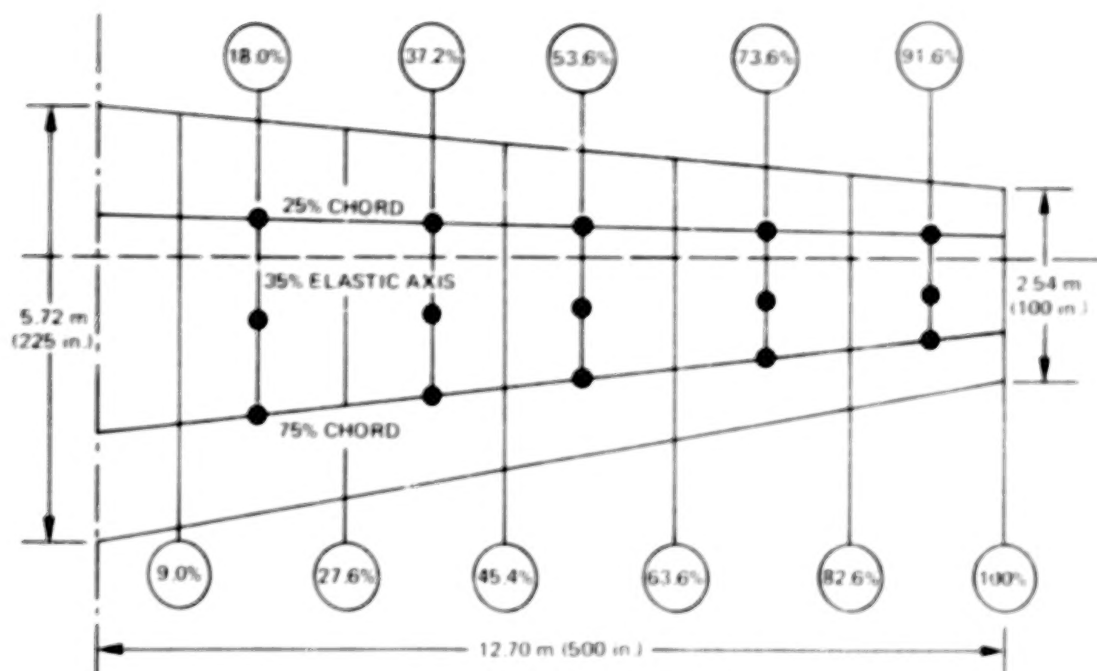


Figure 16. BAI Wing Planform and Aerodynamic Strip Idealization.

The comparisons between results of the P- and the PK-methods are shown in Figs. 17 - 19. The frequencies are compared in Fig. 17. The frequencies are almost identical between the two solutions for the second through the fifth modes. A difference is seen between the two solutions for the first bending mode, and is to be expected from the basic approximation of the British (PK) method of flutter analysis, i.e., it is assumed that the oscillatory aerodynamics are valid for lightly damped motions. The first bending mode is heavily damped and the basic assumption is thereby violated; however, the differences between the two methods are not found in the flutter solution but only in the divergence solution. The damping values in the flutter modes, i.e., the second, third, and fifth modes, are compared in Fig. 18 and are also seen to be almost identical between the two solutions.

Certain peculiarities in the results from the P-method in Ref. 36 deserve further investigation, such as the rapid decrease in frequency of the bending mode and the fact that the divergence root arises from one of the

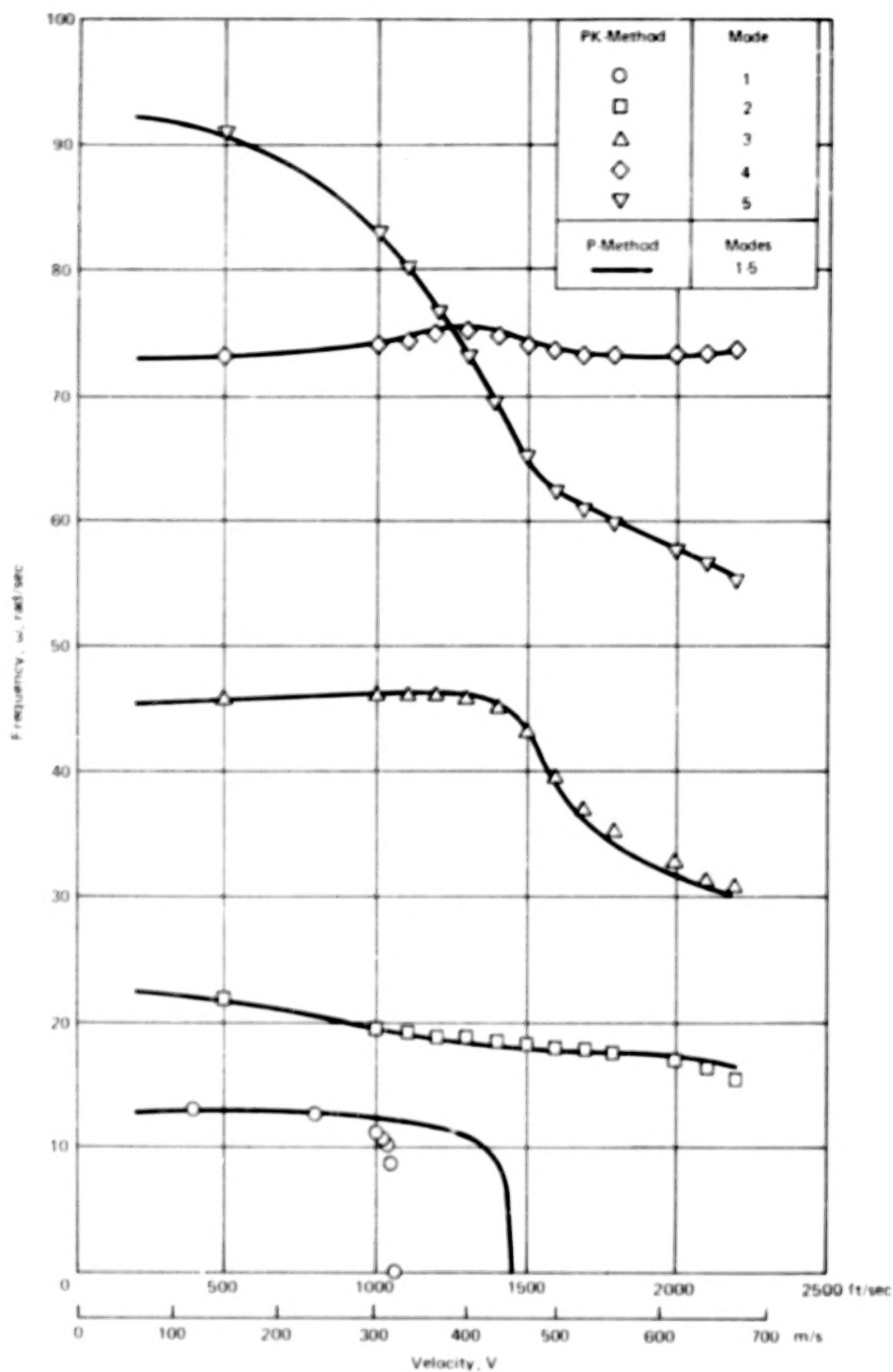


Figure 17. Comparison of BAH Wing Flutter Frequencies Between P- and PK-Methods.

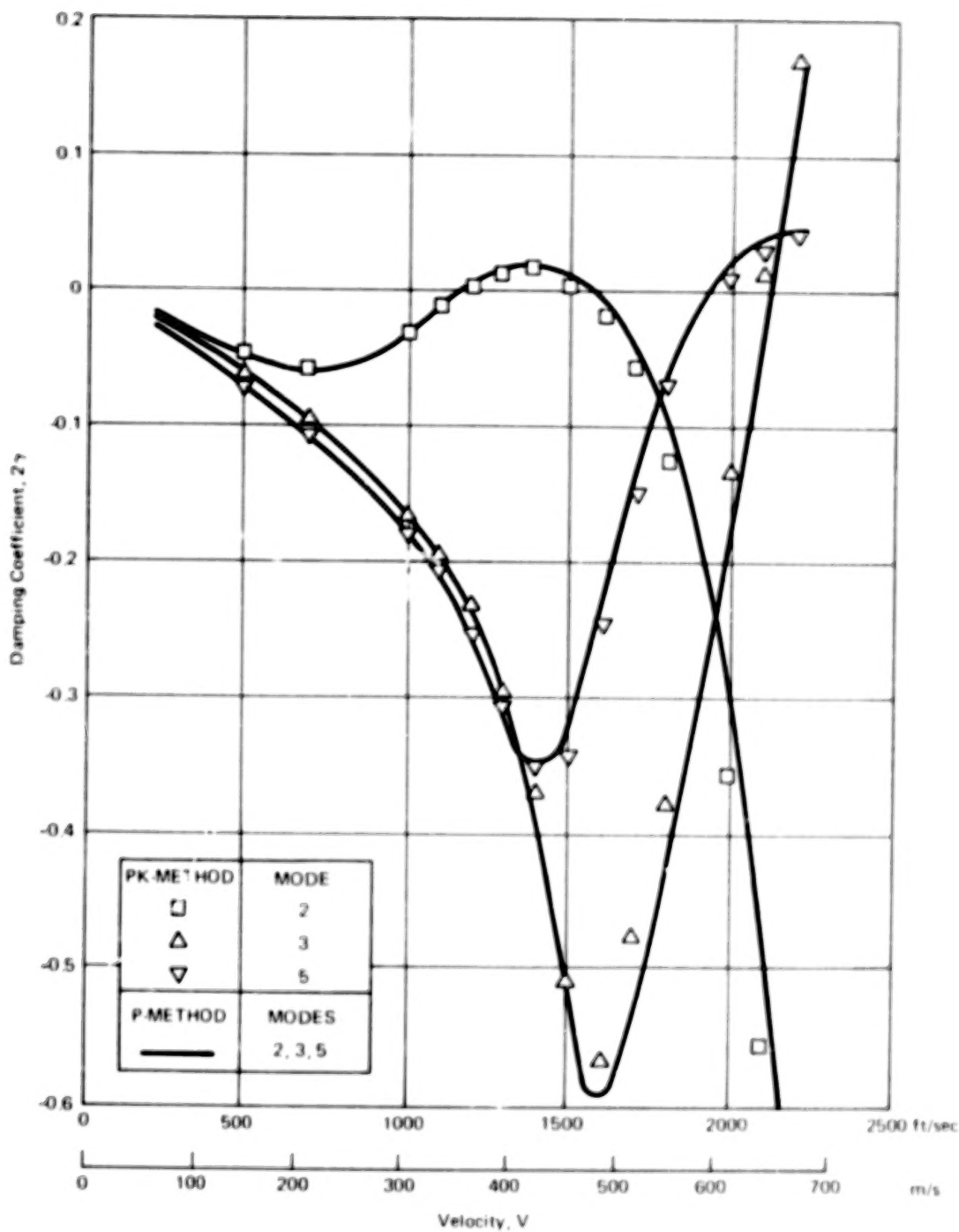


Figure 18. Comparison of BAH Wing Damping Values Between P- and PK-Methods.

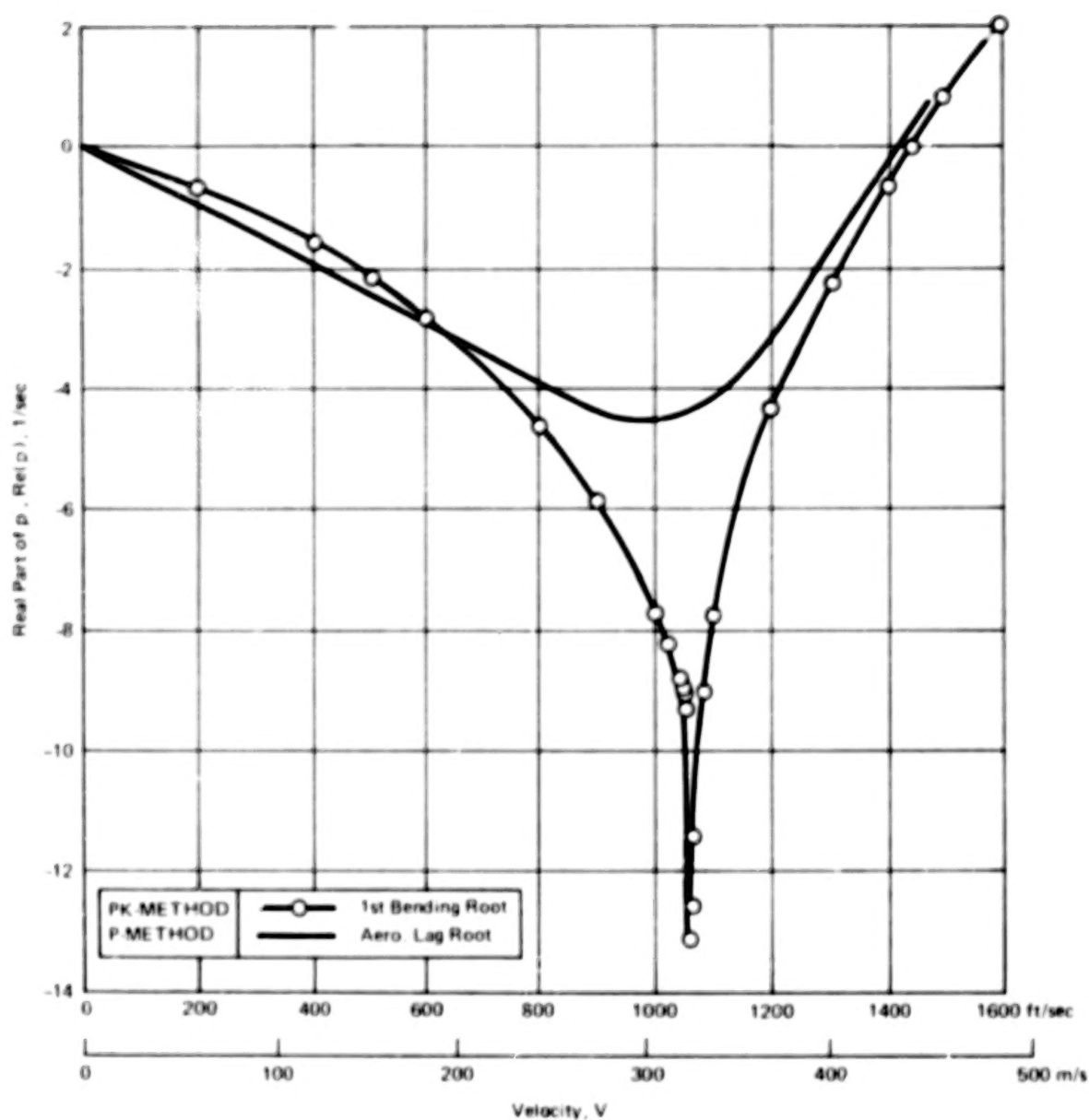


Figure 19. Comparison of BAH Wing Divergence Roots Between P- and PK-Methods.

aerodynamic lag functions introduced in the P-method. However, the P- and PK-methods both give essentially the same divergence speed as shown in Fig. 19. The figure compares the damping in the first bending mode from the PK-method and the critical aerodynamic lag root from the P-method. The significance of these two physically different roots leading to the same divergence speed in the two different methods of flutter analysis remains a subject for future study.

Woodcock, in an appendix to Ref. 8, has suggested that the lag roots "are almost certainly spurious roots to the actual problem"; this cannot be the case since one of them determines the fundamental divergence speed. In any event, the problem of the lag roots does not appear in the PK-method and divergence is predicted as the fundamental vibration mode eventually turns into the static torsional divergence mode.

Servoelastic Stability Analysis. — This example problem is a missile-flipper configuration idealized as a uniform beam with an all-movable aft section as shown in Fig. 20. This is an oversimplification of a typical missile since the entire aft-fuselage/flipper combination was assumed to be hinged in the example problem.

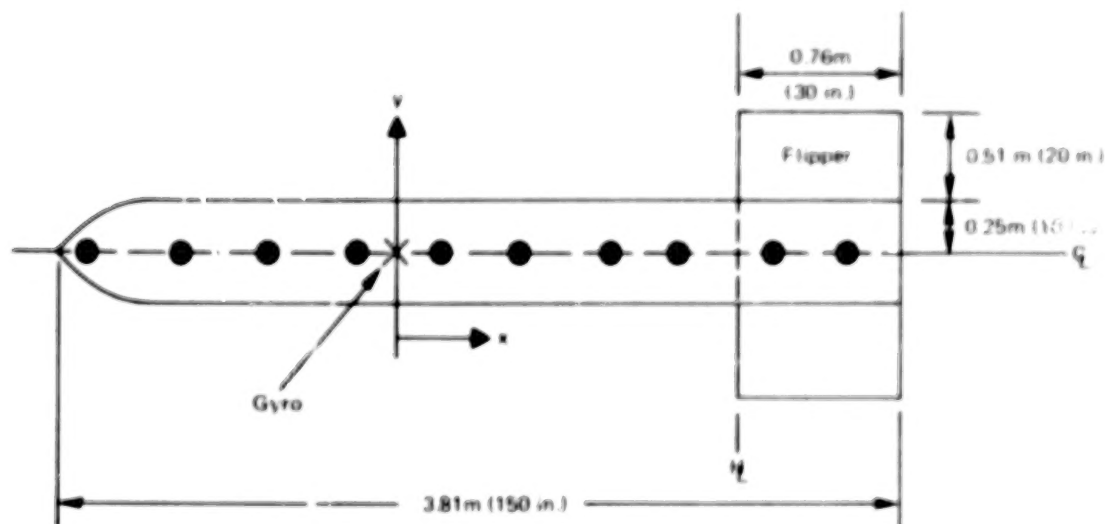


Figure 20. Uniform Missile-Flipper Idealization.



For the numerical example, the missile was assumed to weigh 454 kg (1000 lbs.), to be 3.81 m (150.0 in.) long, and to have a fundamental frequency of 45.0 Hz. The missile was idealized as ten equal concentrated masses connected by a uniform beam as shown in Fig. 20. A rate gyro was located halfway between the fourth and fifth masses and the origin of coordinates was placed there. The structural flexibility was represented by a general element (GENEL) and the flexibility matrix for the missile cantilevered at the origin was taken from Ref. 40. The bending stiffness  $EI$  of the uniform beam was found from the vibration analysis of Ref. 40, and the assumption of the fundamental frequency of  $f_1 = 45.0$  Hz; the bending stiffness was calculated to be  $EI = 3.883 \text{ MNm}^2$  ( $1.353 \times 10^9 \text{ lb-in}^2$ ). The flipper rotation  $\delta$  (positive if trailing edge up) causes mass coupling because of the static unbalance of the flipper about the forward hingeline.

Structural damping was included as a frequency dependent equivalent viscous damping, and the assumed values were  $g_1 = 0.03$  in the first mode,  $g_2 = 0.07$  in the second, and  $g_3 = 0.08$  in the third. From the fundamental frequency  $f_1 = 45.0$  Hz and the vibration analysis of Ref. 40, the higher frequencies were found to be  $f_2 = 125.4$  Hz and  $f_3 = 248.2$  Hz. The damping-frequency sets provided the data necessary for the tabular damping format.

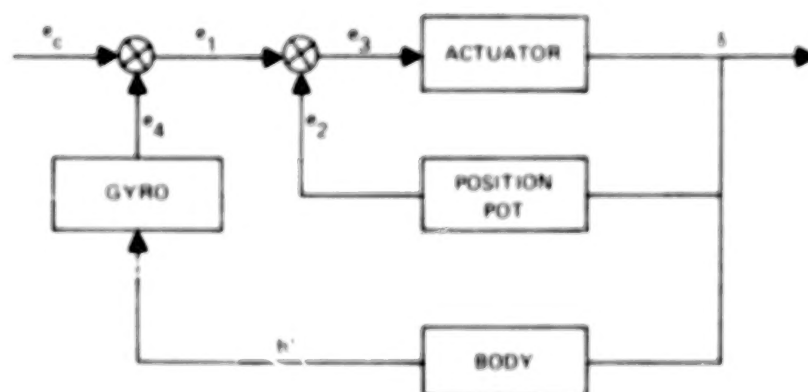


Figure 21. Missile Servo Block Diagram

The servo block diagram is shown in Fig. 21. It is also an oversimplification of a typical air-to-air missile control system. The signals in Fig. 21 denoted by  $e_i$  generally represent voltages or quantities equivalent to voltages output by the various servo elements. The transfer functions were chosen as the following. For the command error,

$$e_1 + e_4 = e_c = 0,$$

for the position potentiometer,

$$e_2/\delta = K_p,$$

for the servoposition error,

$$e_3 - e_1 + e_2 = 0,$$

for the actuator,

$$e_3/\delta = K_a p / (T_a p + 1),$$

in which  $p$  denotes the Laplace transform operator, and for the rate gyro,

$$e_4/\frac{\partial h}{\partial x} = K_g p / (p^2/\omega_g^2 + 2\zeta_g p/\omega_g + 1).$$

The numerical values assumed for the servo time constants were  $K_a = 0.1667$  deg. per deg/sec,  $T_a = 0.01$  sec.,  $K_p = 1.0$  deg/deg,  $\omega_g = 60.0$  Hz = 376.99 rad/sec,  $\zeta_g = 0.70$ , and  $K_g = 0.3$  deg. per deg/sec.

The solution to this problem proceeded through several stages, all in one run on the computer. The first stage was the vibration analysis which obtained the two rigid body modes of pitching and plunging and the first three free-free vibration modes with the locked flipper. Then the modal formulation was made including the coupling with the flipper and servo degrees of freedom. The solution to the modal servoeelastic eigenvalue

problem was carried out by the QR-Transform Method which requires (in NASTRAN) a nonsingular mass matrix. This requirement was met by differentiating the servo equations a sufficient number of times so that all servo elements effectively became second-order systems; the servo equations required seven differentiations, which added seven zero roots to the eigenvalue analysis resulting in a 20th-order eigenvalue problem with 20 real or complex conjugate roots. The roots consisted of: four zero roots from the two rigid body modes; one real actuator damping root; a complex conjugate pair for the rate-gyro; three complex conjugate pairs from the three vibration modes; and the seven zero roots artificially added to use the QR-Transform eigenvalue extraction method.

The nonzero real root and the four complex roots with positive imaginary parts are shown in Table 2 with their corresponding frequencies and damping coefficients. An unsatisfactory design is seen to exist from the negative damping in the second bending mode; the missile will "buzz" in this mode. However, because this example was only illustrative, we were not concerned with any redesign of the oversimplified system.\* The next example shows the effect of atmospheric flight on this configuration.

TABLE 2. - CLOSED LOOP SERVOELASTIC EIGENVALUES, FREQUENCIES AND DAMPING VALUES

Mode	Eigenvalue	Frequency (Hz)	Damping Coefficient
Actuator	-4.840	0.0	0.00385
Rate-Gyro	-260.6+i188.9	30.06	2.759
First Bending	-1.959+i333.1	53.01	0.0118
Second Bending	+135.6+i835.4	133.0	-0.3246
Third Bending	-266.1+i1537.8	244.7	0.3461

\*Subsequent review of this example determined that the correct actuator transfer function should have been  $\delta/e_3 = K_a/p(T_ap+1)$ . This probably explains the "instability."

Aeroservoelastic Stability Analysis. — The effect of atmospheric flight was added to the previous missile-flipper example by using the subsonic Doublet-Lattice/Body aerodynamic theory. This provided air loads on the fuselage and the flipper and accounted for the interference between them. Flight at sea level was assumed at the two velocities of 152.4 m/s (500 fps) and 304.8 m/s (1000 fps), although the air was also assumed to be incompressible (Mach number  $M = 0.0$ ). The planform geometry is shown in Fig. 20. The body has a constant diameter of 0.51 m (20 in.) except in the 0.38 m (15 in.) near the nose where the body tapers to a point. The rectangular flipper had an exposed semispan of 0.51 m (20 in.) and a chord of 0.76 m (30 in.). The flipper chord was used as the reference chord in the unsteady aerodynamic analysis. The aerodynamic idealization consisted of nine boxes on the flipper (one side), six slender body elements on the fuselage and two interference elements between the flipper and the fuselage. The aerodynamic downwashes were found from the motions of the mass points by interpolation; two linear interpolations were made, one for the flipper and the other for the fuselage. The aerodynamic loads were computed from the theory at three reduced frequencies  $k = 0.001$ , 0.2, and 0.4; linear spline interpolation was used for intermediate frequencies, and linear extrapolation was used for  $k > 0.4$ .

The stability analysis was carried out using the PK-method of flutter analysis. This approach led not only to more meaningful estimates of the damping in each of the aeroelastic modes but also led to the rigid body flight characteristics (in this example, the frequency and damping of the short period mode). The results of interest are shown for the two velocities in Tables 3 and 4. There is a difference between the sign conventions for damping coefficients between Table 2 and Tables 3 and 4. The usual sign convention is used in Table 2 in which positive damping indicates stability, whereas, in Tables 3 and 4, the flutter sign convention is used which was established relative to the concept of the artificial structural damping required to sustain an assumed harmonic motion, so that in Tables 3 and 4 a negative damping indicates stability. Table 3 shows the results for  $V = 152.4$  m/s (500.0 fps). The numerical values in parentheses are the results from the first iteration corresponding to  $k = 0.0$  in the PK-flutter solution; the

TABLE 3. — AEROSERVOELASTIC EIGENVALUES, REDUCED FREQUENCIES, FREQUENCIES AND DAMPING VALUES AT SEA LEVEL AT  
V = 152.4 m/s (500 fps)

Mode	Eigenvalue	Reduced Frequency	Frequency (Hz)	Damping Coefficient
Actuator	(-1.694)*	(0.0)	(0.0)	(-0.00135)
Short Period	(-3.165+i13.15)	(0.0329)	(2.093)	(-0.4813)
	-3.172+i13.12	0.0328	2.088	-0.4836
Rate-Gyro	(-260.7+i189.0)	(0.4724)	(30.08)	(-2.759)
	-260.7+i189.0	0.4726	30.09	-2.759
First Bending	(-2.022+i332.8)	(0.8321)	(52.97)	(-0.0122)
	-2.039+i332.6	0.8316	52.94	-0.0123
Second Bending	(135.3+i834.8)	(2.087)	(132.9)	(+0.3242)
	135.5+i834.7	2.087	132.8	+0.3246
Third Bending	(-266.3+i1537.9)	(3.845)	(244.8)	(-0.3463)
	-266.0+i1537.6	3.844	244.7	-0.3460

\* Values in parentheses are first estimates based on  $k = 0.0$ .

TABLE 4. -- AEROSERVOELASTIC EIGENVALUES, REDUCED FREQUENCIES, FREQUENCIES AND DAMPING VALUES AT SEA LEVEL AT  
 $V = 304.8 \text{ m/s (1000 fps)}$

Mode	Eigenvalue	Reduced Frequency	Frequency (Hz)	Damping Coefficient
Actuator	$(-1.822)^*$	(0.0)	(0.0)	(-0.00725)
Short Period	$(-5.409 \pm i26.72)$	(0.0334)	(4.253)	(-0.4048)
	$-5.415 \pm i26.66$	0.0333	4.242	-0.4063
Rate-Gyro	$(-260.0 \pm i188.2)$	(0.2352)	(29.95)	(-2.763)
	$-260.0 \pm i188.3$	0.2354	29.97	-2.762
First Bending	$(-2.154 \pm i332.2)$	(0.4152)	(52.87)	(-0.0130)
	$-2.179 \pm i331.9$	0.4149	52.82	-0.0131
Second Bending	$(135.1 \pm i833.9)$	(1.0424)	(132.7)	(+0.3240)
	$135.3 \pm i833.7$	1.0421	132.7	+0.3246
Third Bending	$(-266.7 \pm i1537.8)$	(1.922)	(244.7)	(-0.3469)
	$-266.4 \pm i1537.4$	1.922	244.7	-0.3465

\* Values in parentheses are first estimates based on  $k = 0.0$ .

# CONTENTS

	Page	
LIST OF TABLES . . . . .	v	1/A7
LIST OF FIGURES . . . . .	vi	1/A8
LIST OF SYMBOLS . . . . .	ix	1/A11
SUMMARY . . . . .	1	1/A14
INTRODUCTION . . . . .	1	1/A14
AEROELASTIC METHODS . . . . .	5	1/B4
Aeroelastic Rigid Formats . . . . .	11	1/B10
Flutter Methods . . . . .	15	1/B12
The K-method of Flutter Solution . . . . .	11	1/B13
The KE-method of Flutter Solution . . . . .	16	1/C1
The PK-method of Flutter Solution . . . . .	17	1/C2
Frequency Response and Random Analysis . . . . .	25	1/C8
Frequency Response . . . . .	25	1/C8
Random Analysis . . . . .	29	1/C14
Transient Analysis by the Fourier Transform Method . . . . .	56	1/D7
Transient Analysis by the Fourier Method . . . . .	56	1/D7
Transformation of Loads . . . . .	59	1/D10
Calculation of Frequency Response . . . . .	11	1/D12
Inverse Transformation of the Response . . . . .	12	1/D13
Practical Considerations for Use of the Fourier Methods . . . . .	11	1/E1
AERODYNAMIC INFLUENCE COEFFICIENTS . . . . .	45	1/E2
Doublet-Lattice Method . . . . .	18	1/E5
Subsonic Wing-Body Interference Theory . . . . .	18	1/E5
Mach Box Method . . . . .	51	1/E11
Strip Theory . . . . .	56	1/E13
Piston Theory . . . . .	57	1/E14
Interconnection Between Structural and Aerodynamic Forces . . . . .	57	1/E14
Theory for Surface Splines . . . . .	59	1/F2
Theory for Linear Splines . . . . .	61	1/F4
Linear Splines . . . . .	61	1/F4
Torsion Bars . . . . .	64	1/F7
Attachment of Splines with Elastic Springs . . . . .	65	1/F8
Rigid Arms on Linear Splines . . . . .	66	1/F9
Coordinate Systems and Constraints . . . . .	66	1/F9

	Page	
DEMONSTRATION PROBLEMS . . . . .	60	1/F9
Flutter Analysis . . . . .	68	1/F11
Swept Wing . . . . .	68	1/F11
The BAH Wing . . . . .	71	1/G3
Servoelastic Stability Analysis . . . . .	79	1/G8
Aeroservoelastic Stability Analysis . . . . .	83	1/G12
Inverse Fourier Transform Characteristics . . . . .	86	2/A3
Aeroelastic Response Analysis . . . . .	96	2/A13
Discrete Gust Response . . . . .	96	2/A13
Random Gust Response . . . . .	98	2/B3
Transient Rolling Maneuver . . . . .	100	2/B5
REFERENCES . . . . .	104	2/B11



converged results for  $k > 0.0$  are shown without parentheses. The only large effect of the airstream that was observed (in comparison with Table 2) was a reduction in the actuator damping from 0.00385 to 0.00135. The short period mode showed up in place of the rigid body pitching mode and its reduced frequency was  $k = 0.0328$  and its damping coefficient was  $2\gamma = -0.4836$ . Table 4 gives the results for  $V = 304.8$  m/s (1000 fps). Although the air-speed is doubled over that in Table 3, a comparison with Table 3 still shows no additionally significant effect of the airstream except the change in the short period frequency. The airstream had no effect on the second bending "buzz" mode: the unstable damping coefficient remained at 0.3246\*. At the higher velocity the short period reduced frequency has increased slightly to  $k = 0.0333$  and the damping coefficient has decreased to  $2\gamma = -0.4063$ .

It should be noted that the aerodynamic forces in the bending modes were not determined accurately because of the high values of reduced frequency. One obvious source of error was the extrapolation above  $k = 0.4$ . However, a more fundamental source of error was the small number of aerodynamic boxes per wave length at the high frequencies.

#### Inverse Fourier Transform Characteristics

A limited study of the Inverse Fourier Transform (IFT) characteristics is presented in Figs. 22 through 28. The example used was a damped oscillator with a unit mass, an undamped frequency of  $f_0 = 5.0$  Hz, and a damping coefficient of  $g_a = 0.1$ . The forcing function was chosen as a unit impulse function. The equation of motion is

$$(p^2 + g_a \omega_0 p + \omega_0^2)u = [p^2 + 0.1 (10\pi)p + (10\pi)^2]u = \delta(t)$$

The frequency response was determined for selected equally or unequally spaced frequencies and a cut-off frequency of 15.0 Hz (3 times  $f_0$ ); the response was calculated for five cycles or 1.0 seconds. All three Inverse Fourier Transform Methods discussed above under Inverse Transformation of the Response

---

\* Note again that an incorrect actuator transfer function was used.

were studied: Method 0 (IFTM = 0), Method 1 (IFTM = 1), and Method 2 (IFTM = 2). No attempt has been made to evaluate the effect of the cut-off frequency on convergence of the responses except to note that the transient was quite close to the exact solution in the case of 61 equally spaced frequencies (Case FREQ105) as shown in Table 5 for IFTM = 0 and 2; excessive damping for IFTM = 1 is apparent in the table and has generally been observed in all the transients using IFTM = 1. The exact solution is:

$$u(t) = 0.03187085 \exp(-1.570796t) \sin 31.376632t$$

The case of FREQ105 with IFTM = 2 is regarded as the most accurate and its computer solution is compared with all the other solutions in Figs. 22 through 28. Case FREQ104 consists of 31 equally spaced frequencies. The other five cases have unequally spaced frequencies. FREQ106 consists of the 21 frequencies: 0.0, 1.0, 2.0, 3.0, 3.5, 4.0, 4.25, 4.5, 4.75, 5.0, 5.25, 5.5, 5.75, 6.0, 6.5, 7.0, 8.0, 9.0, 10.0, 12.5, and 15.0 Hz. The remaining four cases have frequencies selected from FREQ106. FREQ107 consists of the six frequencies of 0.0, 4.0, 5.0, 6.0, 10.0, and 15.0 Hz. FREQ109 consists of the frequencies of FREQ107 with 4.5 and 5.5 Hz added. FREQ111 adds 4.75 and 5.25 Hz to FREQ109, and, finally, FREQ112 adds 3.0 and 7.0 Hz to FREQ111.

A perusal of Figs. 22 through 28 (facilitated by use of dividers) permits some tentative conclusions that deserve further investigation. The range of

TABLE 5. - COMPARISON OF EXACT SOLUTION WITH IFT RESPONSE FOR FREQ105

t(sec)	Exact u(t)	IFTM = 0	IFTM = 1	IFTM = 2
0.05	0.029 463	0.031 181	0.030 168	0.030 182
0.25	0.021 520	0.021 717	0.021 443	0.021 718
0.45	0.015 716	0.015 831	0.015 190	0.015 828
0.65	0.011 477	0.011 554	0.010 595	0.011 538
0.85	0.008 381	0.008 437	0.007 268	0.008 389

the vertical scales in Figs. 22 through 28 is  $-0.04 < u < 0.04$ . Beginning with Fig. 22, the case of 61 equally spaced frequencies, we observe, as in Table 5, no difference between IFTM = 0 and 2, but greater damping for IFTM = 1. In Fig. 23, the case of 31 equally spaced frequencies, IFTM = 0 gives the most accurate solution while IFTM = 2 has more damping; IFTM = 1 has excessive damping. The case of 21 unequally spaced frequencies is typical of practical applications and in Fig. 24 we see IFTM = 2 is very close to the exact solution, IFTM = 1 is also close but with more damping, but that IFTM = 0 is inaccurate, particularly in the last cycle. Figures 25 through 28 consider less frequencies in an attempt to determine some minimum number required for acceptable accuracy. Figure 25 shows the case of only 6 frequencies and no accuracy whatsoever is obtained. Adding two frequencies near the resonance in Fig. 26 shows an improvement for IFTM = 1 and 2 with IFTM = 2 being more accurate, but IFTM = 0 again does not give any accuracy. Adding two more frequencies in Fig. 27 improves the accuracy for IFTM = 2 considerably and for IFTM = 1 somewhat, but no significant improvement is found for IFTM = 0. The final results in Fig. 28 for 12 frequencies show that for IFTM = 2, the exact solution is approximated very well, for IFTM = 1 some small errors still exist, and for IFTM = 0 still no improvement is forthcoming.

Based on this limited investigation, it may be concluded that IFTM = 2 gives the most accurate results when the frequencies are unequally spaced, and that IFTM = 0 gives unreliable results for unequal spacing. For IFTM = 1 the results exhibit more damping than is actually present. The accuracy achieved for IFTM = 2 with 10 and 12 frequencies indicates that at least 7 frequencies are necessary to define the frequency response near a resonant peak in order to obtain reasonable accuracy in the transient response.

The foregoing conclusions have been based on a lightly-damped, single degree-of-freedom system loaded impulsively. More thorough investigations are recommended for two- (and more) degree-of-freedom systems with even less damping and for more general transient loadings. The effect of cut-off frequency, which in this case was three times the resonant frequency, should also be investigated.

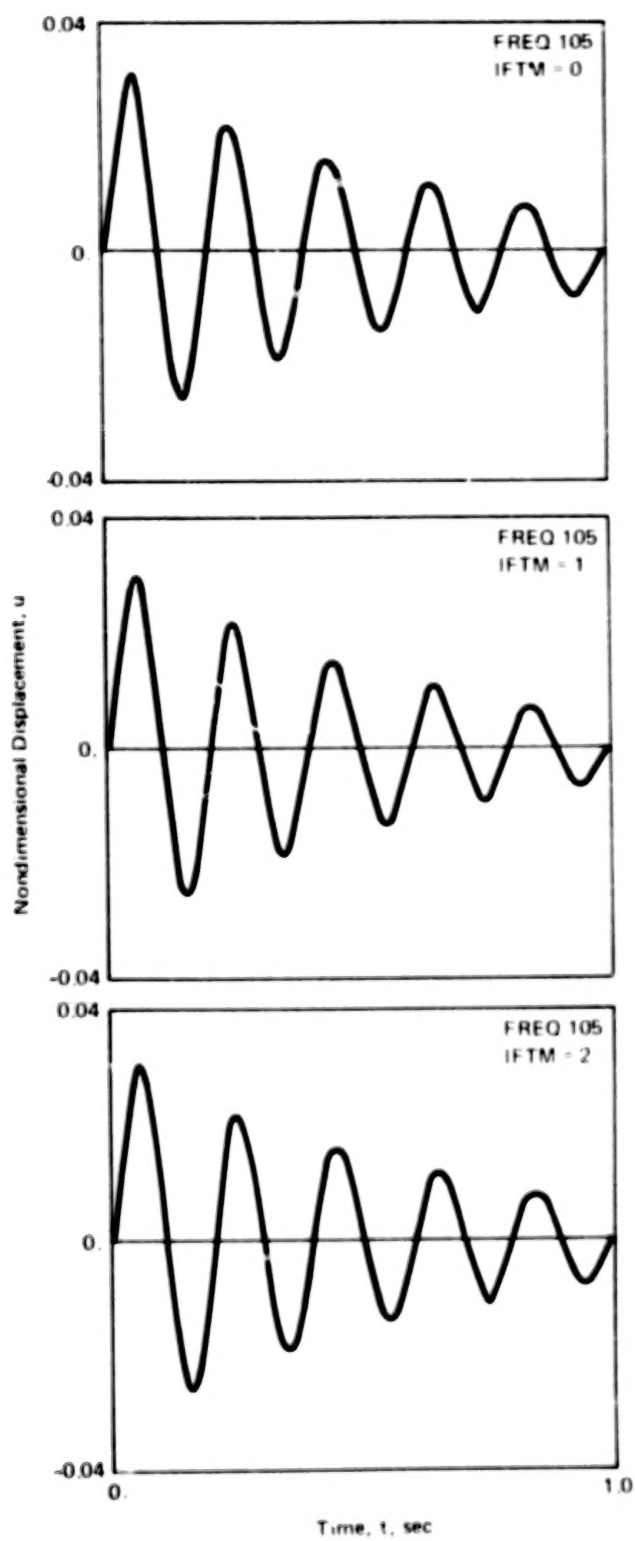


Figure 22. Comparison of the Three Inverse Fourier Transform Methods.

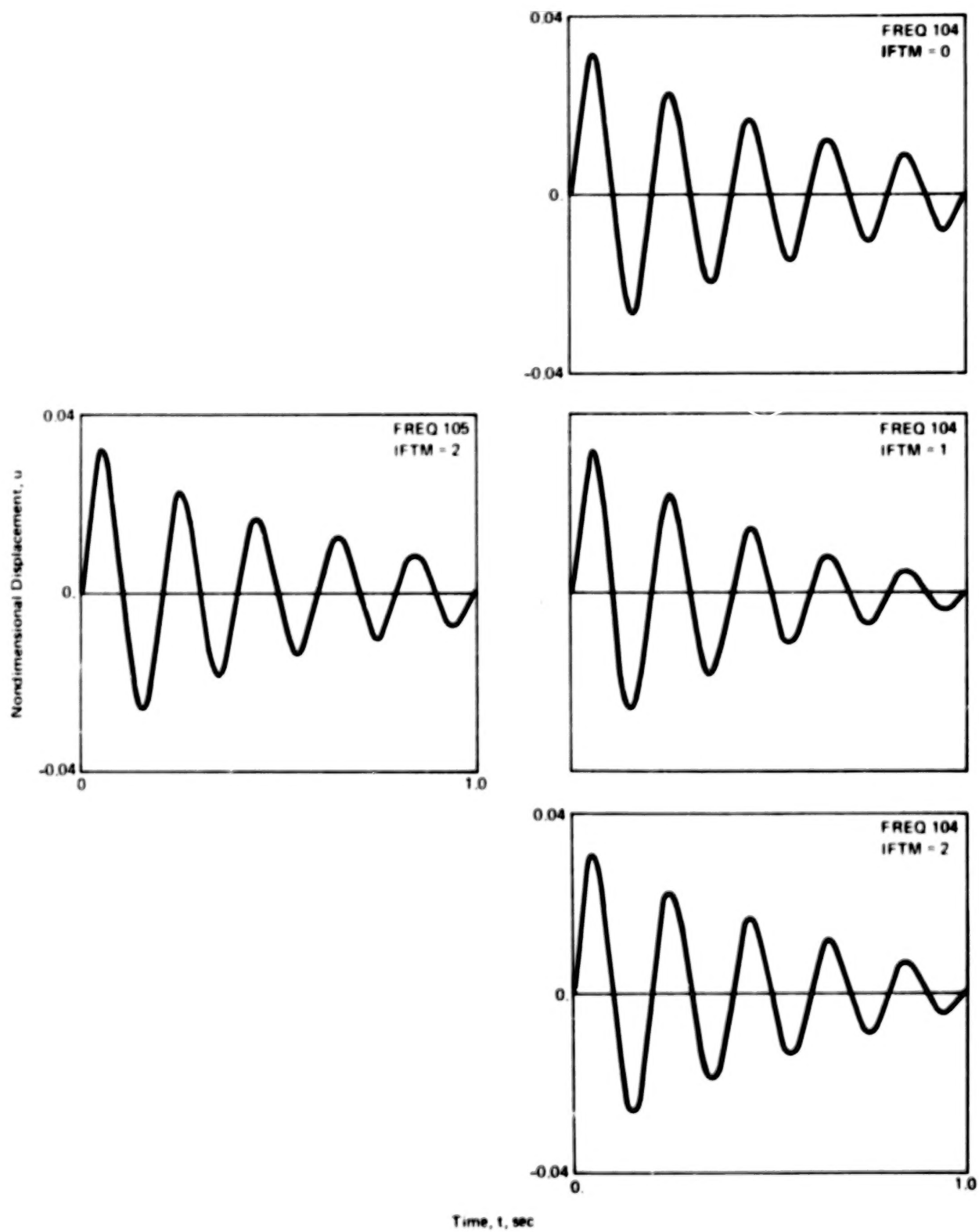


Figure 23. Comparison of FREQ104 (31f's) with Solution (FREQ105, IFTM = 2).

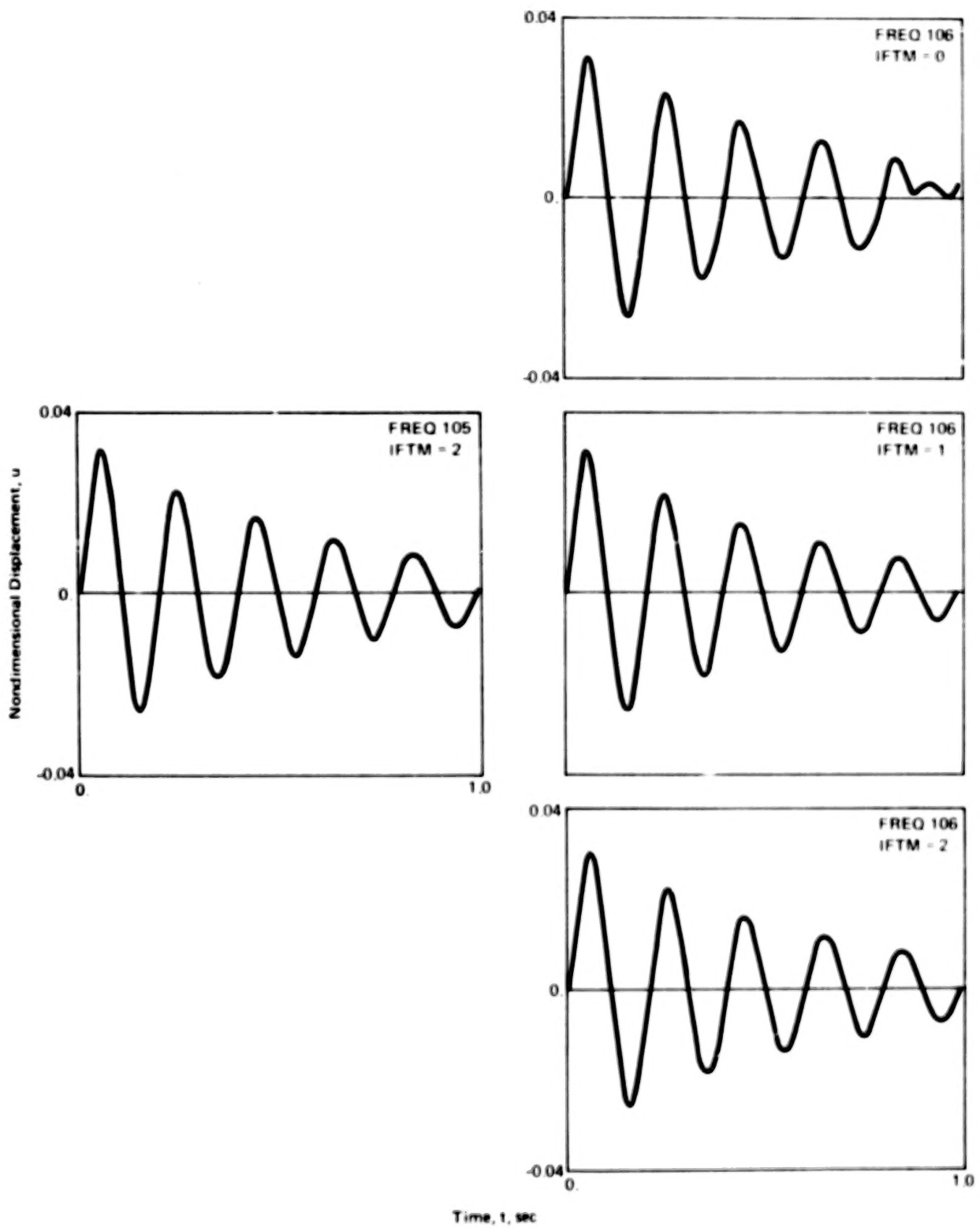


Figure 24. Comparison of FREQ106 (21f's) with Solution (FREQ105), IFTM = 2).

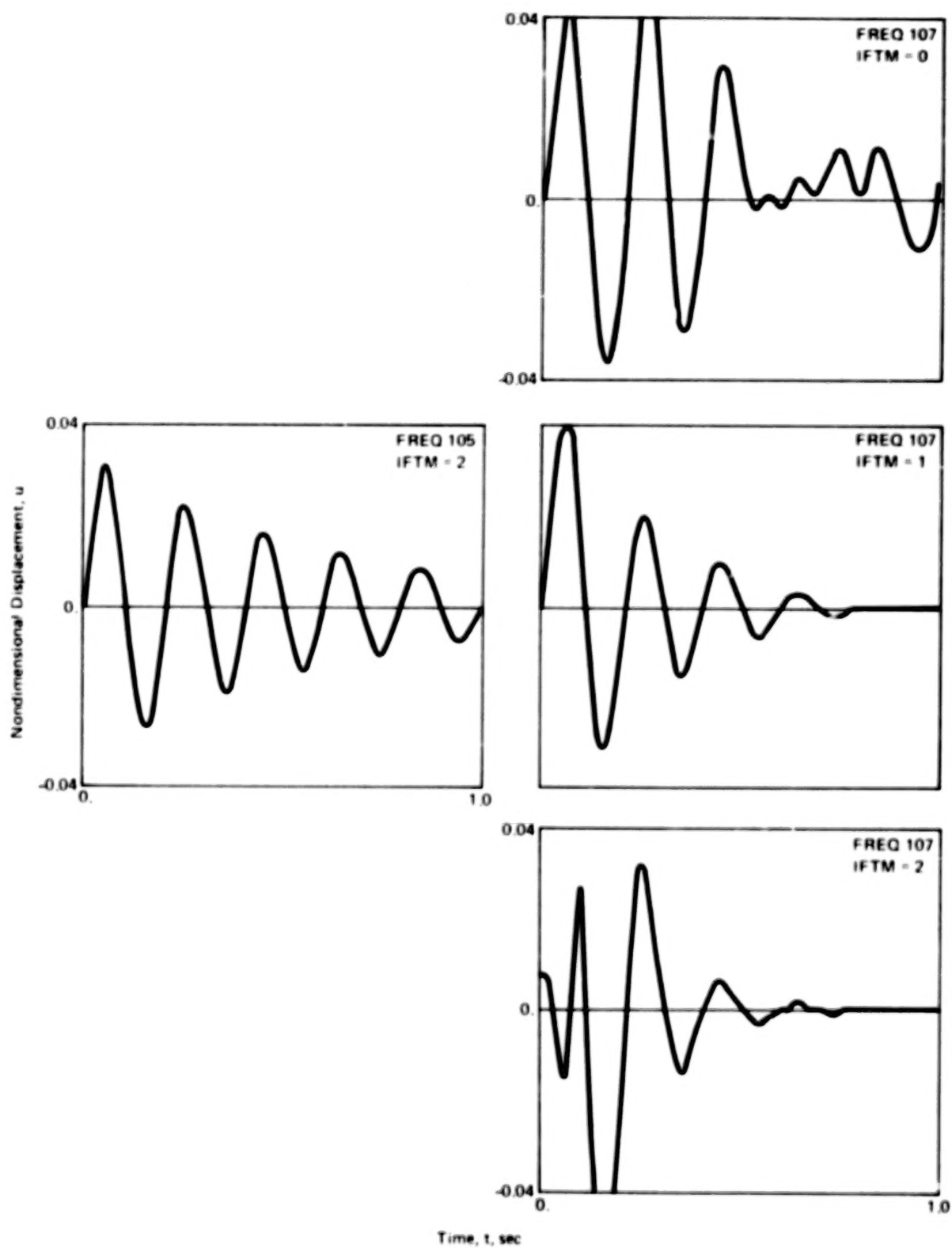


Figure 25. Comparison of FREQ107 (6f's) with Solution (FREQ105, IFTM = 2).

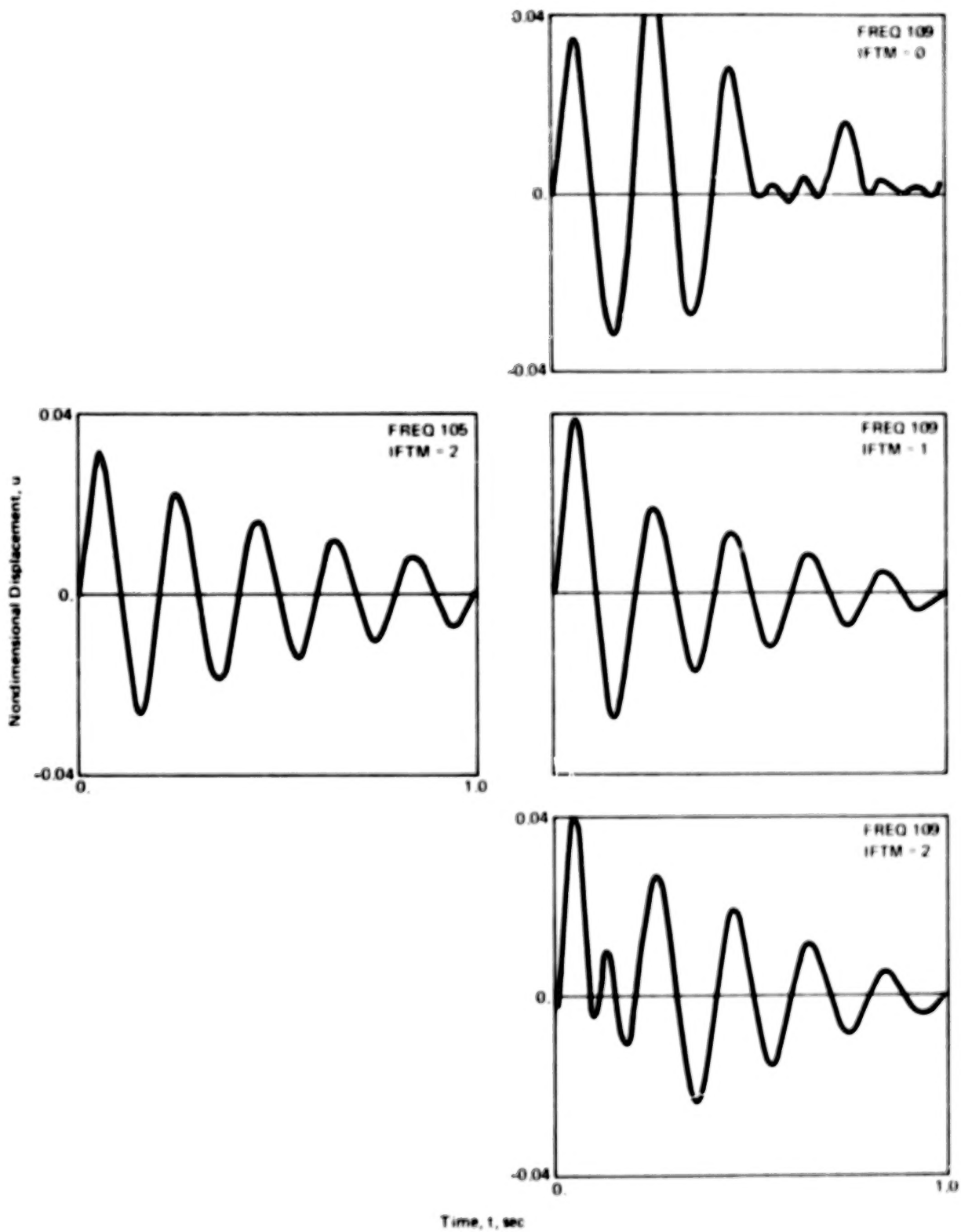


Figure 26. Comparison of FREQ109 (8f's) with Solution (FREQ105, IFTM = 2).



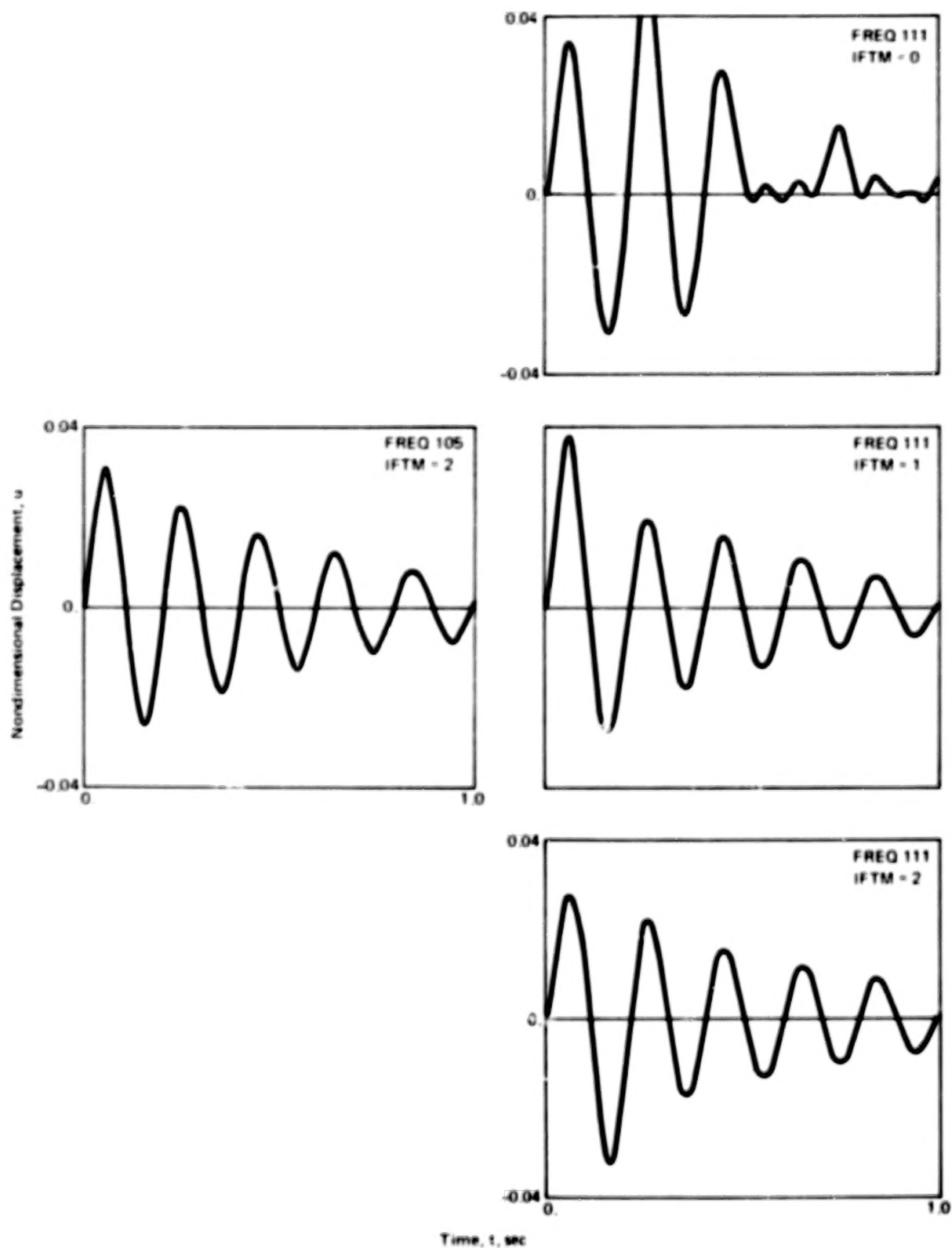


Figure 27. Comparison of FREQ111 (10f's) with Solution (FREQ105, IFTM = 2).

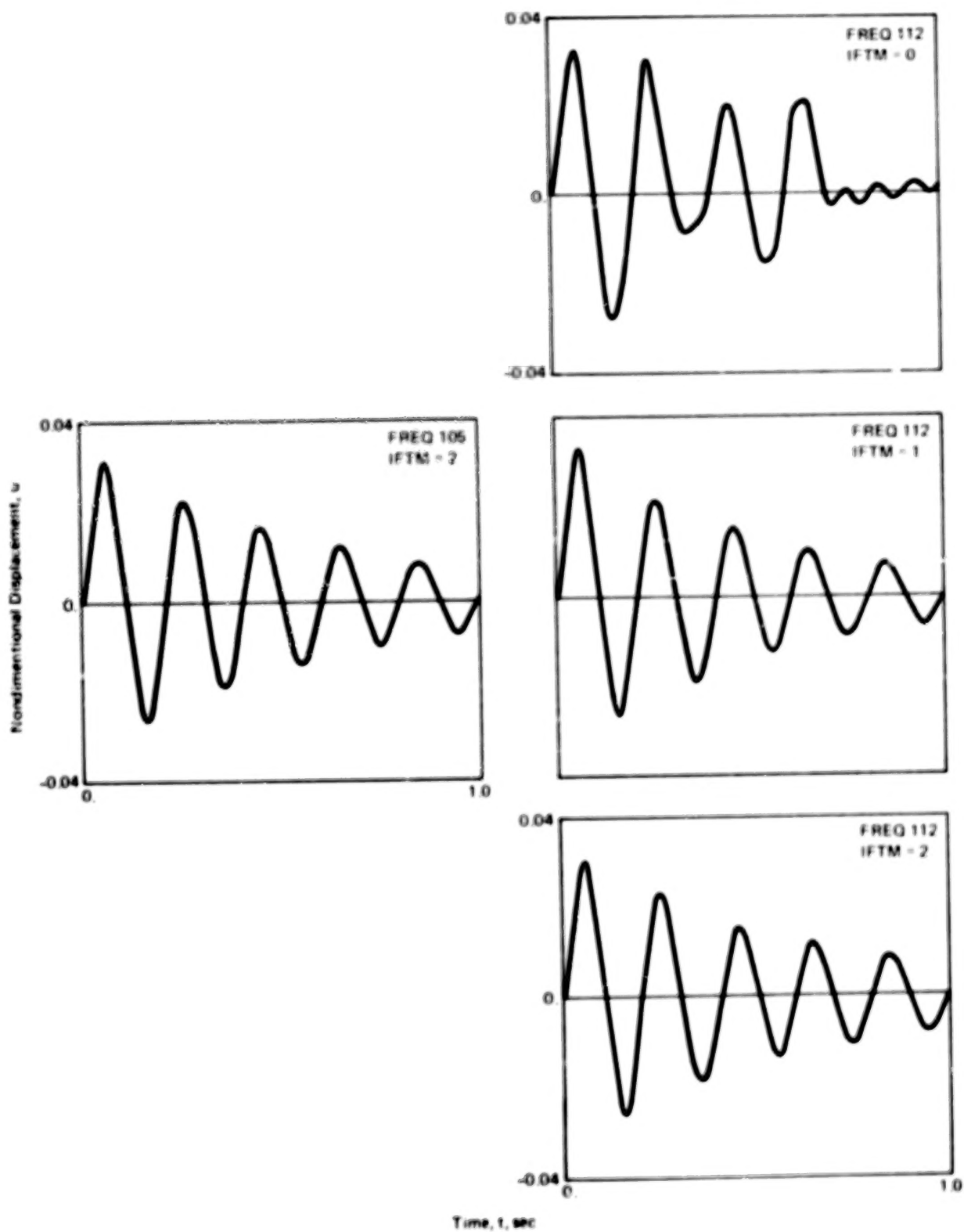


Figure 28. Comparison of FREQ112 (12f's) with Solution (FREQ105, IFTM = 2).

## Aeroelastic Response Analysis

Response analysis is illustrated in three applications to the BAH jet transport wing. The analyses were transient response to a discrete gust, random response to atmospheric turbulence, and transient response to aileron input. Each of these can be compared, to some extent, to the simpler analyses presented in Ref. 16. The structural model was the same as that used in the cantilever flutter analysis above (Fig. 16). However, appropriate rigid body degrees of freedom were permitted. For the discrete and random gust examples, the gust fields were assumed to be symmetric and the aircraft was free to plunge; the pitching and rolling degrees-of-freedom were constrained. For the transient response example, rotation was antisymmetric and the aircraft was free to roll while constrained in pitch and plunge.

Both gust response analyses determined the root bending moment at the side of the fuselage. This required an accurate stress recovery and, hence, all ten of the wing vibration modes were included because NASTRAN uses the Mode Displacement Method (see Ref. 16, pp. 641-650) for stress recovery. The aileron was attached to the wing at its 75%-chord hinge line through a stiff actuator chosen to give an uncoupled aileron rotational frequency of 60 Hz. The aileron was thereby effectively locked in the gust response analyses.

The aerodynamic loads on the wing-aileron combination were calculated by the Doublet-Lattice Method (the only method presently in NASTRAN that considers gust fields as an additional source of downwash) at a Mach number of zero. The planform idealization into 42 boxes is shown in Fig. 29; six boxes were placed on the aileron.

Discrete Gust Response. — Example 10-5 of Ref. 16 (pp. 682-685) calculated the dynamic bending moment at the wing root of the BAH wing at 212 m/s (475 mph) due to a sharp-edged gust, taking into consideration the plunging of the airplane and the fundamental bending mode of the wing and assuming quasi-steady aerodynamic strip theory was satisfactory. The comparison can therefore only be qualitative because of the use of many more vibration modes and unsteady aerodynamic lifting surface theory herein.

**BLANK**

**PAGE**



To simulate the sharp-edged gust in the Fourier transform approach, it was necessary to use a square-wave gust profile of sufficient duration to permit the peak response to occur and then to allow a sufficiently long period such that the response has damped out reasonably well before the next period begins. The square-wave gust profile and the response are shown in Fig. 30. The positive and negative cycles of the square-wave were each chosen as 1.0 sec. and the period was selected as 4.0 secs. The peak response occurred at about 25 semichords into the gust and the response was fairly well damped at the end of the period. The inset in Fig. 30 is Fig. 10-24 of Ref. 16 and the qualitative comparison was good: the NASTRAN peak response is 26 MN·m ( $1.9 \times 10^7$  lb-ft) in a distance of 25 semichords as compared to 23 MN·m ( $1.7 \times 10^7$  lb-ft) in 23 semichords in the simpler solution.

Random Gust Response. — Example 10-6 of Ref. 16 (pp. 691-694) calculates the power spectrum of the root bending moment of the BAH wing at 212 m/s (475 mph) with the same vibration modes and aerodynamic assumptions as in the discrete gust study above, and with the empirical power spectrum of atmospheric turbulence defined by

$$\Phi(\omega/U) = \frac{0.060}{0.000004 + (\omega/U)^2} \quad (136)$$

Because this empirical spectrum is not a standard form in NASTRAN (like the Dryden or von Kármán forms), it must be input in the tabular format. This input provided the frequency content of the gust for the random analysis in a similar manner that the gust profile provided the gust time history for the transient analysis.

The frequency response to the harmonic gust field is shown in Fig. 31. The NASTRAN solution showed a larger peak than Ref. 16; apparently, the lifting surface aerodynamic loads had less damping than the strip theory quasi-steady aerodynamic loads. The power spectral densities of the root bending moment are compared in Fig. 32. The NASTRAN solution had a slightly

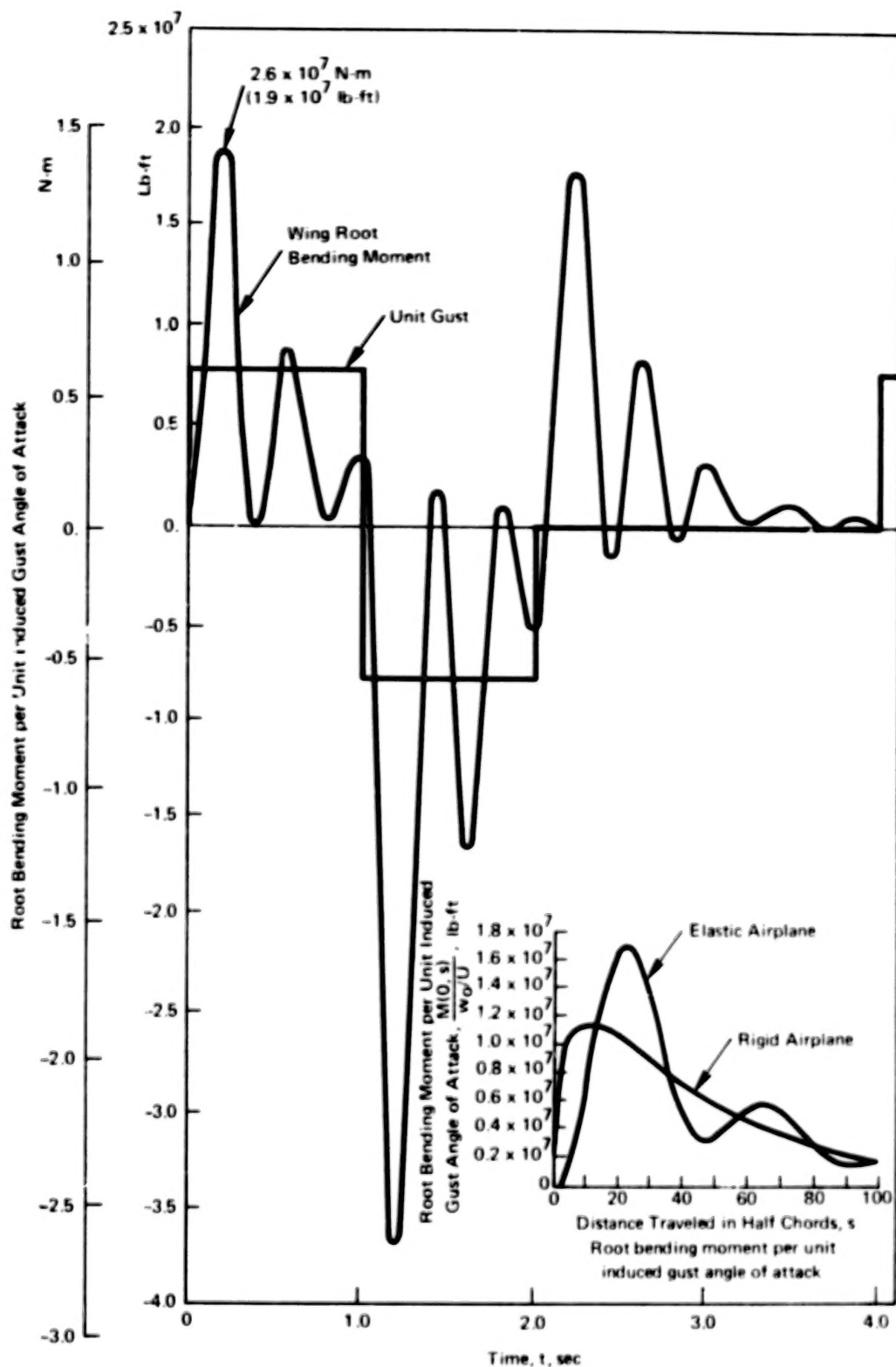


Figure 30. Root Bending Moment per Unit Induced Gust Angle of Attack for BAH Wing due to a Sharp Unit Gust Loading.

lower first peak and a higher second peak, but the average (rms) value is about the same as that obtained in Ref. 16:

$$\bar{A} = \frac{\bar{M}^2 \text{ (elastic)}}{\bar{W}_g^2} = 71.2 \text{ kN}\cdot\text{s} \text{ (} 1.60 \times 10^4 \text{ lb}\cdot\text{sec)}$$

while the NASTRAN value is  $\bar{A} = 74.3 \text{ kN}\cdot\text{s} \text{ (} 1.67 \times 10^4 \text{ lb}\cdot\text{sec)}$ . NASTRAN also obtained the mean frequency of zero crossings as  $N_0 = 1.69 \text{ Hz} = 0.0501 \text{ rad/m}$  (0.0152 rad/ft).

Transient Rolling Maneuver. — Example 8-4 of Ref. 16 (pp. 467-469) calculated the aileron effectiveness of the BAH wing as a function of Mach number using aerodynamic strip theory. The effectiveness was analyzed there as a static aeroelastic problem. The NASTRAN analysis treats the aileron roll as a dynamic maneuver. The desired unit aileron deflection was obtained by applying a hinge moment to the stiff actuator spring. Because of the high actuator stiffness, the relative rotation between the aileron and the wing was proportional to the applied hinge moment. As in the discrete gust response analysis above, the Fourier transform method required a square-wave time history of the forcing function. At 212 m/s (475 mph), right aileron was applied for 1.0 sec. Then the ailerons were neutralized for 2.0 seconds, long enough for the roll rate to damp out reasonably well before the next period. The roll response of the maneuver is shown in Fig. 33. The history was unsymmetrical since the single degree-of-freedom roll can begin from any bank angle and no initial conditions are imposed in the Fourier analysis. However, it was the roll rate that was of interest rather than the bank angle and the steady roll rate (the slope of the bank angle vs. time curve) is seen in Fig. 33 to be  $p = 0.27 \text{ rad/sec}$ . and the rolling helix angle is  $p\ell/2U = 0.16$ . Figure 8-18 of Ref. 16 has been inset into Fig. 33 and a qualitative comparison is shown between the NASTRAN and the earlier estimates of the rolling helix angles. Qualitative agreement is seen between the NASTRAN dynamic Fourier transform solution and the more conventional static aeroelastic analysis.



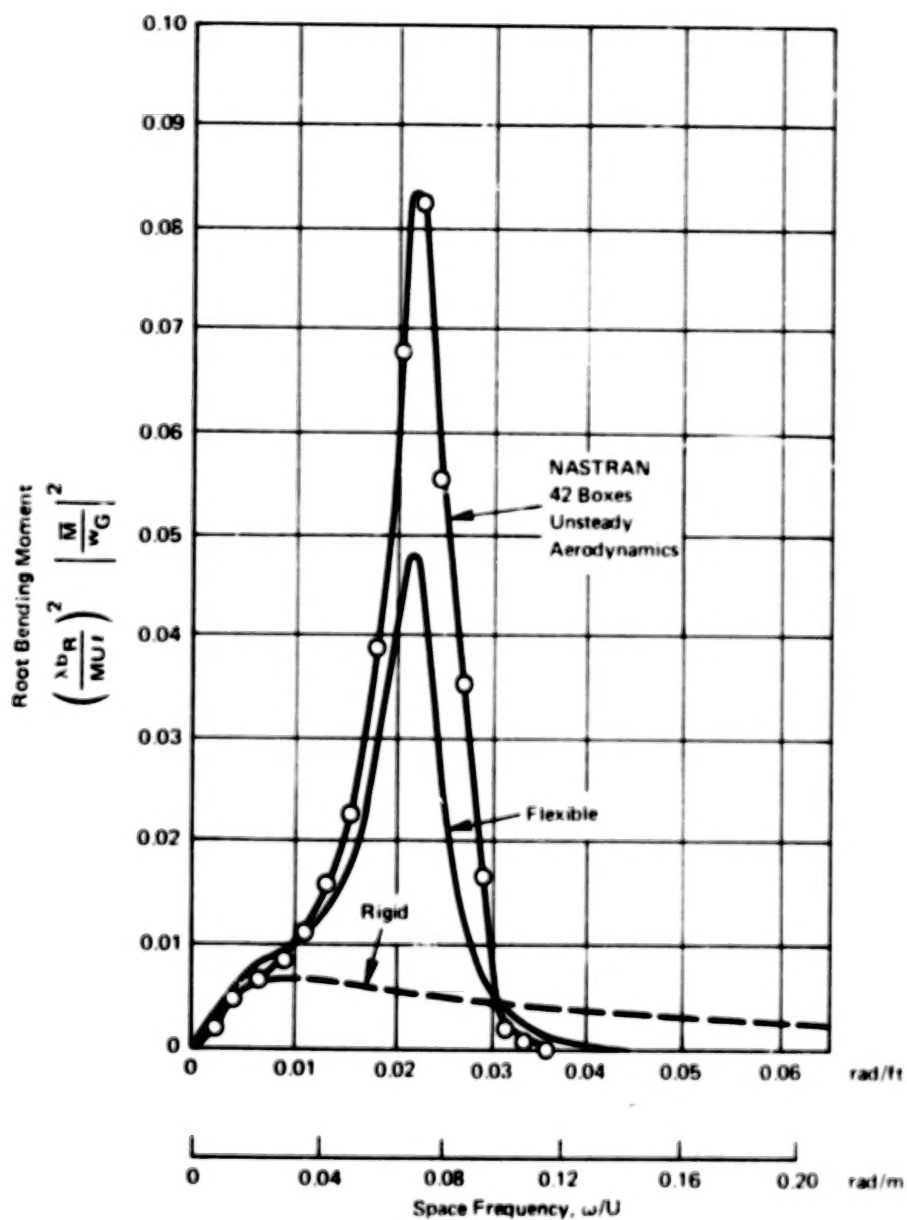


Figure 31. Frequency Response of Root Bending Moment for BAH Wing due to a Random Gust Input.

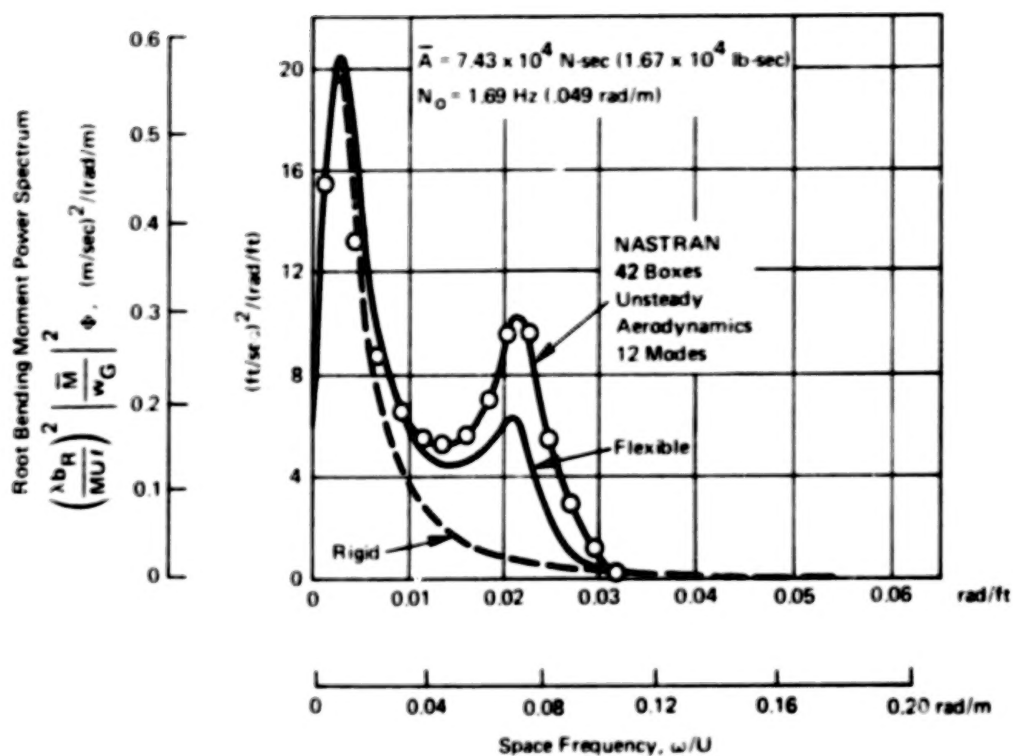


Figure 32. Power Spectral Density of Root Bending Moment for BAH Wing.

**BLANK**

**PAGE**

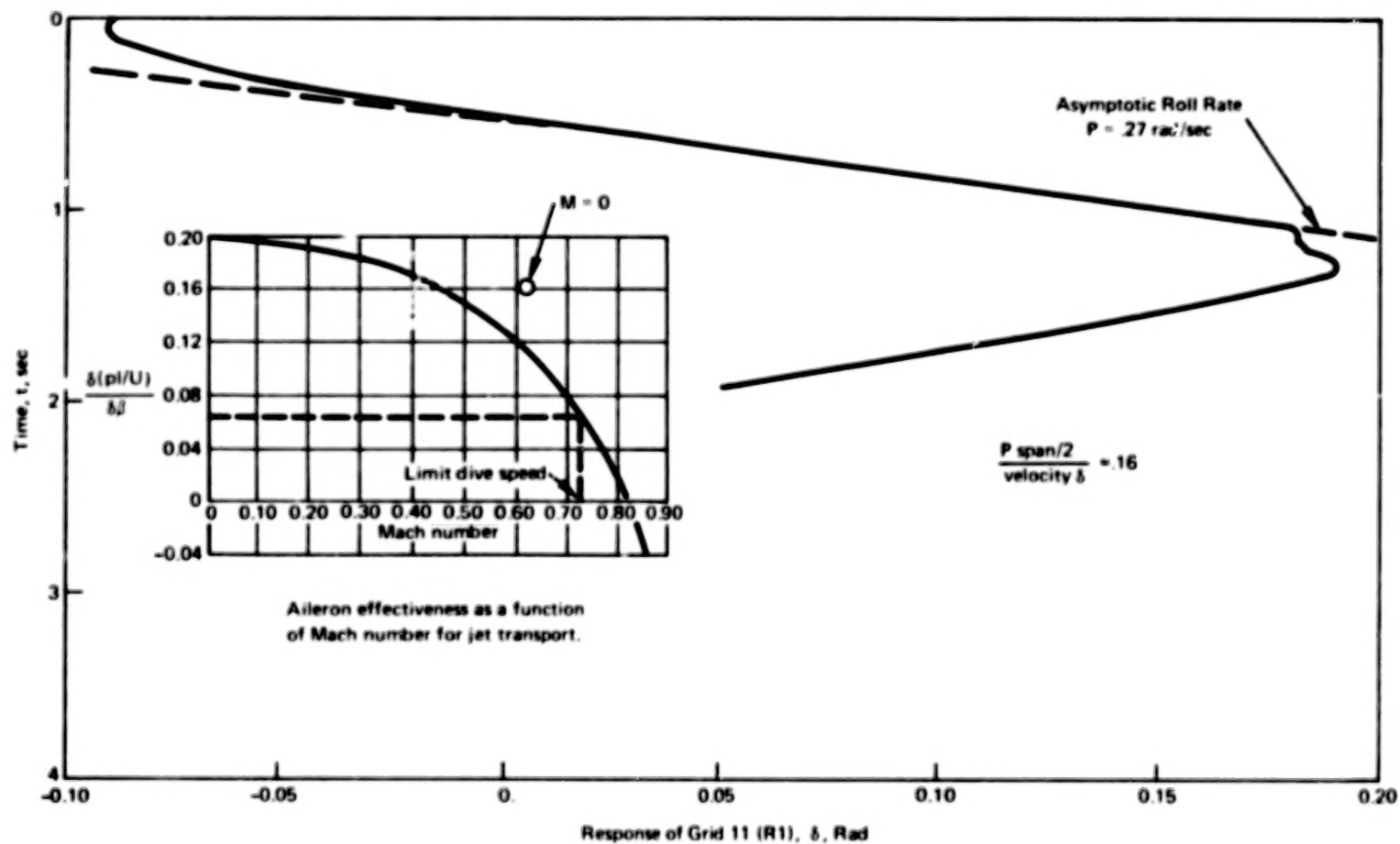


Figure 33. BAH Jet Transport Roll Response.

# REFERENCES

1. Anon., "The NASTRAN Theoretical Manual," NASA SP-221(04), 1978.
2. Anon., "The NASTRAN **User's** Manual," NASA SP-222(04), 1978.
3. Anon., "The NASTRAN Programmer's Manual," NASA SP-223(04), 1978.
4. Harder, R. L., MacNeal, R. H., and Rodden, W. P., "A Design Study for the Incorporation of Aeroelastic Capability into NASTRAN," NASA CR-111918, May 1971.
5. Francis, J. G. F., "The QR Transformation - a Unitary Analogue to the LR Transformation," Parts 1 and 2, *Computer Journal*, Vol. 4, No. 3 (October 1961) and No. 4 (January 1962).
6. Funderlic, R. E., and Rinzel, J., "ALIMAT, A FORTRAN IV Arbitrary Matrix Eigensystem Solver," SHARE Program Library, SDA No. 3411, 2 March 1966.
7. Desmarais, R. N., and Bennett, R. M., "An Automated Procedure for Computing Flutter Eigenvalues," *J. Aircraft*, Vol. 11, No. 2, February 1974, pp. 75-80.
8. Jocelyn Lawrence, A., and Jackson, P., "Comparison of Different Methods of Assessing the Free Oscillatory Characteristics of Aeroelastic Systems," British Aeronautical Research Council, C. P. No. 1084, 1970.
9. Woodcock, D. L., and Jocelyn Lawrence, A., "Further Comparisons of Different Methods of Assessing the Free Oscillatory Characteristics of Aeroelastic Systems," Royal Aircraft Establishment, Tech. Rpt. 72188, 14 Sept. 1972.
10. Hassig, H. J., "An Approximate True Damping Solution of the Flutter Equation by Determinant Iteration," *J. Aircraft*, Vol. 8, No. 11, Nov. 1971, pp. 885-889.
11. Ralston, A., and Wilf, H. S. (Ed), Mathematical Methods for Digital Computers, Vol. II, New York, John Wiley and Sons, Inc., 1968, pp. 116-130.
12. Anon., "Subroutine HSBG," IBM 360 Library Subroutine Manual, Form H20-0205-3, 14 Feb. 1969.
13. Anon., "Subroutine ATEIG," IBM 360 Library Subroutine Manual, Form H20-0205-3, 14 Feb. 1969.
14. Wilkinson, J. H., The Algebraic Eigenvalue Problem, Oxford: Clarendon Press, 1965.
15. Guyan, R. J., "Reduction of Stiffness and Mass Matrices," *AIAA J.*, Vol. 3, No. 2, Feb. 1965, p. 380.

16. Bisplinghoff, R. L., Ashley, H., and Halfman, R. L., Aeroelasticity, Reading: Addison-Wesley Publishing Co., 1955.
17. Taylor, J. (Ed), "Manual on Aircraft Loads," AGARDograph 85, Pergamon Press, 1965, pp. 200-202.
18. Rodden, W. P., and Revell, J. D., "The Status of Unsteady Aerodynamic Influence Coefficients," I.A.S. Fairchild Fund Paper No. FF-53, 23 Jan. 1962.
19. Albano, E., and Rodden, W. P., "A Doublet-Lattice Method for Calculating Lift Distributions on Oscillating Surfaces in Subsonic Flows," AIAA J., Vol. 7, No. 2, Feb. 1969, pp. 279-285, and Vol. 7, No. 11, Nov. 1969, p. 2192.
20. Rodden, W. P., Giesing, J. P., and Kálmán, T. P., "Refinement of the Nonplanar Aspects of the Subsonic Doublet-Lattice Lifting Surface Method," J. Aircraft, Vol. 9, No. 1, Jan. 1972, pp. 69-73.
21. Giesing, J. P., Kálmán, T. P., and Rodden, W. P., "Subsonic Unsteady Aerodynamics for General Configurations; Part I, Vol. I - Direct Application of the Nonplanar Doublet-Lattice Method," Air Force Flight Dynamics Laboratory Report No. AFFDL-TR-71-5, Part I, Vol. I, Nov. 1971.
22. Giesing, J. P., Kálmán, T. P., and Rodden, W. P., "Subsonic Unsteady Aerodynamics for General Configurations; Part II, Vol. II - Computer Program N5KA," Air Force Flight Dynamics Laboratory Report No. AFFDL-TR-71-5, Part II, Vol. II, April 1972.
23. Giesing, J. P., Kálmán, T. P., and Rodden, W. P., "Subsonic Unsteady Aerodynamics for General Configurations; Part I, Vol. I - Application of the Doublet-Lattice Method and the Method of Images to Lifting-Surface/Body Interference," Air Force Flight Dynamics Laboratory Report No. AFFDL-TR-71-5, Part II, Vol. I, April 1972.
24. Giesing, J. P., Kálmán, T. P., and Rodden, W. P., "Subsonic Steady and Oscillatory Aerodynamics for Multiple Interfering Wings and Bodies," J. Aircraft, Vol. 9, No. 10, Oct. 1972, pp. 693-702.
25. Pines, S., Dugundji, J., and Neuringer, J., "Aerodynamic Flutter Derivatives for a Flexible Wing with Supersonic and Subsonic Edges," J. Aero. Sci., Vol. 22, No. 10, Oct. 1955, pp. 693-700.
26. Moore, M. T., and Andrew, L. V., "Unsteady Aerodynamics for Advanced Configurations; Part IV - Application of the Supersonic Mach Box Method to Intersecting Planar Lifting Surfaces," Air Force Flight Dynamics Laboratory Report No. FDL-TDR-64-152, Part IV, Feb. 1965.
27. Donato, V. M., and Huhn, C. R., Jr., "Supersonic Unsteady Aerodynamics for Wings with Trailing-Edge Control Surfaces and Folded Tips," Air Force Flight Dynamics Laboratory Report No. AFFDL-TR-68-30, Jan. 1968.

28. Theodorsen, T., "General Theory of Aerodynamic Instability and the Mechanism of Flutter," NACA Report 496, 1955.
29. Kussner, H. G., and Schwarz, I., "Der schwingenden Flügel mit aerodynamisch ausgeglichenem Ruder," *Luftfahrtforschung*, Vol. 17, No. 11/12 Dec. 1940, pp 337-354; translated as "The Oscillating Wing with Aerodynamically Balanced Elevator," NACA TM-991, 1941.
30. Smilg, B., and Wasserman, L. S., "Application of Three-Dimensional Flutter Theory to Aircraft Structures," Army Air Force Tech. Rpt. 4798, July 1942.
31. Ashley, H., and Zartarian, G., "Piston Theory - A New Aerodynamic Tool for the Aeroelastician," *J. Aero. Sci.*, Vol. 23, No. 12, Dec. 1956, pp. 1109-1118.
32. Rodden, W. P., Farkas, E. F., Malcom, H. A., and Kliszewski, A. M., "Aerodynamic Influence Coefficients from Piston Theory: Analytical Development and Computational Procedure," Aerospace Corp., Report No. TDR-169(3230-11)TN-2, 15 Aug. 1962.
33. Van Dyke, M. D., "A Study of Second-Order Supersonic Flow Theory," NACA Report 1081, 1952.
34. Harder, R. L., and Desmarais, R. N., "Interpolation Using Surface Splines," *J. Aircraft*, Vol. 9, No. 2, Feb. 1972, pp. 189-191; see also, Comment and Reply, *J. Aircraft*, Vol. 9, No. 12, Dec. 1972, pp. 869-871.
35. Tuovila, W. J., and McCarty, J. L., "Experimental Flutter Results for Cantilever Wing Models at Mach Numbers Up to 3.0," NACA RM L55E11, June 1955.
36. Rodden, W. P., and Stahl, B., "A Strip Method for Prediction of Damping in Subsonic Wind Tunnel and Flight Flutter Tests," *J. Aircraft*, Vol. 6, No. 1, 1969, pp. 9-17.
37. Jones, W. P., "Aerodynamic Forces on Wings in Non-Uniform Motion," British Aeronautical Research Council, R&M 2117, 1945.
38. Burkhart, T. H., "Subsonic Transient Lifting Surface Aerodynamics," Paper No. 75-758, AIAA, ASME, and SAE 16th Structures, Structural Dynamics and Materials Conference, Denver, Colo., 27-29 May 1975.
39. Rodden, W. P., "A Matrix Approach to Flutter Analysis," Institute of the Aeronautical Sciences, Fairchild Fund Paper No. FF-23, 1959.
40. Rodden, W. P., "A Method for Deriving Structural Influence Coefficients from Ground Vibration Tests," *AIAA J.*, Vol. 5, No. 5, May 1967, pp. 991-1000.

1. Report No. NASA CR-3094		2. Government Accession No.		3. Recipient's Catalog No.	
4. Title and Subtitle Aerelastic Addition to NASTRAN				5. Report Date March 1979	
				6. Performing Organization Code	
7. Author(s) William P. Rodden, Robert L. Harder, and E. Dean Bellinger				8. Performing Organization Report No.	
9. Performing Organization Name and Address  The MacNeal-Schwendler Corp. 7442 N. Figueroa Street Los Angeles, CA 90041				10. Work Unit No. 505-17-23-02	
				11. Contract or Grant No. NAS1-13034	
12. Sponsoring Agency Name and Address  National Aeronautics and Space Administration Washington, DC 20546				13. Type of Report and Period Covered Contractor's Report (Final)	
				14. Sponsoring Agency Code	
15. Supplementary Notes Langley Technical Monitor: Deene J. Weidman Final Report					
16. Abstract  This report describes the additions made to the NASTRAN program to allow analysis of aeroelastic phenomena. Several methods for flutter analysis (termed K, PK, KE methods) are included, as well as the means for calculating random and gust response of aerodynamic surfaces and bodies under fluid flow. Doublet lattice, mach box, and piston theory aerodynamics are all incorporated. Interference between bodies and surfaces is accounted for, and several basic illustrative examples are presented.					
17. Key Words (Suggested by Author(s)) NASTRAN Finite Elements Aerodynamics Aeroelasticity Flutter				18. Distribution Statement  Unclassified - Unlimited Subject Category 02	
19. Security Classif. (of this report) Unclassified	20. Security Classif. (of this page) Unclassified		21. No. of Pages 116	22. Price* \$6.50	

\* For sale by the National Technical Information Service, Springfield, Virginia 22161



90%

**END**